การประเมินปริมาณรังสียังผลในผู้ป่วยจากการตรวจกล้ามเนื้อหัวใจด้วยเครื่องสเปก-ซีที (SPECT-CT)

นางสาวนี นีตา

วิทยานิพนธ์นี้เป็นส่วนหนึ่งของการศึกษาตามหลักสูตรปริญญาวิทยาศาสตรมหาบัณฑิต
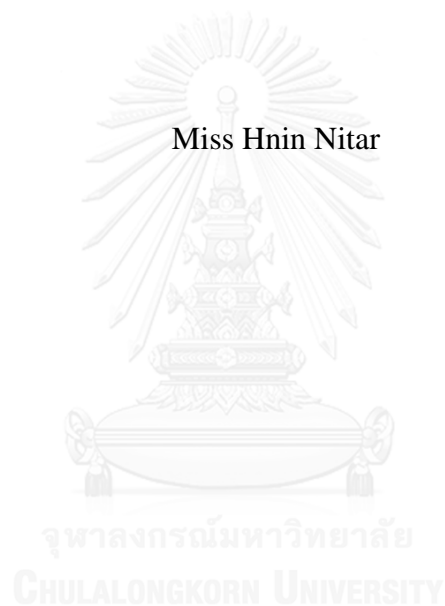สาขาวิชาฉายาเวชศาสตร์ ภาควิชารังสีวิทยา
คณะแพทยศาสตร์ จุฬาลงกรณ์มหาวิทยาลัย
ปีการศึกษา 2559
ลิขสิทธิ์ของจุฬาลงกรณ์มหาวิทยาลัย

ESTIMATION OF EFFECTIVE DOSE TO PATIENTS UNDERGOING
MYOCARDIAL PERFUSION SPECT/CT

Miss Hnin Nitar

A Thesis Submitted in Partial Fulfillment of the Requirements
for the Degree of Master of Science Program in Medical Imaging
Department of Radiology
Faculty of Medicine
Chulalongkorn University
Academic Year 2016
Copyright of Chulalongkorn University

Thesis Title	ESTIMATION OF EFFECTIVE DOSE TO PATIENTS UNDERGOING MYOCARDIAL PERFUSION SPECT/CT
By	Miss Hnin Nitar
Field of Study	Medical Imaging
Thesis Advisor	Associate Professor Anchali Krisanachinda, Ph.D.
Thesis Co-Advisor	Kitiwat Khamwan, Ph.D.

Accepted by the Faculty of Medicine, Chulalongkorn University in Partial Fulfillment of the Requirements for the Master's Degree

.... Dean of the Faculty of Medicine
(Professor Suttipong Wacharasindhu, M.D.)

THESIS COMMITTEE

.... Chairman
(Associate Professor Tawatchai Chaiwatanarat, M.D.)
.... Thesis Advisor
(Associate Professor Anchali Krisanachinda, Ph.D.)
.... Thesis Co-Advisor
(Kitiwat Khamwan, Ph.D.)
.... Examiner
(Associate Professor Supatporn Tepmongkol, M.D.)
.... External Examiner
(Professor Franco Milano, Ph.D.)

นี นีตา : การประเมินปริมาณรังสียังผลในผู้ป่วยจากการตรวจกล้ามเนื้อหัวใจด้วยเครื่องสเปก-ซีที (SPECT-CT) (ESTIMATION OF EFFECTIVE DOSE TO PATIENTS UNDERGOING MYOCARDIAL PERFUSION SPECT/CT) อ.ที่ปรึกษาวิทยานิพนธ์หลัก: อัญชลี กฤษณจินดา, อ.ที่ปรึกษาวิทยานิพนธ์ร่วม: กิติวัฒน์ คำวัน, 119 หน้า.

^{99m}Tc-sestamibi SPECT / CT เป็นที่นิยมสำหรับการประเมินโรคหัวใจและหลอดเลือด การใช้สเปคร่วมกับซีทีให้ผลในด้านคุณภาพของการถ่ายภาพที่ดีกว่าการใช้สเปคเพียงอย่างเดียวซึ่งจะมีผลให้ปริมาณรังสียังผลที่ผู้ป่วยเพิ่มขึ้นด้วย วัตถุประสงค์ของการศึกษานี้เพื่อประเมินปริมาณรังสียังผลที่ผู้ป่วยได้รับจากการตรวจกล้ามเนื้อหัวใจด้วยเครื่องสเปคซีที โดยเปรียบเทียบกับระยะเวลาของการรับรังสีแบคกราวด์ (BERT) ปริมาณรังสียังผลได้รับการประเมินในผู้ป่วย 10 รายที่อยู่ในสภาวะปกติ(rest study)และในผู้ป่วยที่มีการออกกำลังกายและถ่ายภาพด้วยเครื่องสเปคซีที ที่โรงพยาบาลจุฬาลงกรณ์สภากาชาดไทย ปริมาณรังสีดูดกลืนและรังสียังผลจากการใช้สาร ^{99m}Tc-MIBI ถูกคำนวณด้วยสมการและปัจจัย โดย Medical Internal Radiation Dosimetry (MIRD) คณะกรรมการของสมาคมเวชศาสตร์นิวเคลียร์แห่งสหรัฐอเมริกา ด้วยตาราง"S" ซึ่งได้รับการแก้ไขเพื่อใช้กับขนาดอวัยวะของคนเอเชีย ปริมาณรังสีดูดกลืนและรังสียังผลจากเครื่องซีทีสแกนถูกประเมินโดยใช้โปรแกรมมอนติคาโล ซิมูเลชั่น ImPACTSCANเวอร์ชั่น 1.0.4

ผลการศึกษาพบว่าอวัยวะที่ได้รับปริมาณรังสีดูดกลืนสูงสุดคือถุงน้ำดีในผู้ป่วยที่อยู่ในสภาวะปกติ (rest study) มีค่าเท่ากับ 35.80 ± 6.00 ไมโครเกรย์ต่อเมกะเบเคอเรล และสำหรับผู้ป่วยที่มีการตรวจกล้ามเนื้อหัวใจด้วยเสปคซีทีภายหลังการออกกำลังกาย (stress study)มีค่าเท่ากับ 34.81 ± 7.33 ไมโครเกรย์ต่อเมกะเบเคอเรล อวัยวะที่เกี่ยวข้องในทางเดินขับถ่ายของ MIBI (ลำไส้เล็ก upper large intestine, lower large intestine และไต) จะได้รับปริมาณรังสีดูดกลืนสูง ค่าเฉลี่ย ± SD ในช่วงที่ฉีด ^{99m}Tc-MIBI ของผู้ป่วยสภาวะปกติ rest study มีค่าเท่ากับ 935.00 ± 60.00 (821.00-993.00) เมกะเบเคอเรล และมีค่าเท่ากับ 886.28 ± 108.60 (577.00 – 993.00) เมกะเบเคอเรล สำหรับผู้ป่วยที่ออกกำลังกาย (stress study) ค่าเฉลี่ย ± SD และช่วงของค่าสัมประสิทธิ์ ของ ^{99m}Tc-MIBI ในผู้ป่วยสภาวะปกติ rest study มีค่าเท่ากับ 11.64 ± 0.70 (10.30 – 12.40) ไมโครซีเวิร์ตต่อเมกะเบเคอเรล และ ในผู้ป่วยที่ออกกำลังกาย stress study มีค่าเท่ากับ 10.18 ± 0.40 (10.70 – 9.30) ไมโครซีเวิร์ตต่อเมกะเบเคอเรล ค่าเฉลี่ย ± SD และช่วงค่าของรังสียังผลสำหรับ rest study ของ ^{99m}Tc-MIBI มีค่าเป็น 10.85 ± 1.24 (8.45 – 12.29) ไมโครซีเวิร์ต และสำหรับผู้ป่วยที่ออกกำลังกาย stress study จะมีค่าเท่ากับ 9.01 ± 1.25 (5.73 – 10.23) ไมโครซีเวิร์ต ค่าเฉลี่ย ± SD และช่วงรังสียังผลจาก CT สำหรับ rest study มีค่าเท่ากับ 1.14 ± 0.11 (0.9 – 1.3) และสำหรับ stress study มีค่าเท่ากับ 1.12 ± 0.13 (0.9 – 1.34) ไมโครซีเวิร์ด ค่าเฉลี่ย± SD และค่ารังสียังผลรวมสำหรับ rest study ของสเปคซีทีมีค่าเท่ากับ 11.99 ± 1.2 (9.75 – 13.49) ไมโครซีเวิร์ต และมีค่าเฉลี่ย BERT เป็น 3.99 ± 0.4 (3.25 – 4.50) ปี ค่าเฉลี่ย ± SD รังสียังผลของการตรวจด้วยเสปคซีที มีค่าเท่ากับ 10.35 ± 1.2 (6.83 – 11.45) ไมโครซีเวิร์ต และมีค่า BERT เท่ากับ 3.5 ± 0.2 (2.28 – 3.82) ปี ปริมาณรังสีเหล่านี้สามารถใช้เป็นข้อมูลอ้างอิงของประชากรในเอเชียสำหรับการกำหนดปริมาณรังสีที่ผู้ป่วยได้รับจากประเมินโรคหัวใจและหลอดเลือดด้วยเครื่องเสปคซีที และช่วยเพิ่มประสิทธิภาพของการถ่ายภาพ

ภาควิชา รังสีวิทยา	ลายมือชื่อนิสิต	_____
สาขาวิชา ฉายาเวชศาสตร์	ลายมือชื่อ อ.ที่ปรึกษาหลัก	_____
ปีการศึกษา 2559	ลายมือชื่อ อ.ที่ปรึกษาร่วม	_____

5874114230 : MAJOR MEDICAL IMAGING

KEYWORDS: SPECT/CT / MYOCARDIAL PERFUSION / 99MTC- SESTAMIBI / MIRD

HNIN NITAR: ESTIMATION OF EFFECTIVE DOSE TO PATIENTS UNDERGOING MYOCARDIAL PERFUSION SPECT/CT. ADVISOR: ASSOC. PROF. ANCHALI KRISANACHINDA, Ph.D., CO-ADVISOR: KITIWAT KHAMWAN, Ph.D., 119 pp.

^{99m}Tc-sestamibi SPECT/CT has become widely used for the assessment of cardiovascular diseases. The integrated SPECT/CT results in better quality corrected SPECT imaging with higher patient exposure than SPECT alone. The purpose of this study is to investigate the effective doses to patients undergoing myocardial perfusion SPECT/CT and compare with background equivalent radiation time (BERT). The effective doses had been evaluated in 10 patients at rest and 10 patients at stress study of myocardial perfusion SPECT/CT at King Chulalongkorn Memorial Hospital. The absorbed dose and effective dose from ^{99m}Tc-MIBI were calculated by the equations and factors provided by Medical Internal Radiation Dose (MIRD) committee of the Society of Nuclear Medicine with the "S" tables modified with the organ masses of the Asian reference man . The absorbed dose and effective dose from CT scan were determined by using Monte Carlo simulation, ImPACTSCAN program version 1.0.4.

The result showed that the organ received the highest absorbed dose was the gall bladder of 35.80 ± 6.00 µGy/MBq for rest study and 34.81 ± 7.33 µGy/MBq for stress study respectively. The organs involved in the excretory pathway of MIBI (small intestine, upper large intestine, lower large intestine and kidneys) received the high absorbed doses. The mean±SD and range of injected activity of ^{99m}Tc-MIBI for rest study was 935.00 ± 60.00 ($821.00 - 993.00$) MBq. For stress study, the mean±SD and range of injected activity was 886.28 ± 108.60 ($577.00 - 993.00$) MBq. The mean±SD and range of dose coefficients of ^{99m}Tc-MIBI was 11.64 ± 0.70 ($10.30 - 12.40$) µSv/MBq for rest study and 10.18 ± 0.40 ($9.30 - 10.70$) µSv/MBq for stress study. The mean±SD and range of effective dose from ^{99m}Tc-MIBI was 10.85 ± 1.24 ($8.45 - 12.29$) mSv for rest study and 9.01 ± 1.25 ($5.73 - 10.23$) mSv for stress study. The mean±SD and range of effective dose from CT was 1.14 ± 0.11 ($0.9 - 1.3$) mSv for rest study and 1.12 ± 0.13 ($0.9 - 1.34$) mSv for stress study. The mean±SD and range of total effective dose from rest study of myocardial perfusion SPECT/CT was 11.99 ± 1.2 ($9.75 - 13.49$) mSv, and its related mean BERT was 3.99 ± 0.4 ($3.25 - 4.50$) years. The mean±SD and range of total effective dose from stress study of myocardial perfusion SPECT/CT was 10.35 ± 1.2 ($6.83 - 11.45$) mSv, and its related BERT was 3.5 ± 0.2 ($2.28 - 3.82$) years. These dose values can be used as reference of Asian population for determination of patient radiation dose undergoing myocardial perfusion SPECT/CT and assist for optimization of myocardial perfusion imaging.

Department:	Radiology	Student's Signature	
Field of Study:	Medical Imaging	Advisor's Signature	
Academic Year:	2016	Co-Advisor's Signature	

ACKNOWLEDGEMENTS

CONTENTS

LIST OF TABLES

Table   **Page**

LIST OF FIGURES

Figure   **Page**

LIST OF ABBREVIATIONS

Abbreviation	Terms
2D	Two dimensions
3D	Three dimensions
ACR	American College of Radiology
AEC	Automatic exposure control
BERT	Background equivalent radiation time
BMI	Body mass index
CAD	Coronary artery disease
COR	Center of rotation
cpm	Count per minute
CT	Computed tomography
CTDI	Computed tomography dose index
DLP	Dose length product
ECG	Electrocardiogram
FOV	Field of view
FWHM	Full width at half maximum
GE	General Electric
h	Hour
HU	Hounsfield unit
ICRP	International Commission on Radiological Protection
ImPACT	Image Performance Assessment in Computed Tomography
keV	KiloelectronVolt

Abbreviation	Terms
kVp	Kilovoltage peak
LPO	Left posterior oblique
LLI	Lower large intestine
mA	Milliampere
MBq	MegaBecquerel
mCi	MilliCurie
MIBI	Methoxy isobutyl isonitrile
min	minute
MIRD	Medical Internal Radiation Dosimetry
mSv	MilliSievert
NaI(Tl)	Sodium iodide thallium activated
NEMA	National Electrical Manufacturers Association
PMMA	Polymethyl methacrylate
PSF	Point spread function
PVE	Partial volume effect
QPS	Quantitative perfusion SPECT
RAO	Right anterior oblique
RSNA	Radiological Society of North America
SPECT	Single Photon Emission Computed Tomography
TAC	Time activity curve
TEW	Triple energy window
TIAC	Time-integrated activity coefficient
TLD	Thermoluminescent dosimeter
ULI	Upper large intestine

CHAPTER 1

INTRODUCTION

1.1 Background and rationale

Cardiovascular disease is the leading worldwide cause of death, accounting for 17.3 million deaths each year. Therefore, the use of a diagnostic test such as electrocardiogram (ECG)-gated single photon emission computed tomography (SPECT) is essential to improve outcome and significantly reduce mortality and morbidity from ischemic heart disease. The sensitivity and specificity of cardiac SPECT are affected by image artifacts caused by tissue attenuation [1].

Therefore, the integrated SPECT/CT has become widely used in MPI to overcome these artifacts and improve the diagnostic accuracy. Hybrid cardiac imaging SPECT and CT depicts cardiac and vascular anatomical abnormalities and their physiologic consequences in a single setting and appears to offer superior information compared with either stand-alone or side-by-side interpretation of the data sets in patients with known or suspected coronary artery disease (CAD) [2]. This system allows the accurate localization of the functional findings to a specific anatomic structure, improvement in the characterization of SPECT imaging and detection of anatomical lesions not detected by SPECT. In addition, an algorithm that allows CT information-based attenuation correction has been implemented in SPECT/CT system. The role for CT in myocardial perfusion SPECT/CT is the attenuation correction and anatomical correlation of functional SPECT. This results in better quality corrected SPECT imaging and enables quantitative SPECT.
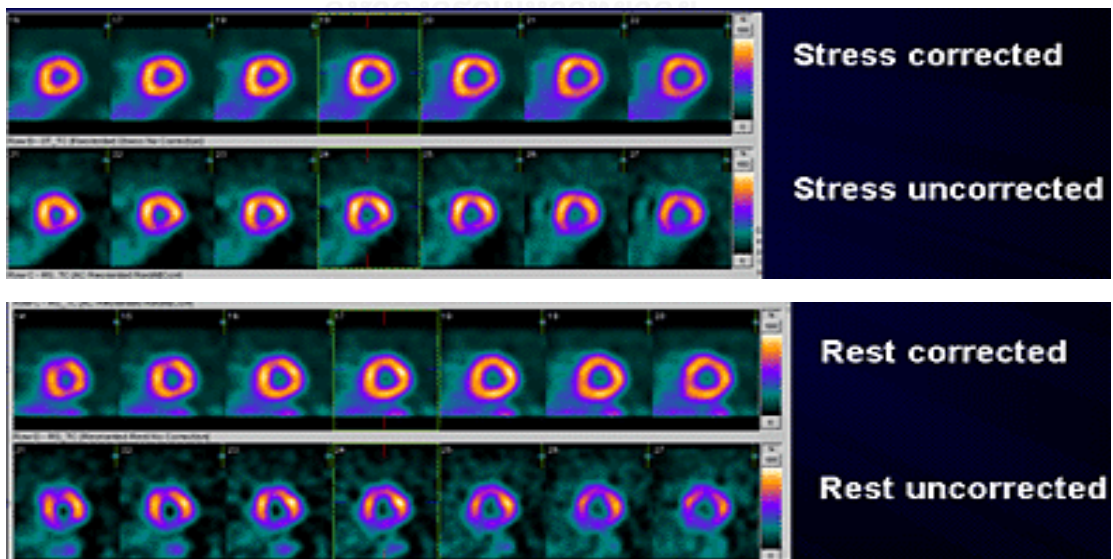
Figure 1.1 Short axial images of CT-based attenuation correction and without attenuation correction in the same patient

On the other hand, SPECT/CT examinations involve higher patient exposure than with SPECT alone. With SPECT/CT, the radiation dose to the patient is the combination of the radiation dose from the radiopharmaceutical injected for SPECT imaging and radiation dose from CT.

The radiation exposure from myocardial perfusion imaging might lead to increasing risk of cancer development in the group of investigated patients [3]. Effective dose, an indicator of stochastic effect, is a useful parameter that enables patient exposure to different medical procedures using ionizing radiation to be evaluated and compared. Effective dose is a calculated age- and sex-averaged value that is used as a robust measure to compare detriment from cancer and hereditary effects due to various procedures involving ionizing radiation. It is especially important to establish early mean absorbed dose to organs and tissues from each investigations. To estimate the radiation exposure of patients undergoing myocardial perfusion SPECT/CT, the effective doses due to both radiopharmaceutical and CT should be determined.

In the aspect of internal dosimetry, it is not possible to perform direct measurements of the mean absorbed dose to the various organs and tissues from radionuclides within the body. The biodistribution or biokinetics of radiopharmaceutical, i.e. the uptake and retention in different organs and tissues, must be known to evaluate the radiation absorbed doses to organs and tissues resulting from an administered radionuclide. In contrast to diagnostic radiology where normally only the organs or tissues of diagnostic interest and their surroundings are irradiated, nuclear medicine examinations cause the radiation exposure of the whole body. In the case of CT, absorbed doses to the organs or tissues can be measured by using thermoluminescent dosimeters (TLDs) or calculated by using the voxel-based Monte Carlo simulation technique.

Background radiation is the radiation that comes from environmental sources including earth's crust, atmosphere, cosmic rays and naturally occurring radioisotopes. Three mSv is the worldwide average annual natural background radiation [4]. As the effective dose is not a magnitude that is easily understood by patients and the general public, the radiation dose from diagnostic procedure can be compared with the background radiation, mostly from natural sources to provide an equivalent background equivalent radiation time (BERT) estimate. Thus, the amount of radiation received from a radiological procedure can be expressed in terms of a certain number of days or years of background radiation, as follows:

$$\text{BERT(years)} = \frac{\text{E(mSv)}}{3\text{mSv}} \qquad [1.1]$$

Where, E is the effective dose from radiological procedure.
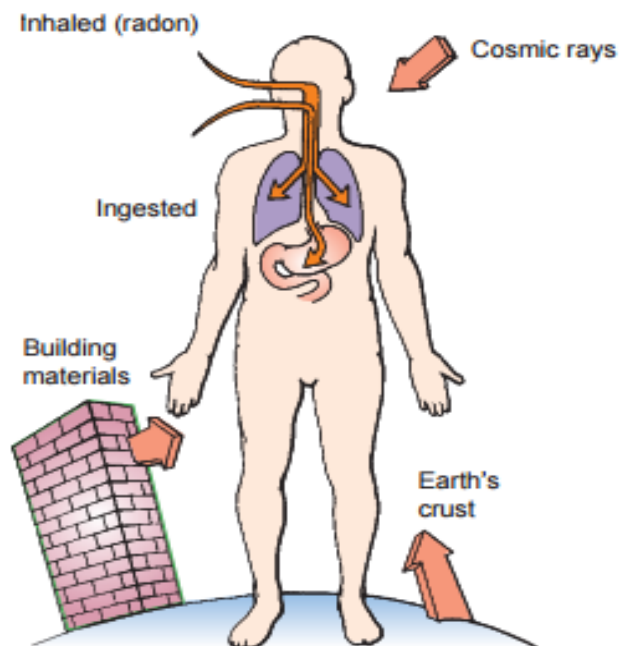
Figure 1.2 Natural background radiation from environmental sources [5]

As recommended by American College of Radiology (ACR) and Radiological Society of North America (RSNA), the qualitative risk level of radiation exposure from radiological procedure with BERT are as follows: [6]

Negligible risk: less than 2 days of natural background exposure

Minimal risk: more than 2 days and up to 1 month of natural background exposure

Very low risk: more than 1 month and up to 8 months of natural background exposure

Low risk: more than 8 months and up to 6 years of natural background exposure

Moderate risk: more than 6 years of natural background exposure.

Increased awareness of the risk of exposure to ionizing radiation has resulted in efforts to minimize radiation dose incurred during diagnostic and nuclear medical imaging investigations. Furthermore, the specific dosimetric information assists in justification of risk and optimization of myocardial perfusion imaging. That is why this study was designed to determine the effective doses to patients from myocardial perfusion SPECT/CT.

1.2 Research objectives

1.2.1 To evaluate the effective doses to patients undergoing myocardial perfusion SPECT/CT

1.2.2 To express these effective doses in relation with background equivalent radiation time (BERT)

1.3 Definition [7]

Attenuation

A process by which the number of particles or photons entering through the medium is reduced by the combined effect of absorption and scattering.

Background radiation

Radiation that comes from environmental sources including earth's crust, atmosphere, cosmic rays and naturally occurring radioisotopes. **3mSv** is the worldwide average annual natural background radiation.

Becquerel (Bq)

The unit of radioactivity, corresponding to one disintegration per second.
($1Ci = 3.7 \times 10^{10}$ disintegration per second).

Biological half-life

The time required to eliminate half of the amount of a substance administered by the biological system, such as that of a living organism.

Computed Tomography

A technique for constructing images of the structures at a particular depth within the body done by taking several x-ray images at different angles and then using a computer to reconstruct and analyze the resulting images.

Decay, radioactive

The decrease in the amount of any radioactive material with the passage of time due to the spontaneous breakdown of an atomic nucleus resulting in the release of energy and matter from the nucleus.

Dose, Absorbed dose

The amount of energy deposited in any substance by ionizing radiation per unit mass of the substance. It is expressed numerically in rad (traditional units) or grays (SI units).

Effective half-life

The time required to be diminished 50 percent of the amount of a radionuclide deposited in a living organism by the combined action of physical decay of radionuclide and biological elimination.

External dose

Radiation exposure from a source outside the body.

Gray (Gy)

The international system (SI) unit of radiation dose expressed in terms of absorbed energy per unit mass of tissue. The gray is the unit of absorbed dose and has replaced the rad. 1 gray = 1 Joule/kilogram and also equals 100 rad.

Internal dose
Radiation exposure from a source inside the body.

Myocardial perfusion imaging
It is non-invasive imaging that shows how well blood flows through the heart muscle. It can show an area of the heart muscle that is not getting enough blood flow.

Reference man
A person assumed to have the anatomical and physiological characteristics of an average individual. These assumed characteristics are used in calculations assessing internal dose.

Sestamibi (methoxyisobutylisonitrile)
It is a myocardial perfusion agent that is indicated for detecting coronary artery disease by localizing myocardial ischemia and infarction, in evaluating myocardial function and developing information for use in patient management decisions.

Sievert (Sv)
The international system (SI) unit for dose equivalent equal to 1 Joule/kilogram. The sievert has replaced the rem. (1 Sievert = 100 rem)

Single Photon Emission Computed Tomography (SPECT)
An imaging modality that allows to visualize functional information about a patient's specific internal organ or body system using the distribution of radionuclide in the target organ.

Stochastic effects
Effects that occur by chance and consist primarily of cancer and genetic effects. The effect may occur without a threshold level of dose, whose probability is proportional to the dose and the severity is independent of the dose.

Tissue weighting factor
A multiplier that is used to convert the equivalent dose to a specific organ or tissue into what is called the "effective dose." The goal of this process was to develop a method for expressing the dose to a portion of the body in terms of an equivalent dose to the whole body that would carry with it an equivalent risk in terms of the associated fatal cancer probability. It applies only to the stochastic effects of radiation.

Thermo-luminescent dosimeter (TLD)
A small device used to measure the radiation dose by measuring the amount of light emitted from nonmetallic crystalline solids in the detector when the crystal is heated after being exposed to the radiation.

CHAPTER 2

REVIEW OF RELATED LITERATURE

2.1 Theory

2.1.1 Principle of myocardial perfusion imaging

SPECT myocardial perfusion imaging performed with ^{99m}Tc-sestamibi is a widely utilized noninvasive imaging modality for the diagnosis and management of coronary artery diseases. This modality permits three dimensional assessment and quantitation of perfused myocardium and functional assessment through electrocardiogram (ECG)-gating of perfusion images.

The diagnosis of occlusive coronary disease using radionuclide imaging is made by detection of relatively decreased myocardial perfusion distal to the site of vascular obstruction, compared with the more normally perfused surrounding myocardium. The fundamental principle of rest/stress myocardial perfusion imaging is the assessment of heterogeneity of regional myocardial blood flow that the impaired myocardium received less blood flow than the normal myocardium in stress perfusion images compared with rest images. In figure 2.1, perfusion images of myocardium supplied by two branches of a coronary arteries, one is normal (left) and one with significant stenosis (right). However, myocardial blood flow is homogenous in both coronary artery branches at rest perfusion image because of autoregulation of coronary blood flow. Decrease in vessel resistance to achieve the increased coronary blood flow can accomplish oxygen demand caused by exercise, resulting in approximately two to three folds increased above the level at rest and four to five folds increased in pharmacologic stress than the baseline [8]. In the impaired region, peripheral vessel resistance distal to stenosis cannot decrease anymore. Therefore, in stress perfusion image, regional myocardial perfusion is heterogeneous due to stenosis in the right branch.
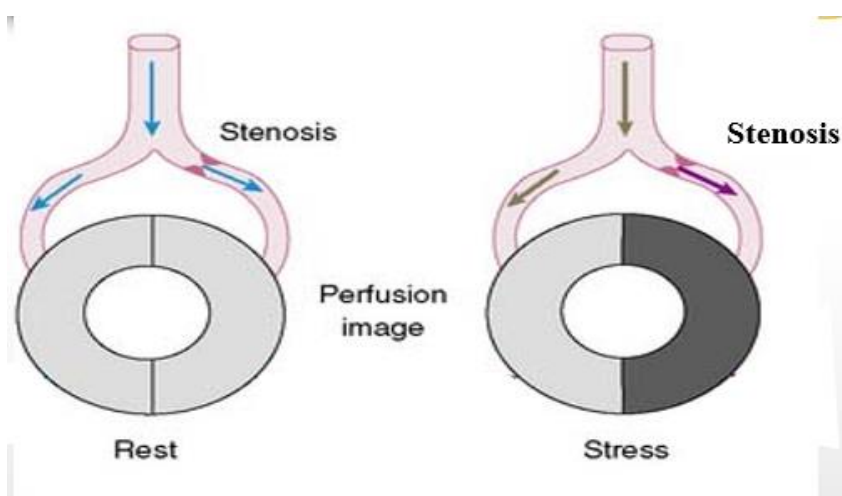
Figure 2.1 Principle of rest and stress myocardial perfusion imaging [9]

Even severe stenosis may not demonstrate detectable blood flow abnormalities at rest, one kind of stress, either exercise or pharmacologic stress, is usually needed to distribute a flow differential that can be seen on myocardial perfusion imaging. Although stenosis of up to 90% of the arterial diameter may not produce a decrease in blood flow significant enough to be detected at rest, stenosis of 50% or more are reliably detected with myocardial perfusion imaging under conditions of maximal myocardial stress (Fig.2.2). By comparing myocardial perfusion at rest (baseline blood flow) to perfusion under conditions of stress (maximal blood flow), areas of reduced coronary reserve indicative of stenosis and resultant stress-induced ischemia can be identified.
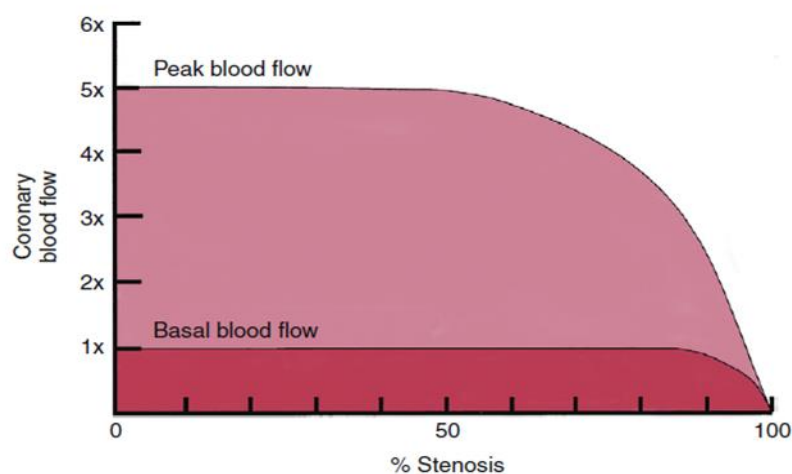
Figure 2.2 Coronary blood flow. Relationship of coronary blood flow at exercise (peak blood flow) and rest (basal blood flow) relative to the percentage diameter of coronary artery stenosis

2.1.2 Gated SPECT Imaging

Cardiac gating allows heart motion and contraction to be resolved by dividing the projection into discrete time parts coupled with the cardiac cycle. The electrocardiogram is used to determine the heart rate and the onset contraction at the QRS complex. Two successive R-wave peaks (R-R interval) define a cardiac cycle. The cardiac cycle is divided a set number of predetermined time intervals, called frames and counts collected during each frame are directed to a different projection set. The electrocardiographic QRS information is matched to the imaging data. The ECG QRS complex is detected by a gating circuit that defines the QRS by a rapid change in voltage per unit time (dV/dt) and produces a gating signal. Counts are directed into the first frame during the initial T/N seconds after the QRS complex is detected, where N is the number of frames and T is the length in second of the cardiac cycle. Then, counts are directed into the second frame for the second T/N seconds, and so on. This is repeated for each heartbeat during the acquisition, at every angle. At the end of the acquisition, there are N sets of complete projection images. When these are reconstructed, the result is N 3D sets of slides showing the heart at N points during the cardiac cycle. These four-dimensional data allow 3D analysis of motion and myocardial thickening, as well as perhaps enabling better discrimination of the extent and location of perfusion abnormalities.

Local variables such as left ventricular volume, mass and ejection fraction can be calculated. Local properties of wall motion and myocardial thickening can be also obtained; these can then be displayed using either polar maps or 3D graphics. Most commercially available programs for quantifying cardiac function are fully 3D approaches, which start by detecting endocardial and epicardial surface points through the cardiac cycle.

2.1.3 SPECT Data acquisition

Data acquired by rotation of the detector head around the long axis of the patient over 180 or 360 degree, while 180-degree right anterior oblique (RAO) to left posterior oblique (LPO) data collection is commonly used for cardiac study since it minimizes the effects of attenuation and variation of resolution with depth. Data can be collected in either continuous motion or step and shoot mode. In continuous acquired data are later binned into the number of segments equal to the number of projections desired. In the step and shoot mode, the detector moves around the patient at selected incremental angles and collects the data for the projection at each angle.

Pixels 6 to 6.5 mm in size have proved to be adequate for cardiac SPECT. This size is obtained by using a 64x64 pixel matrix for systems with a field of view of 38 to 40 cm. 64 projections over 180 degrees are preferred but 32 projections are used with satisfactory results [10].

2.1.4 Myocardial perfusion SPECT/CT imaging protocol

2.1.4.1 One-day protocol

If two-day imaging protocol is impractical for some patients, stress and rest studies are usually performed using one-day imaging protocol. This requires the administration of a lower dose (approximately one-fourth of the total dose) for the first injection and a higher dose (approximately three-fourths of the total dose) for the second injection. One-day stress/rest and rest/stress Tc-99m protocols are now typically performed with no significant delay between obtaining the first set of images and injection of the second dose of Tc-99m at stress or rest. In patients without a high pre-test probability of a stress perfusion defect or left ventricular dysfunction or dilatation, a low-dose stress/high-dose rest Tc-99m protocol is advantageous because a significant percentage of these patients will have normal stress imaging, thereby enabling obviating the need for the rest imaging with its additional radiation exposure, and permitting performance of stress-only imaging [11].

2.1.4.2 Two-day protocol

Ideally, stress and rest imaging with Tc-99m agents should be performed on two separate days to avoid having residual activity (''shine-through'' or ''crosstalk'') from the first injection interfere with interpretation of images reflecting the second injection. In larger patients (e.g., >250 lbs or BMI >35) or in female patients where significant breast attenuation is anticipated, a low dose of Tc-99m radiotracer may result in suboptimal images and a 2-day imaging protocol with higher activities (18 to 30 mCi) for each injection may be preferable [11].

2.1.5 SPECT reconstruction

Methods of image reconstruction using the acquired data introduce two categories: iterative methods and analytic methods. Analytic methods are based on the exact mathematical solution to the image reconstruction problem, whereas iterative methods estimate the distribution through successive approximations. Accurate correction for attenuation and their degradations require more complex iterative reconstruction techniques.

2.1.5.1 Filtered backprojection

Filtered back projection is an analytic reconstruction algorithm designed to overcome the limitations of conventional back projection; it applies a convolution filter to remove blurring. This method provides accurate estimation of 2D radiotracer distribution when projection data are noise free. The basic principles are to perform Fourier transform of angular projections, apply the ramp filter in the frequency anti transform. This method is simple to implement and fast in performing reconstruction. However, the ramp filter used to eliminate star artifact also amplifies the noise component, which is particularly important at low counting statistics.

2.1.5.2 Iterative reconstruction

Iterative reconstruction is a method of algorithms used to reconstruct 2D and 3D images from the projections of an object. The algorithm starts with an assumed image, computes projections from the image, compares the original projection data and updates the images based upon the difference between the calculated and the actual projections.

The major advantages of the iterative approach include improved in sensitivity to noise and the capability of reconstructing an optimal image in the case of incomplete data, however it needs increased in processing time. The type of iterative reconstruction currently used is the ordered subset expectation maximization (OSEM) method, in which the projection data are ordered into subsets, which are used in the iterative steps of the reconstruction to speed up the process. The advantage of OSEM is that an order of magnitude increase in computational speed can be obtained.

2.1.5.3 Reorientation and reslicing

Transverse or transaxial slices of three dimensional block perpendicular to the body axis can be obtained by reconstruction of raw data. However, due to an oblique axis of heart position in the chest wall, cardiac images need to be standardized slices that are perpendicular or parallel with the long-axis of the heart and oblique to the axis of the body such as short-axis, horizontal long-axis and vertical long-axis, Fig (2.3). Short-axis sections through the left ventricle are from the base of the heart to the apex with its anterior wall towards the top, the inferior wall towards the bottom, the septal wall towards the left and the lateral wall towards the right. Serial short-axis images are displayed from the apex to the base and the left to the right.

Vertical long-axis sections through the left ventricle are from septum to the lateral wall with the base of left ventricle towards bottom of the image and apex towards the right. Serial vertical slices are displayed from the medial to the lateral, from the left to the right.

Horizontal long-axis sections through the left ventricle are from the anterior to the inferior wall with the base towards the bottom of the image and apex towards the top. The right ventricle can be visualized on the left side of the image. Serial horizontal images are displayed from the inferior to the anterior, from the left to the right.
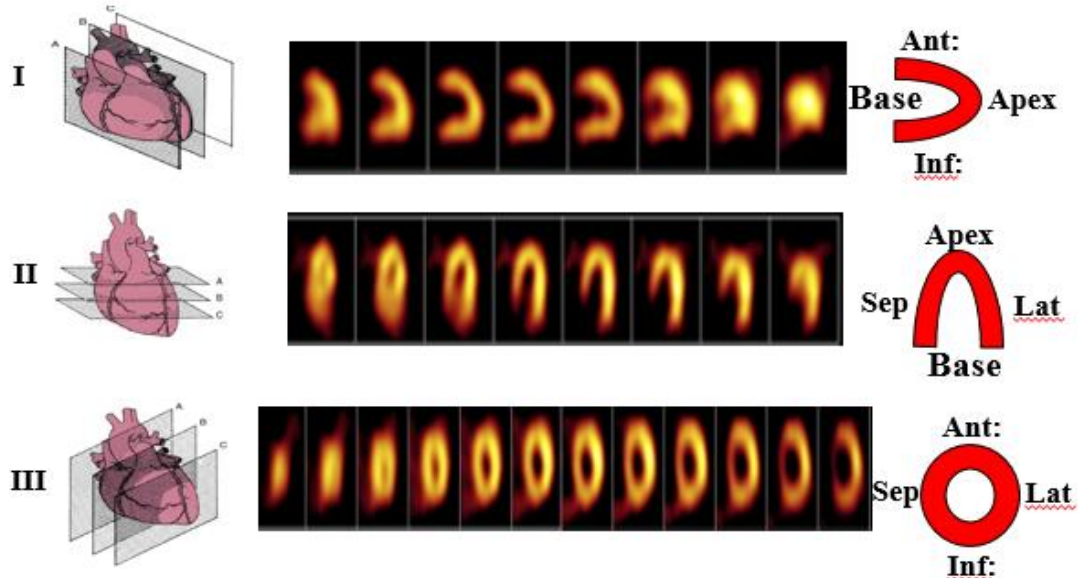
Figure 2.3 Vertical long-axis slices (I) Horizontal long-axis slices (II) and short-axis slices (III) of myocardial perfusion imaging

2.1.6 Quantitative analysis

The counts per pixel value within the cardiac region are related to some parameters of cardiac performance. Therefore, quantitative methods have been used to measure cardiac function as well as regional cardiac function from SPECT images during the past of 10 years. In myocardial perfusion imaging, the counts per pixel value of the region are related to the concentration of radionuclide and blood flow. Two standard types of quantification are: absolute quantification, which is the ability to extract number of counts per pixel from radionuclide concentrations at the source locations and the true relative quantification, which is able to extract the ratio of the pixel counts expected from a given ratio of radionuclide concentrations at two source locations. In the present, the most widely used approach is using data based methods of quantification. The concept of data based quantification involved three major steps:

1. To enhance the image in term of image processing.
2. To extract pertinent measurement to use in determining normality versus abnormality in term of image analysis
3. To qualify the degree of abnormality by comparing the extracted measurement to normal database.

Many of the techniques illustrate reflect computer method developed at Cedars-Sinai Medical Center. The Cedars-Sinai quantitative approach to SPECT is based on sampling the patient's short and vertical long axis myocardial tomogram using maximum count circumferential profiles and comparing this profile to profile derived

from a database of normal patients. Patient profile points that fall below the normal limit and meet a criterion for abnormality are considered abnormal. The quantitative output of the program includes a polar map display design being abnormality and a report indicating the percent of abnormal pixel within the total and individual vascular territories. Quantitative perfusion SPECT (QPS) provides three perfusion polar maps and 3D parametric surfaces (stress, rest and reversibility).

2.1.7 Physical factors influencing image quality of cardiac SPECT imaging

The important physical factors affected the quality of cardiac SPECT images are as followings:

2.1.7.1 Photon attenuation

Attenuation of photons in the body tissue is the most significant factor that influenced the quantitation of tracer distribution and image quality in myocardial perfusion imaging. Gamma ray photons are attenuated in body tissue while passing through a patient. The degree of attenuation depends on the photon energy, the thickness of the tissue and the linear attenuation coefficient of the photons in tissue. Since attenuation is depth-dependent, regions deeper in the body are more attenuated. Attenuation can result in the number of photons incident on the medium to reduce exponentially with the source depth in the medium. Due to highly differences in tissue composition in the thorax region, attenuation produces attenuation artifacts as non-uniform myocardial wall uptake expected in normal scan. These include breast attenuation artifacts occurred in female patients, diaphragmatic attenuation artifacts mostly seen in male patients and chest wall attenuation artifacts frequently identified in obese patients. As a result, attenuation correction of these images is necessary to accurately determine the amount of radionuclides present in various organs of the body.

2.1.7.1.1 Methods of attenuation correction

Several methods were employed to correct for attenuation. In one method, an uncorrected image is taken and the thickness of tissue through which the photons attenuated are estimated. Using constant linear attenuation coefficient of the photons in the tissue, each pixel data is corrected to this equation to reconstruct the image.

$$I_t = I_0 e^{-\mu x} \tag{2.1}$$

If the photon beam initial intensity I_0 passes through an absorber of thickness x, then the transmitted beam I_t is given by an exponential equation, where μ is the linear attenuation coefficient of absorbing for photon of interest and has a unit of cm^{-1}. The factor of $e^{-\mu x}$ represents the transmission factor of the photon.

However, estimation of a constant linear attenuation coefficient can only be useful for symmetric organs with similar tissue density since gamma ray traverses different thicknesses of various body tissues. Therefore a constant correction factor may not be adequate for attenuation correction and the patient-specific information on spatial distribution of attenuation coefficient (attenuation map) is required.

Consequently, the use of CT is essential integrated with SPECT to generate a patient specific attenuation map for correcting the radionuclide image for photon

attenuation. The linear attenuation coefficient measured with CT is calculated at the x ray energy rather than at the energy of the photon emitted by the radiopharmaceutical acquired during the radionuclide imaging study. Therefore, it is required to transform the linear attenuation coefficients obtained from the CT scan to those corresponding to the energy of the emission photons used for the SPECT imaging study.

2.1.7.2 Physical interaction of photon by Compton scattering

Photons can interact with atoms in the body via Compton scattering prior to detection and are scattered in a new direction. Most scattered photons are incorrectly detected, leading to degradation of contrast resolution and quantification.

2.1.7.2.1 Methods of scatter correction

Generally, the methods of scatter compensation can be divided into two different categories. The first category, which referred as energy based scatter compensation method, estimates the scatter contributions to the projections based on the acquired emission data. The data used may be information from the energy spectrum or a combination of the photopeak data and an approximation of scatter point spread function (PSF's). The scatter PSF gives the spatial distribution of the relative probabilities of detecting scattered photons at each location in the projection for a given location in the source distribution. The scatter estimate can be used before, during, or after reconstruction. The second category consists of those methods that model the scatter PSF's during the reconstruction process. The second approach is referred as reconstruction-based scatter compensation.

One example of an energy based scatter compensation method is the triple-energy-window (TEW) method. Triple energy window scatter-correction method uses centered the photopeak of the radionuclide's energy spectrum with adjacent to upper and lower scattered energy windows to determine the number of scattered photons. The subtraction is carried out using two sets of data: the count acquired with the main window centered at photopeak energy, and the count with two sub-windows on both sides of the main window. The scattered photons included in the main window are estimated from the counts acquired with the sub-windows. To obtain the primary count in the main window, the scattered photons are subtracted from the count acquired with the main window.

2.1.7.3 Partial volume effect (PVE)

Another important factor affecting count quantification in myocardial perfusion imaging is partial volume effect. This phenomenon is usually related to the limitations resulting from the sampling of image with pixels that are of finite size. Marked partial volume effects occur in myocardial single photon emission computed tomographic (SPECT) studies because of limited resolution in imaging the myocardial wall and contractile motion of the heart. The partial volume effect can lead to both under/overestimation of activities around small structures in the reconstruction image. The Recovery coefficient (RC) value is the ratio between the reconstructed count activity and true count activity of region of interest and should be 1 for the larger object. Recovery coefficient is applied for correcting the over/underestimation of activities from partial volume effect in a small structure.

2.1.8 Technicium-99m-sestamibi

^{99m}Tc hexakis-2-methoxyisobutyl isonitrile (^{99m}Tc sestamibi) is a monovalent cation consisting of a central Tc(I) core surrounded in an octahedral configuration by six identical methoxyisobutyl isonitrile ligands coordinated through the isonitrile carbon atoms (Fig. 2.4). Technicium-99m is a metastable radionuclide produced from molybdenum-99m generator. It is a gamma ray emitter with physical half-life of 6.02h. The substance is taken by myocytes in proportion to regional myocardial blood flow.
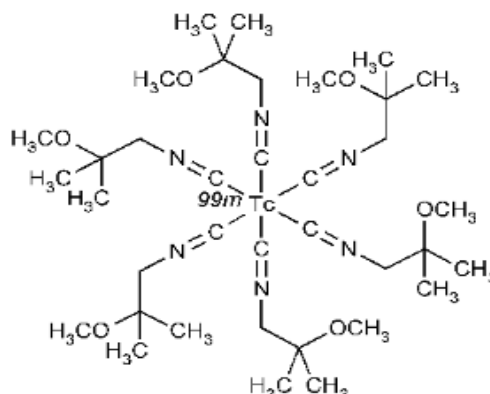
Figure 2.4 Schematic chemical structure of ^{99m}Tc-sestamibi

The cationic charge of the compound provides hydrophilic properties, while six isonitrile groups allow hydrophilic interaction with cell membrane. The 140keV photon energy of ^{99m}Tc-MIBI can provide higher myocardial image quality with reduced soft tissue attenuation effect in comparison with low photon energy. It can also provide sufficient counting statistics to allow gating of perfusion images.

2.1.9 Pharmacologic coronary vasodilatation

The pharmacologic coronary vasodilatation can be used to promote directly coronary blood flow independent of myocardial oxygen demand. The advantage of pharmacologic stress is that the patient does not need to have the physical and mental ability to do exercise. The commonly used agents for clinical SPECT stress imaging are adenosine which directly produces vasodilatation and dipyridamole which indirectly acts through its effect on adenosine metabolism.

2.1.9.1 Adenosine [12]

Adenosine is produced endogenously by endothelial and vascular smooth muscle cells in small amount during normal cellular condition and in larger amount under ischemic condition. It functions as a physiologic regulator of blood flow in most vascular beds, including coronary circulation. The pharmacologic effect of adenosine is much more rapid than that of dipyridamole, but the degree of coronary dilatation is comparable, producing about three to five times baseline blood flow. Adenosine has very short half-life of less than two seconds and rapid onset of action. Its peak hyperemic action is reached within two minutes after starting of its infusion and back to baseline within two minutes after termination of infusion. The usual dose is 0.14 mg/kg/6min.

Caffeine and theophylline inhibit the vasodilatation effect of adenosine and therefore caffeine should be withheld for 24h and theophylline for 72h if the patients can tolerate before the studies.

The three most common side effects of adenosine are flushing, shortness of breath, and chest pain. These are usually transient and require no action or treatment. An uncommon but more serious side effect is atrioventricular block, which usually occurs in the first few minutes of infusion and is also transient.

Contraindications to adenosine include severe obstructive lung disease, acute myocardial infarction or unstable coronary syndrome (< 24h), second- or third-degree atrioventricular block with a functioning pacemaker and systolic pressure less than 90 mmHg.

2.1.10 Rationale for integrating SPECT and CT in myocardial perfusion imaging

The efficiency of SPECT myocardial perfusion imaging to investigate coronary artery disease and to conclude cardiovascular events had been reported extensively in the literature. Nevertheless, SPECT cardiac imaging has extensive limitations:

- The spatial resolution of conventional imaging equipment is inferior (Table 2.1)
- The full range of myocardial blood flow is poorly visualized, particularly at higher flow levels
- Non-uniform soft tissue attenuation may be misleading as regional myocardial perfusion deficiency.

Therefore, to overcome these problems, the integration of SPECT with CT was imperative to provide a unique opportunity to delineate cardiac and vascular abnormalities and their physiologic consequences in a single setting.

The roles for CT in myocardial perfusion study are as follows:

- Correction of nonuniform attenuation artifacts
- Anatomic co-registration of functional SPECT with anatomic imaging techniques that have high spatial resolution
- Coronary artery calcium scoring

Although the dual-modality imaging may improve the potential diagnostic accuracy, it poses with regard to the added radiation dose to the patients.

Table 2.1 Spatial resolution of different imaging modalities [13]

Modality	Resolution (FWHM) (mm)
Nuclear Medicine (SPECT)	7-15
Nuclear Medicine (PET)	4-10
Computed Tomography	0.5-2
Magnetic Resonance Imaging	0.5-1.5

FWHM, full width half maximum

2.2 Radiation dosimetry

2.2.1 Radiopharmaceutical kinetics data

In addition to the requirements of physical factors of radionuclide, the biokinetic behavior of a radioactive substance which includes the activity uptake and retention in different organs and tissues as the function of time, i.e. the time-dependent distribution in an organ or whole-body is required in order to assess the internal radiation dosimetry. Radioactivity deposited in an organ of interest or whole-body can be estimated by extrapolation from animal data, external measurements by using a scintillation camera and in vitro measurements of excretory fluids and blood. Among these, serial whole-body measurement by using gamma camera is most commonly used for performing biokinetic studies of radiopharmaceuticals labelling with gamma-emitting radionuclides in vivo.

The calculation of the absorbed dose to a given target region initially requires the determination of the time-integrated activities of the various source regions. The time-integrated activity is the total number of nuclear transformations (radioactive decay) in the source region r_S. The activity in that region is necessary to measure over time and integrates over time to yield the residence time of time-integrated activity coefficient ($\tilde{a}\ (r_S, T_D)$). That coefficient represents the total number of nuclear transformations occurring in source region over dose-integration period per unit administered activity, determined by the equation as:

$$\tilde{a}\ (r_S, T_D) = \frac{1}{A_0} \int_0^{T_D} A(r_S, t)dt \tag{2.2}$$

Where, $\tilde{a}\ (r_S, T_D)$ is the time-integrated activity coefficient (s). $A(r_S,t)$ is the time-integrated activity (Bq.s). A_0 is the administered activity in Bq. The residence time is correlated to the characteristics of both physical decay and biological removal in the source organ.

The Conjugate-view method first proposed by Thomas and collaborators in the 1970s is the most commonly used method to obtain the whole-body data needed for biodistribution in vivo. In the conjugate-view counting, whole body anterior and posterior emission scans of the subject are taken simultaneously with gamma camera in 180 degree opposite direction.

The quantitative uncertainty at each measurement point is 10% or more, by using SPECT. The patient's general condition as well as the access to the imaging facilities renders further limitations. Consequently, the data collection has to be limited to a few time points, which add to the uncertainty concerning the kinetics and the calculation of the total number of decays. This error is likely to be dominating and may be as high as 20% or more.

2.2.2 Medical Internal Radiation Dose (MIRD)

It is crucial to determine the radiation dose received in patient from radionuclide labelled drugs used in nuclear medicine to ensure the safe use of that radiopharmaceuticals. The radiation dose received from radioactive materials within the body, also known as internal dose, cannot be directly measured, somewhat, the dose integrated over time is calculated based on standardized assumptions and anatomical models. Medical Internal Radiation Dose (MIRD) Committee of the Society of Nuclear Medicine provided its first set of instructions on nuclear medicine

dosimetry calculations in 1968. The latest publication on the formalism was published in 2009 in MIRD Pamphlet No. 21 which provides the schema for standardizing nomenclature and dosimetry quantities used in comparative evaluation of potential risks of radiation in nuclear medicine. Even several methodologies provided to calculate internal radiation dosimetry, the schema developed by MIRD committee is more versatile and gives more accurate results. Therefore it has been widely adopted as the standard method for performing internal radiation dosimetry.

The MIRD formalism takes into account the physical factors associated with characteristics of radionuclide used and biological factors associated with retention and clearance rate of the investigated subjects. It provides a calculation of the mean absorbed dose (i.e., the integral of the absorbed dose over a defined dose-integration period) to a target region due to a time-dependent varying amount of activity in a source organ. The absorbed dose contributions to the target region from various target organs are summed and the result provides the total absorbed dose to the target region.

2.2.2.1 Basic concepts of MIRD [14]

The MIRD formalism gives a framework for the calculation of the absorbed dose to a target region, recipient of radiation energy irradiated from a source region in which activity localizes time-independently.

The general approach for calculating the absorbed dose to a target organ from radioactivity in a source organ is as follows:

Firstly, the amount of activity and time spent by the radioactivity in the source organ is determined and time-integrated activity needs to calculate by the integral of the area under the time activity curve. The activity as a function of time A (t) can often be described by the sum of exponential functions as the following equation:

$$A(r_S, t) = \sum_j A_j \cdot e^{-t(\lambda_P + \lambda_b)} \tag{2.3}$$

Where, $A(r_s,t)$ is the activity in the source region at time, t. j represents the number of exponentials, A_j the initial activity for the jth exponential, λ_p is the physical decay constant for the radionuclide, λ_b is the biological decay constant and t is the time after the administration of the radiopharmaceutical.

Time-integrated activity in source region ($\tilde{A}$ (r_s, T_D))

The amount of cumulated activity present in the source organ over dose-integration period represents the time-integrated activity or total number of nuclear transformation in the source region. The time-integrated activity can be obtained by the integral of the area under the time-activity curve (Fig 2.5). It can be mathematically expressed as:

$$\tilde{A}(r_s, T_D) = \int_0^{T_D} A(r_s, t) \, dt \tag{2.4}$$

Where, $\tilde{A}(r_s,T_D)$ is time-integrated activity in the source region (Bq-sec), T_D is dose-integration period, $A(r_s,t)$ is the activity, Bq, in the source region at time, t .
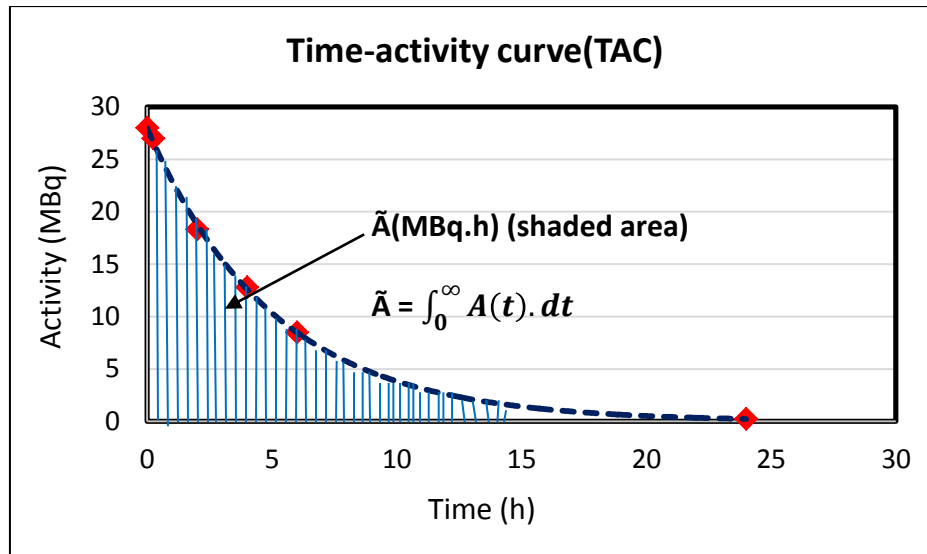
Figure 2.5 Time-activity curve for radioactivity in a source organ

The time-integrated activity depends on the amount of activity administered to patients (A_0) and life-time of the radiotracer within the body or organ of interest. Therefore, characteristics of both physical and biological factors had influenced time-integrated activity and the radiation dose delivered by activity in a source organ is proportional to its time-integrated activity.

S-factor

The mean absorbed dose to the target organ per unit of time-integrated activity in a specified source organ is denoted as S-factor in unit of Gy/Bq.s. It is determined by the number of factors including type and amount of ionizing radiation emitted per disintegration, absorbed fraction and mass of the target organ. Each S-factor is specific to particular source-target organ pair and it has been tabulated with variety of anatomic reference models based on Monte Carlo simulation for a wide variety of radionuclides commonly used in diagnostic and therapeutic nuclear medicine [15, 16].
S-factor is given as follows:

$$S(r_T \leftarrow r_S) = \frac{1}{M(r_T)} \sum_i \Delta_i \emptyset (r_T \leftarrow r_S, E_i) \qquad (2.5)$$

Where, Δ_i is equilibrium absorbed dose constant, i.e. mean energy of the ith transition per nuclear transformation. $\emptyset (r_T \leftarrow r_S, E_i)$ is the absorbed fraction and $M(r_T)$ is the time-dependent mass of target tissue r_T in the reference individual. Energy emitted per unit of cumulated activity is the equilibrium absorbed dose constant Δ_i in unit of (Gy.kg/Bq.s). This factor needs to calculate for each type of emission of radionuclide as follows:

$$\Delta_i = 1.6 \times 10^{-13}. N_i E_i \qquad (2.6)$$

Where, E_i is the average energy (in MeV) of the ith emission and N_i is the relative frequency of that emission (number emitted per disintegration) by the radionuclide. Equilibrium absorbed dose constant depends primarily on the energy of the radionuclide emissions and their frequency of emission (number per disintegration).

Absorbed fraction, ø

The fraction of radiation energy E_i emitted within the source organ, r_s that is absorbed by the target organ, r_T is defined as absorbed fraction and represented by symbol ø. The formalism of absorbed can be simply denoted as:
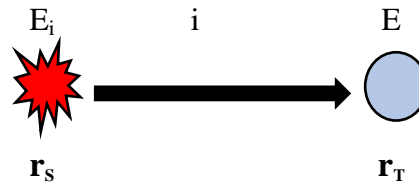
$$\text{Ø}(r_T \leftarrow r_s) = \frac{E\text{ (energy absorbed by target)}}{E_i\text{(energy emitted by source)}} \qquad (2.7)$$

So, the fraction absorption depends on:
- The distance between the source and target organs
- The composition of the tissue between the source and target organs
- The penetrating ability of the radiation.

Monte Carlo is used to model the probabilistic interaction laws. ø is calculated by summing up initial energy in the source organ and comparing to the total energy absorbed by the target organ. The absorption properties may be differed depending on the penetrating ability of the radiation. For penetrating radiation like X-ray and γ-ray, some of the emitted energy will escape objects of the size and composition of interest to internal dosimetry, mostly soft tissue organs with diameter of the order of centimeters. For electron and beta particles referred as non-penetrating radiation, most energy is considered to be absorbed. So, absorbed fraction is equal to one. Absorbed fraction property for various type of radiation was illustrated in figure (2.6).

Values of ø have been calculated based on mathematical reference man models incorporating organs and anatomic structures of average size and shape Fig (2.7).
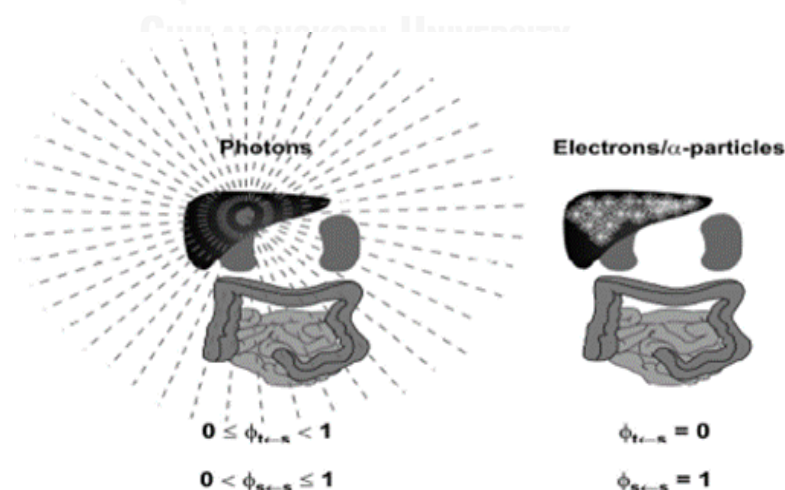
Figure 2.6 Different absorption properties of penetrating and non-penetrating radiation

Absorbed fraction, ø is normalized by the mass of target tissue M (r_T), denoted as specific absorbed fraction, Φ, measured in unit of g^{-1}.

$$\Phi(r_T \leftarrow r_s, E_i) = \frac{\text{ø }(r_T \leftarrow r_s, E_i, t)}{M(r_T)} \qquad (2.8)$$

Mean absorbed dose to the target organs

The total mean absorbed dose to the target region D (r_T, T_D) is given by summing the separate contributions from each source region r_S as follows:

$$D(r_T, T_D) = \sum_{r_s} \tilde{A}(r_s) . S(r_T, r_s) \qquad (2.9)$$

The self-absorbed dose commonly gives the largest fractional contribution to the total absorbed dose in a target region. The self-absorbed dose refers to the case in which the source and target regions are identical, whereas the cross-absorbed dose refers to the case in which the source and the target regions are different from each other.
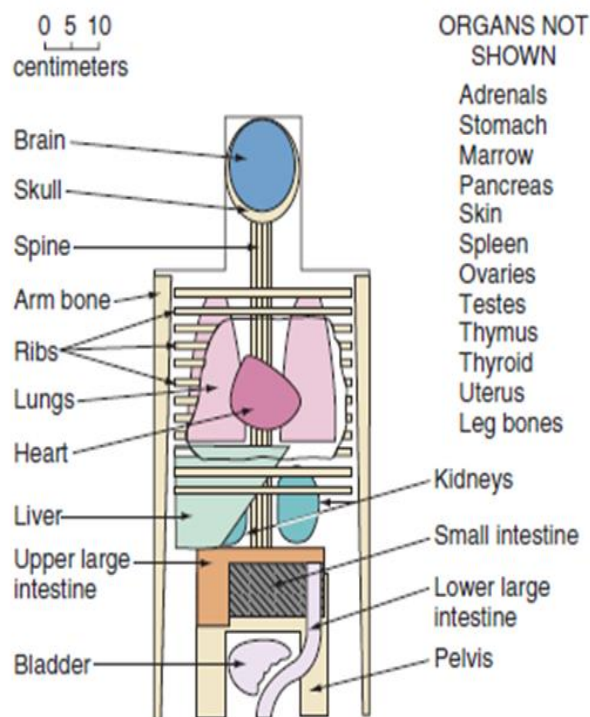
Figure 2.7 Representation of anatomical reference man used for calculation of absorbed fraction [17]

2.2.2.2 Limitation of MIRD method

Values of absorbed fraction are based on models of human anatomy that assume specific relationships in the shape, size, and location of various organs, not individual subject. The MIRD formalism also implicitly assumes that activity is distributed uniformly within each organ and, moreover, that energy is uniformly deposited throughout the organ. The assumption can cause a significant error in the calculated

dose from non-penetrating radiation when the activity is taken up in specific regions or cell types within an organ.

In regardless of these limitations, the MIRD method is a useful tool for comparing the average dose to various organs in patients for a wide variety of nuclear medicine procedures.

2.2.3 Basic dosimetric quantities

2.2.3.1 Absorbed dose and equivalent dose

In radiation biology and radiological protection, the absorbed dose is the basic physical dose quantity and is used for all types of ionizing radiation and any irradiation geometry. The mean energy imparted by ionizing radiation per unit mass of the substance is called absorbed dose, designated by symbol D.
Absorbed dose is defined as

$$D = \frac{d\varepsilon}{dm} \tag{2.10}$$

Where, $d\varepsilon$ is the mean energy imparted by ionization radiation to matter of mass dm. The SI unit of absorbed dose is $J\ kg^{-1}$ and its special name is gray (Gy).

Depending on the type and energy of radiation causing the dose, absorbed dose can result in different biological effects. Equivalent dose is based on the physical quantity of absorbed dose but takes into account the biological effectiveness of the radiation, which is dependent on the type and energy of the radiation R. The equivalent dose (H_T) is calculated as:

$$H_T = \sum W_R . D_{T,R} \tag{2.11}$$

Where, $D_{T,\ R}$ is the mean absorbed dose from radiation R deposited in body tissue or organ T, W_R is the radiation weighting factor which is dependent on the type and energy of the radiation. The unit is the Joule per kilogram (Jkg^{-1}) and is given the special name Sievert (Sv). Current values recommended by International Commission on Radiation Protection (ICRP 1979), are given. (Table 2.2)

Table 2.2 Radiation weighting factors recommended by ICRP 30

Particle or photon	Radiation weighting factor (W_R)
Alpha particles	20
Protons > 2MeV	2
Beta particles (+/-)	1
x-rays, Gamma rays	1

2.2.3.2 Effective Dose

When the body is irradiated after nuclear medicine examination, individual organ and tissue are likely to receive different equivalent dose. Effective dose is a quantity defined by International Commission on Radiological Protection (ICRP) publications 60 and 103 as a weighted sum of equivalent doses to all relevant tissues and organs. Its calculation is based on the application of tissue-weighting factors (W_T) on the equivalent doses (H_T) absorbed by the various radiosensitive organs of the human body. The effective dose (E) is calculated as:

$$E = \sum_T W_T . H_T \tag{2.12}$$

The unit is the Joule per kilogram (J kg^{-1}) and is given the special name Sievert (Sv). The ICRP 103 recommendations update tissue weighting factors for the calculation of effective dose from a reference population of equal number of both sexes and wide range of age. (Table 3.3).

2.2.4 Health Effect of ionizing radiation

All nuclear medicine investigations cause exposure to ionizing radiation of the whole body. In general, radiation doses to the investigated subjects in diagnostic nuclear medicine examinations are low. However, the risk of health effects due to radiation from diagnostic nuclear medicine should not be negligible, since it may cause the stochastic effect. Therefore radiation protection is always essential. The risk associated with ionizing radiation is dependent on the age of the patient from exposure. Children are more sensitive to radiation and they are expected to have a longer life-time during which cancers can develop [18].

2.2.4.1 Stochastic Effects

These effects result from an alteration in the genome of a cell, which, in the case of cancer gives rise to a clone of uncontrolled, rapidly dividing cells. Various mechanisms might be involved in the mutation of the DNA. These may include the activation of an oncogeny (a cancer-causing gene), the inactivation of a tumor-suppressor gene or the loss of function of a repair-mutator gene. These can give rise to carcinogenesis and hereditary effects. In this effect, the severity of radiation damage is not related to the dose and the probability of occurrence increases with increasing radiation dose, e.g., development of cancer. There is no threshold for stochastic effects.

2.2.5 Dosimetry Toolkit [19]

Dosimetry toolkit uses multi WB SPECT/CT and/or WB planar datasets for quantifying changes in radiopharmaceutical uptake over time and calculating residence time per organ. The purpose of dosimetry toolkit is to replace tedious manual tools for organs definition and activity calculations, in order to enable improved processing workflow and productivity. The accuracy of the dosimetry toolkit results depends heavily on the user provided quantitative input: consecutive patient scans, injected activity, organ definition, system sensitivity and reconstruction parameters.

Time activity curve is created for each of the organs defined. These curves are fitted to an exponential function of the form:

$$y = A\,e^{-BX} \tag{2.13}$$

Usually exponential fit is done by taking the logarithm of the function and looking for the parameters that give the least square fit. This fit gives greater weights to small y values so, in order to weight the points equally, it is often better to minimize the function:

$$N = \Sigma\ y_i\ (\ln y_i - a - bx_i)^2 \tag{2.14}$$

i= 1

The equal weight exponential fit is used in Dosimetry Toolkit.

2.3 Review of related literatures

Tootell A K et al [20], investigated the radiation dose of myocardial perfusion SPECT/CT performed with ^{99m}Tc-sestamibi and ^{99m}Tc-tetrofosmin from four different scanners based on phantom for external dose and human studies for internal dose. They reviewed the patient data undergoing myocardial perfusion SPECT/CT and estimated the patient dose by using the dose coefficients for ^{99m}Tc-sestamibi and ^{99m}Tc-tetrofosmin from ICRP publications 80 and 106 for internal dose and from thermoluminescent dosimeter measurements performed on CIRS ATOM dosimetry verification phantom for CT dose. The total injected activity of 1600 MBq of ^{99m}Tc-tetrofosmin or ^{99m}Tc-sestamibi for two-day (stress and rest) procedure was used. The radiation exposure of patients from myocardial perfusion SPECT/CT on four different scanners was summarized in Table (2.4).

Table 2.3 Protocols used for attenuation correction for myocardial perfusion imaging SPECT/CT

Scanner	Scout view	kVp	mA	Rotation time	Slice thickness	Pitch	AEC/dose modulation
GE Infinia Hawkeye (one slice)	No	140	2.5	30 s per rotation (214° exposure)	10 mm	NA	NA
GE Infinia Hawkeye (4 slice)	No	140	2.5	30 s per rotation (214° exposure)	5 mm	1.9 mm per rotation	NA
Siemens Symbia T6	Yes	130	20	0.6 s	3 mm	0.938	AEC & dose modulation
Philips Precedence 16	Yes	120	30	1.5 s	5 mm	0.938	NA

kVp, tube voltage   mA, tube current
AEC, automatic exposure control   NA, not applicable

Table 2.4 Summary of radiation exposure from myocardial perfusion SPECT/CT on four different scanners

Organ	^{99m}Tc-tetrofosmin	^{99m}Tc-MIBI	GE Infinia Hawkeye (single slice)	GE Infinia Hawkeye (four slice)	Siemens Symbia T6	Philips Precedence
Lung (mGy)	5.1	7.1	3.6	5.4	3.1	5.5
Esophagus (mGy)	5.3	6.5	2.5	3.8	2.4	5.6
Colon (mGy)	28.8	34.0	0.2	0.2	0.6	0.5
Liver (mGy)	5.3	16.0	2.6	4.7	2.7	4.9
Stomach (mGy)	7.4	10.0	1.1	2.4	1.7	3.1
Breast (mGy)	3.7	5.7	7.1	6.6	4.1	8.2
E (mSv)	11	13.3	1.9	2.5	1.8	3.0

E, effective dose

Leide S et al [21], estimated the biodistribution and radiation dosimetry from myocardial perfusion studies. Biodistribution of MIBI was studied by scanning the patients at 15 min, 6 h and 24 h after injection of MIBI with single-head gamma camera (Toshiba GCA 901A) and uptake was corrected for physical decay of technetium-99m. For patients at rest, 900 MBq of Tc-99m MIBI was intravenously injected and for stress test, the patients were done bicycle ergometer according to Scandinavian standard following the injection of Tc-99m MIBI. The cumulated activity and absorbed doses to the different organs were calculated according to ICRP publication 53 with absorbed fraction based on organ masses of ICRP reference man. There were significant differences in uptake of MIBI between stress and rest for thyroid, gall bladder intestine and muscle. The upper large intestine (ULI) received the highest absorbed dose from both rest and stress study, absorbed dose coefficient of 76 μGy/MBq in rest and 59 μGy/MBq in stress study. Another organ received the high absorbed dose was gall bladder with absorbed dose coefficient of 28 μGy/MBq in rest study and 30 μGy/MBq in stress study. The effective dose from the examination with Tc-99m MIBI (both rest and stress) study was 13mSv in this study.

Montes C et al [22], reported estimation of total effective dose from low-dose CT scans and radiopharmaceutical administrations delivered to patients undergoing SPECT/CT explorations. These studies were performed on a dual-headed SPECT gamma camera with an integrated 2-slice CT scanner (Symbia T2 Emotion Duo, Siemens, Erlangen, Germany). In this study, they determined the radiation exposure of patients from routine SPECT/CT examinations and expressed the effective dose in relation with the Background Equivalent Radiation Time (BERT). The contribution of total effective dose imparted by the radiotracer was calculated by using the effective dose coefficients from ICRP publications 53, 80 and 106. The CT contribution was estimated by multiplying the Dose-Length Product (DLP) and specific conversion factors. The patient effective dose associated with a SPECT/CT procedure was calculated as the sum of the effective dose from the radiopharmaceutical administered and the effective doses from the CT scan and compared with background radiation. The radiation doses from routine SPECT/CT explorations were summarized in Table (2.5).

Table 2.5 Effective doses and related BERT from routine SPECT/CT examinations

SPECT/CT procedure	Radiopharmaceutical	Activity administered (MBq)	Effective dose (mSv)		BERT (years)	
			$E_{(SPECT)}$	$E_{(CT)}$	SPECT	CT
[67]Ga-citrate in lymphoma	^{67}Ga-citrate	260	26.5	-	11	-
[67]Ga-citrate for infection and inflammation	^{67}Ga-citrate	185	18.9	-	7.9	-
Parathyroid scan	^{99m}Tc-MIBI	740	6.4	1.2	2.7	0.5
Cardiac (stress/rest) one-day protocol	^{99m}Tc-Tetrofosmin	330+1000	8.5	2.4	3.5	1
[111]In-octreotide	^{111}In-DTPA	185	8.5	-	3.5	-

CHAPTER 3

RESEARCH METHDOLOGY

3.1 Research Design

This study was designed as a prospective descriptive study. The steps of the procedure are shown as the following figure 3.1.

3.2 Research design model
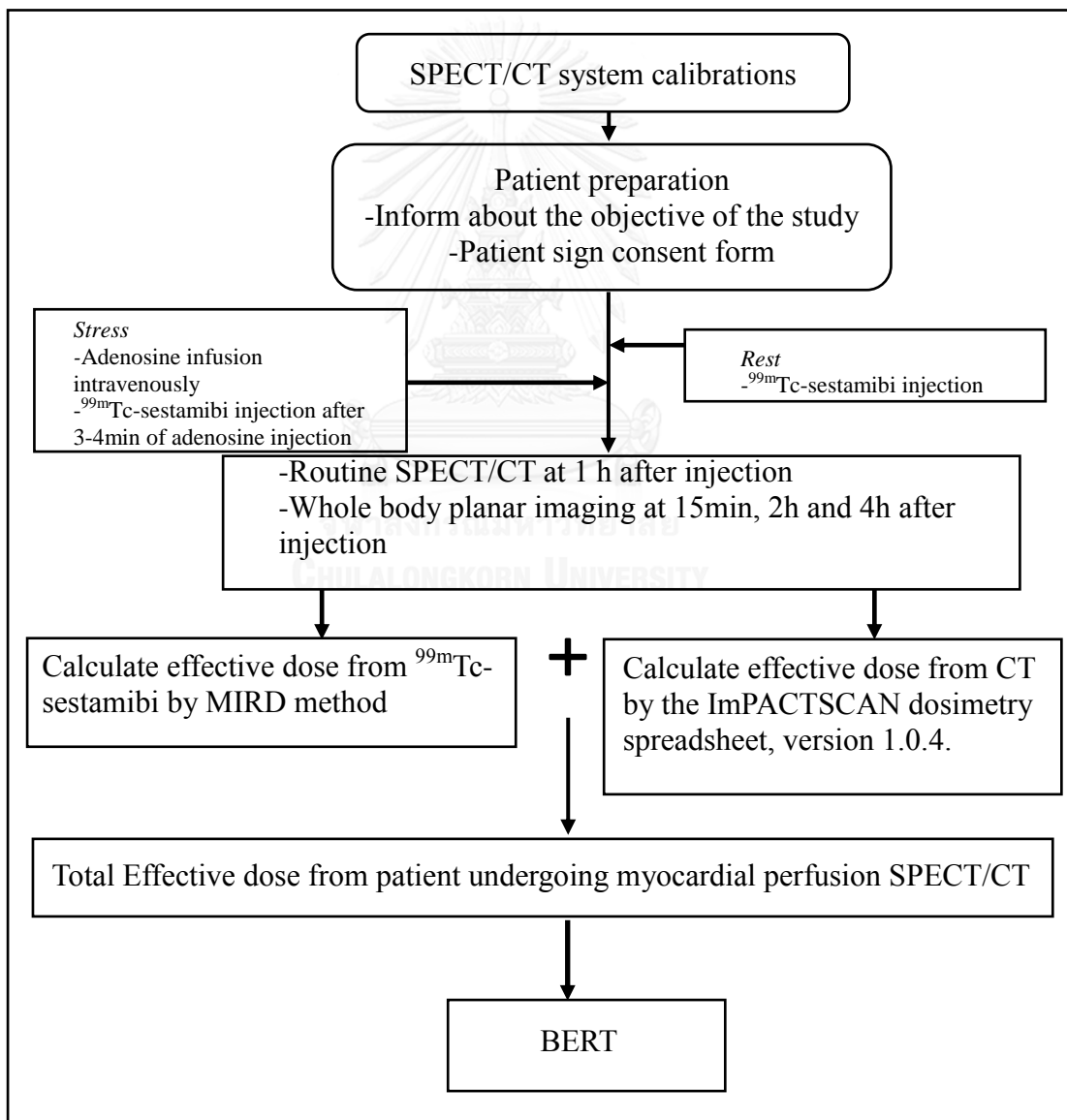
Figure 3.1 Research design model

3.3 Conceptual framework

The effective dose in patient undergoing myocardial perfusion SPECT/CT is the combination of the effective dose from radiopharmaceutical injected for SPECT imaging and effective dose from CT. The biological factors of individual, physical factors of radionuclide and injected activity of ^{99m}Tc-sestamibi influence the dose from radiopharmaceutical. The dose from CT is affected by kVp, effective mAs, collimation, added filtration, scan length, pitch, slice thickness, and patient size. The conceptual framework of this study is shown in figure 3.2.
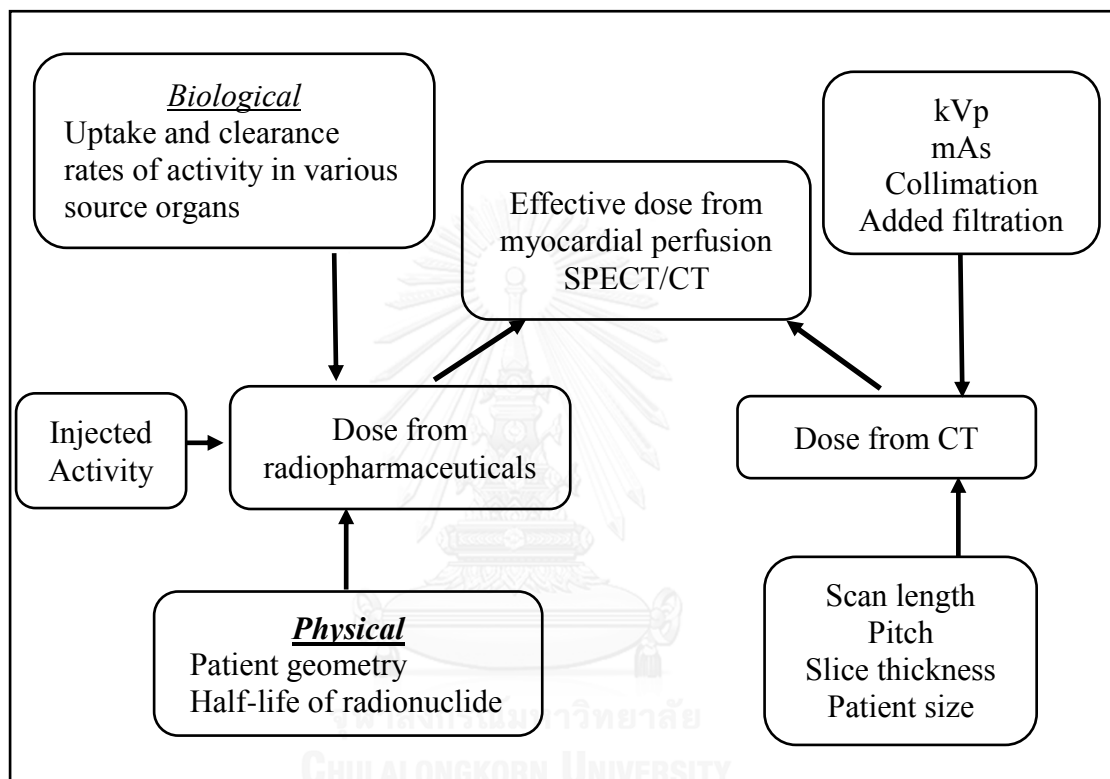
Figure 3.2 Conceptual framework

3.4 Research questions

3.4.1 Primary research question

What is the effective dose received in patients undergoing myocardial perfusion SPECT/CT?

3.4.2 Secondary research question

How many BERTs related with myocardial perfusion SPECT/CT imaging?

3.5 Key words

SPECT/CT
Myocardial perfusion
^{99m}Tc-sestamibi
MIRD

3.6 The sample

3.6.1 Target population

All patients who were requested for myocardial perfusion SPECT/CT examination at King Chulalongkorn Memorial Hospital.

3.6.2 Sample population

The patients who underwent myocardial perfusion SPECT/CT examination at King Chulalongkorn Memorial Hospital from August, 2016 to March, 2017 and met the eligible criteria.

3.6.3 Eligible criteria

3.6.3.1 Inclusion criteria

Patients who underwent myocardial perfusion SPECT/CT of the age from 18 to 70 years old.

3.6.3.2 Exclusion criteria

Unconscious patients

Pregnant women

3.6.4 Sample size determination

The sample population is continuous, prospective data and is determined by formula:

$$N = \frac{z_\alpha{}^2 \sigma^2}{d^2}$$

N = sample size
σ^2 = variance of data (7.1)
d is acceptable error (1.45)
Zα for 90% CI = 1.64

$$N = \frac{2.6896 \times 7.1}{2.1025} = 9.08$$

Therefore, the sample size (N) for 90% confidence interval is 10.

20 patients (10 patients for rest and 10 patients for stress) were performed for this study.

3.7 Materials

3.7.1 Single Photon Emission Computed Tomography/ Computed Tomography (SPECT/CT)

The SPECT/CT system model Discovery 670 manufactured by General Electric as shown in figure 3.3 was installed in 2016 at Division of Nuclear Medicine, King Chulalongkorn Memorial Hospital, Bangkok, Thailand. The system integrates a SPECT system with BrightSpeed Elite sixteen-slice CT scanner using Xeleris[3] processing & review workstation. Dual SPECT detector of NaI (Tl) crystal is 59.1x44.5 cm. The useful field of view is 54x40 cm and the total number of photomultiplier tubes is 59. Energy range of the detector is 40-620 keV. The maximum scan field for CT is 50 cm and gantry - bore diameter is 70 cm. Four tube voltage settings are available at 80, 100, 120 and 140 kVp. The tube current ranges from 10 to 440 mA.

Figure 3.3 SPECT/CT system

3.7.2 Technetium-99m-sestamibi (99mTc-MIBI)

99mTc-MIBI (methoxy isobutyl isonitrile) is a radiopharmaceutical used for myocardial perfusion imaging.Technetium-99m is a metastable nuclear isomer of technetium-99, symbolized as 99mTc. The "m" indicates a metastable nuclear isomer. Technetium-99m is used as a radioactive tracer detected in the body. It is well suited to the role of diagnosis because it emits readily detectable 140 keV gamma rays and its half-life for gamma emission is 6.01 hours. The structure of 99mTc-MIBI is shown in figure 2.4.

3.7.3 Monte Carlo simulation program

ImPACT (Imaging Performance Assessment of CT scanners) (ImPACTSCAN, Knightsbridge Wing, St George's Hospital, London) CT Patient Dosimetry Calculator version 1.0.4, as shown in figure 3.4, is a spread sheet for calculating patient organ and effective doses from CT examinations. It makes use of the NRPB Monte Carlo dose data sets produced in report SR250. SR250 provides normalized organ dose data for irradiation of a mathematical phantom by a range of CT scanners. The exposure factors were entered into the ImPACTSCAN spread sheet, along with CTDI in air which the measurements performed with pencil ionization chamber. The spread sheet uses these data and normalized organ dose data by matching with the manufacturer CT machine. These are combined according to the tissue weighting factors given in ICRP publications 103, to calculate an effective dose. In addition, the weighted CTDI ($CTID_w$), volume CTDI ($CTDI_{vol}$) and dose length product (DLP) are also displayed.

Figure 3.4 ImPACT CT Dosimetry Calculator

3.7.4 The pencil ionization chamber

A 100 mm length pencil ionization chamber: RaySafe Xi CT detector is shown in figure 3.5. The RaySafe Xi CT detector is a hybrid ion chamber with 10 cm active length designed by Unfors RaySafe. The center and the edges (+ 5 cm and - 5 cm) of the active volume are marked on the phantom adapter. An automatic correction of temperature and pressure will be applied for all dose measurements. The temperature sensor is positioned inside the active ionization chamber and the measurement is corrected for the true temperature inside the phantom. The pressure sensor is placed inside the RaySafe Xi CT detector housing and is calibrated to show the actual pressure at the measurement facility's altitude. The measured temperature and pressure for each exposure can be displayed when using the RaySafe Xi view. All measurements are performed with the RaySafe Xi CT detector communication with the RaySafe base unit.

Figure 3.5 The pencil ionization chamber

3.7.5 The RaySafe Xi Base Unit

Measurements of radiation parameters can be obtained with the detector placed in the radiation field connected with RaySafe Xi base unit is illustrated in figure 3.6. The three row alphanumerical display clearly presents all measured parameters. All functions are accessed by pressing one of the RaySafe two buttons. The RaySafe Xi supports both RS-232 and the optional Bluetooth data communications protocols.

Figure 3.6 RaySafe Xi base unit

3.7.6 CTDI Polymethyl Methacrylate Acrylic (PMMA) Phantoms

The CTDI phantoms are made from polymethyl methacrylate (PMMA) for 16 cm diameter head phantom and 32 cm diameter body phantom. The phantom is constructed with a center hole and eight peripheral holes (four in the head phantom and four in the body phantom) for CT ionization chamber placement. It also includes PMMA inserts for peripheral holes.
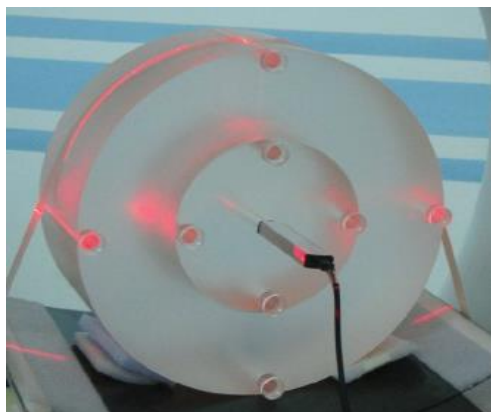
Figure 3.7 CTDI head and body phantoms

3.7.7 Catphan ® 700

Catphan ® 700 phantom was used for the performance study of the CT scanner as shown in Figure 3.8.
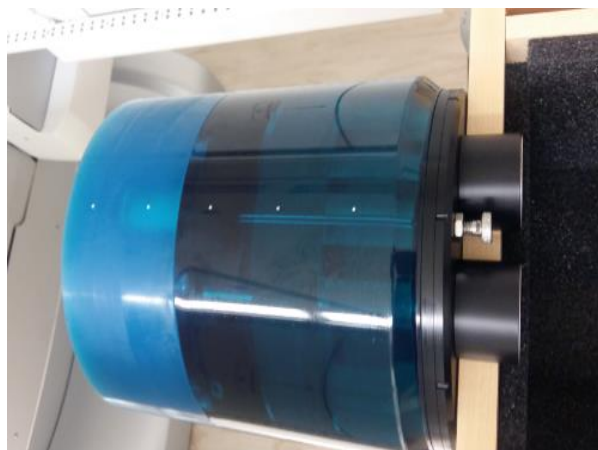
Figure 3.8 .Catphan ®700

3.8 Methods

This study was carried out as the following:

3.8.1 SPECT/CT Quality Control [APPENDIX E]

For SPECT system, background count rate, energy peak, extrinsic energy resolution and extrinsic uniformity were evaluated as daily QC tests. The weekly QC is center of rotation (COR) test which must be accurately aligned with the center of the acquisition matrix in the computer. The X-ray CT tube warm-up and fast calibration were performed daily.

3.8.2 Subjects

Twenty subjects (ten subjects at rest and ten subjects under stress) who underwent myocardial perfusion SPECT/CT at King Chulalongkorn Memorial hospital were performed for this study. Some of them were patients for diagnostic investigation and became the volunteers for this research and some of them were volunteer throughout the study. The subjects were clearly informed about the objective of the study. The written consent form was obtained from the patient before examination [APPENDIX D]. This study had been approved by the Institutional Review Board (IRB) of Faculty of Medicine, Chulalongkorn University [APPENDIX B].

The information of the subject such as age, gender, height, weight, injected activity, injection time and scanning times were recorded in the case record form [APPENDIX C]. The subject information is summarized in Table 3.1.

The examination consists of two parts: examination at rest and examination under stress. The subjects were fasting during four to six hours before the examination. In examination under stress, calcium-channel blockers and β-blockers were discontinued for a sufficient length of time prior to the examination to avoid any

interference with obtaining an adequate stress examination by limiting heart rate response. Xanthine-containing medications, including theophylline (aminophylline), were withheld for 48 hours, if tolerated by the patient, and caffeine-containing beverages were avoided for 12 hours before the study.

For ten subjects at rest, mean activity 933.7±60 MBq (ranged from 821 to 993 MBq) was injected intravenously. For the other ten subjects, stress condition was achieved by the infusion of adenosine followed by an intravenous injection of 886.3±108.6 MBq (ranged from 577 to 993 MBq) of ^{99m}Tc-MIBI after four minutes. The subjects were encouraged to have fat meal at 30min after injection to activate gall bladder contraction that decreases the uptake of MIBI in the gall bladder and the liver. To avoid the biological decay between the injection time and first scanning time, it was sure that the subjects did not void between that periods.

Table 3.1 Summary of subject parameters

No. subjects	Gender	Age (years)	Body weight (kg)	Injected activity (MBq)	Last scanning time
10 subjects at rest	4 male 6 female	60.0± 13.0 (26.0-70.0)	60.0±8.5 (49.0-70.0)	933.7±60.0 (821.0-993.0)	4 h (8 subjects) 24 h(2 subjects)
10subjects under stress	5 male 5 female	58.0±8.0 (47.0-70.0)	59.0±5.5 (50.0-70.0)	886.3±108.6 (577.0-993.0)	4 h

All data are expressed with mean ± SD (range).

3.8.3 Whole-body scanning and SPECT/CT procedures

Imaging was performed by SPECT/CT system (GE Discovery NM/CT 670) which utilizes Bright Speed Elite 16 slices. Whole-body emission scans were acquired with square field-of-view (54x40 cm) dual-head SPECT detectors equipped with low energy high resolution parallel-hole collimators. Whole-body planar imaging was obtained at 15 min, 2 h, 4 h and 24 h with scanning speed of 14 cm/min in craniocaudal direction after administration of ^{99m}Tc-MIBI to investigate the time-activity curves (TAC) in various source organs. A 20% energy window around the photopeak of ^{99m}Tc was used.

Routine myocardial perfusion SPECT/CT was performed at 1 h after injection for diagnostic purpose. For CT scan, the parameters such as tube voltage (kVp), tube current (mA), rotation time (s), slice width and pitch factor were fixed for all patients except the scan length (ranged from 16.0 to 20.5 cm). The parameters for CT scanning are summarized in Table 3.2.

Table 3.2 CT technique summary

Scanner	Scout view	Axial/ Helical	kVp	mA	Rotation	Slice thickness	Pitch
SPECT/CT (GE Discovery670)	No	Helical	120	20	0.8 s	5 mm	0.938

3.8.4 Data analysis

3.8.4.1 Calculation the absolute activity in each source region

The regions of interest (ROI) were manually drawn within the boundary of the organ in order to determine the time-integrated activity. For each time interval of the scan, absolute organ activity (MBq) was determined by geometrical mean calculation as the following equation:

$$A = \frac{1}{F} \cdot \sqrt{N_A . N_P}$$ [3.1]

Where N_A and N_P are the number of counts in ROI of anterior and posterior images. F is ratio between whole body count and the decay corrected injected activity in terms of counts per unit activity. It is used as the conversion factor from counts to activity.

The first whole-body images at 15 min with no patient excretion were used to determine the count-to-activity conversion factor. Division of geometrical mean of the counts in anterior and posterior images by decay-corrected injected activity (counts per unit activity) represented the factor for conversion from count to absolute activity.

Detector background was subtracted and injected activity was corrected for physical decay of Technetium-99m. Background ROI was drawn over some region of the body that is close to the ROI of the source organ.

For overlapping structures such as liver and right kidneys, corrections were performed by using the mean count concentration (mean count/pixel) in the overlapped liver region multiplied by projected area of the liver. The image of the right kidney was treated in the same way.

3.8.4.2 Curve fitting and determination of time-integrated activity

Time activity curves (TAC) were obtained for eleven source organs (gall bladder, heart, intestine, kidneys, liver, lungs, muscle, salivary glands, spleen, thyroid and urinary bladder) with absolute organ activity in each source organ as function of time. The half-time of the radionuclide in each source organ and time-integrated activity (total number of nuclear transformations) were obtained from the curve, as shown in figure 3.7. The area under the time activity curve represents the time-integrated activity in the source organ.

The time activity curve for each subject was fitted with nonlinear least squares fitting by using curve fitting toolbox 3.5.1 of MATHLAB program, version 8.5.0. The activity as a function of time in each source organ $A(r_S,t)$ can often be described by the sum of exponential functions as:

$$A(r_S, t) = \sum_j A_{j_{(0)}} \cdot e^{-(\lambda_P + \lambda_P)t}$$ [3.2]

Where, j represents the number of exponentials, $A_{j(0)}$ denotes the initial activity for the jth exponential, λ_p is the physical decay constant for the radionuclide, λ_b is the biological decay constant and t is the time after the administration of the radiopharmaceutical.

The time-integrated activity ($\tilde{A}_{(rS, \ TD)}$) in each source organ for the dose integration period (T_D) was calculated as the time integral of an exponential function as the following:

$$\tilde{A}\,(r_S, T_D) = \int\limits_0^\infty A(t).\,dt$$

$$= \sum_j A_{j_{(0)}}.\,e^{-(\lambda_P+\lambda_P)t}.\,dt \qquad [3.3]$$

Where, $\tilde{A}\,(r_S, T_D)$ is the time-integrated activity in the source region in the unit of MBq.s.
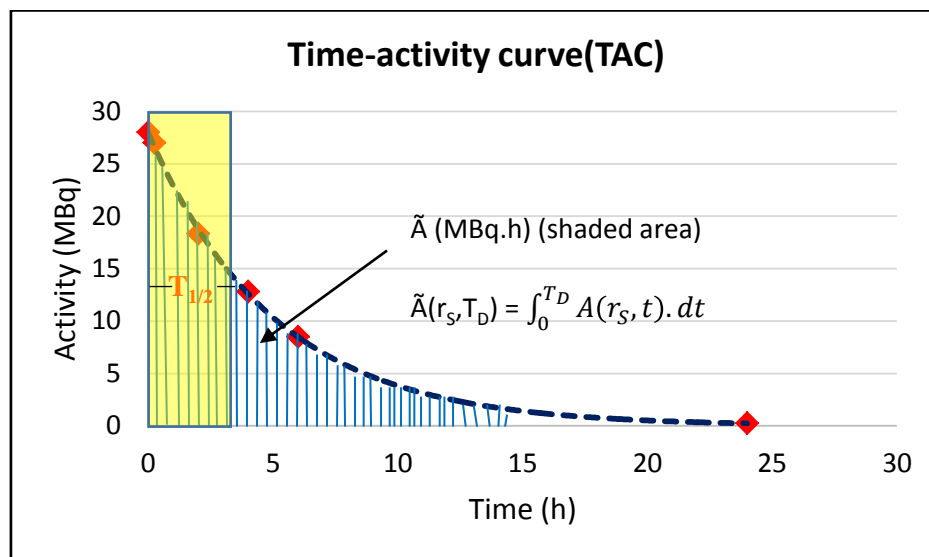
*$T_{1/2}$ = effective half time of radionuclide (biological + physical half-life)

Figure 3.9 Illustration of $\tilde{A}\,(r_S, T_D)$ and average lifetime (1.44 T_p) of a radionuclide from time-integrated activity curve

3.8.4.3 Biokinetics of ^{99m}Tc-MIBI

The quantitative biodistribution was determined by expressing specific organ uptake by the decay-corrected injected activity. The residence time or time-integrated activity coefficient is defined as the cumulative number of nuclear transformations (MBq.h) occurring in source tissue r_S over a dose-integration period T_D per unit administered activity A_0 (MBq), determined by the equation:

$$\tilde{a}\,(r_S, T_D) = \frac{1}{A_0}\int_0^{T_D} A(r_S, t).\,dt \qquad [3.4]$$

Where, $\tilde{a}\,(r_S, T_D)$ is the time-integrated activity coefficient (s). $A(r_s,t)$ is the activity in each source organ as function of time (MBq). T_D is the dose-integration period (s). A_0 is the administered activity (MBq).

The residence time or time-integrated activity coefficient is related to the characteristics of both physical decay and biological removal in the source organ.

Effective half-time of ^{99m}Tc-MIBI in each source organ

The effective half-life ($T_{1/2}$) of a radionuclide is the time required for it to decay to 50% of its initial activity level by both physical and biological decay, as the following equation:

$$\frac{1}{T_e} = \frac{1}{T_p} + \frac{1}{T_b}$$ [3.5]

Where, T_e is the effective half-time, T_p is the physical half-time and T_b is the biological half-time.

The half-life and decay constant (λ) of a radionuclide are related as:

$$T_{1/2} = \frac{\ln 2}{\lambda}$$ [3.6]

3.8.4.4 Internal dose assessment

The internal radiation dose from ^{99m}Tc-MIBI was estimated by using the techniques, equations and factors according Medical Internal Radiation Dose (MIRD) Committee of the Society of Nuclear Medicine. As MIRD method, the mean absorbed dose D (r_T,T_D) to target tissue r_T over a defined dose-integration period T_D after administration of radioactive material to the subject is given:

$$D(r_T, T_D) = \sum_{r_s} \tilde{A}(r_S, T_D) \cdot S(r_T \leftarrow r_s)$$ [3.7]

Where, $D(r_T,T_D)$ is the mean absorbed dose to the target organ (mGy)

$\tilde{A}(r_S,T_D)$ is the time-integrated activity (MBq.s) in the source region r_S over dose-integration period T_D.

$S(r_T \leftarrow r_S)$ is the radionuclide-specific quantity representing the mean absorbed dose rate to target tissue r_T at time t after administration per unit activity present in source tissue r_S (mGy/MBq.s).

The value of S may be based on reconstructed whole-body computational phantoms representing reference individual of a given age, sex, total-body mass, and standing height. S is given as:

$$S(r_T \leftarrow r_S) = \frac{1}{M(r_T)} \sum_i E_i Y_i \phi(r_T \leftarrow r_S, E_i)$$ [3.8]

Where, E_i is the mean energy of the ith nuclear transition

Y_i is number of ith nuclear transitions per nuclear transformation

$\phi(r_T \leftarrow r_S, E_i)$ is the absorbed fraction (defined as the fraction of radiation energy

E_i is the emitted energy within the source tissue r_S at time t that is absorbed in the target tissue r_T)

$M(r_T)$ is the mass of the target tissue r_T in the reference individual.

The S-values for various radionuclides are provided in tabular form. Due to differences in physique between ICRP reference man and Asian population, S values were generated with the organ masses of Asian reference man in the present study [APPENDIX H].

S-values based on Asian reference man for 253 source-target organ pairs were scaled by the masses of target organs as the following equation:

$$S_{(ARM)} = S_{(Cristy\ and\ Eckerman)} \cdot \frac{M_{r_{T(cristy\ and\ Eckerman)}}}{M_{r_{T(ARM)}}} \qquad [3.9]$$

Where, $S_{(ARM)}$ is S-value based of the organ masses of Asian reference man. $S_{(Cristy\&Eckerman)}$ is S-value based of the organ masses of Cristy & Eckerman phantom [23]. M (r_T) $_{(ARM)}$ is the mass of target organ (Asian reference man) [24]. M (r_T) $_{(Cristy\&Eckerman)}$ is the mass of target organ (Cristy & Eckerman phantom)

Selection of source and target organs for internal dose calculation

The organs with significant uptake of radiopharmaceuticals were considered as source organs by the sight of investigators on the anterior and posterior whole-body planar images. The organs with those being irradiated by the source organs were selected as target organs. The following were source and target organs set up for this study.

Source organs

Gall bladder, heart, intestine, kidneys, liver, lungs, muscle, salivary glands, spleen, thyroid and urinary bladder were set up as source organs in this study.

Target organs

Adrenals, bone surface, brain, breasts, gall bladder, lower large intestine, small intestine, stomach, upper large intestine, heart, kidneys, liver, lungs, muscles, pancreas, red marrow, skin, spleen, thymus, thyroid, urinary bladder, gonads and other remaining organs were selected as target organs in this study.

Calculation of effective dose from ^{99m}Tc-MIBI

The effective dose from administration of ^{99m}Tc-MIBI was calculated as following:

$$E = \sum_T W_R \cdot W_T \cdot D_{T,R} \qquad [3.10]$$

Where, W_R is the radiation weighting factor. ($W_R = 1$ for gamma ray)

W_T is the relative radiation sensitivity of organ or tissue T or tissue weighting factor provided by ICRP-103 as shown in Table 3.3.

$D_{T,R}$ is the mean absorbed dose from radiation R in tissue or organ T.

3.8.4.5 External dose assessment

For CT scan, the absorbed dose and effective dose were calculated by using ImPACT CT patient dosimetry calculator as the following:

Input data and parameters

When ImPACT spread sheet was started, the input screen had been shown in figure 3.4. The manufacturer, type of scanner, kVp, scan region and scan range were selected. In the section of "Acquisition Parameters", tube current, rotation time, spiral pitch and CTDI values were entered into the ImPACT software to calculate the organ absorbed doses and effective doses.

The Computed Tomography Dose Index (CTDI) measurements were performed by using the pencil ionization chamber, RaySafe Xi CT detector designed by UNFORS connected with Raysafe Xi base unit for dose reading as followed:

Firstly, CTDI in air measurement was performed at the isocenter by placing the Raysafe pencil ionization chamber in air with the support stem. Then, it was connected with the RaySafe Xi Base Unit for dose reading and exposed for three times with selected protocol.

Secondly, the CTDI center and peripheries measurements were performed by using CTDI phantoms. For CTDI center, the chamber was inserted at the center of the phantom. The other peripheral holes were filled with PMMA inserts. Then, chamber was connected with the dosimeter for dose reading and exposed for three times with selected protocol. The mean dose was taken from three times reading and the normalized CTDI center was calculated.

For CTDI peripheries, the chamber was placed at the twelve, three, six and nine o'clock positions. For each position, the above measurement steps (as CTDI center) were followed. After that, normalized CTDI periphery was calculated for each position (center and peripheries).

Table 3.3 Tissue weighting factors for calculation of effective dose provided by ICRP-103 [25]

Tissue/ Organ	ICRP 103 (W_T)
Red bone-marrow	0.12
Colon	0.12
Lung	0.12
Stomach	0.12
Breast	0.12
Gonads	0.08
Bladder	0.04
Liver	0.04
Esophagus	0.04
Thyroid	0.04
Skin	0.01
Bone surface	0.01
Brain	0.01
Salivary gland	0.01
Reminder organs *	0.12

*Remainder organ of extra thoracic region, lymphatic nodes and oral mucosa, are approximated by thyroid, muscle and brain.

3.8.4.6 Calculation of effective dose from myocardial perfusion SPECT/CT and comparison with background radiation

The effective dose from myocardial perfusion SPECT/CT was calculated by the combination of effective dose from SPECT and effective dose from CT in both rest

and stress studies. The received effective dose was expressed as background equivalent radiation time (BERT).

3.9 Statistical analysis

The data were expressed as mean ± SD (min-max). The study involved the correlation of the data from independent and dependent variables. Correlation coefficient between the effective dose and patient characteristics, protocols of myocardial perfusion SPECT/CT were determined by Pearson's correlation.

- Independent variable: Patient's body weight, scan length, injected activity of ^{99m}Tc-MIBI, patient's height and age.
- Dependent variable: Effective dose

Data analysis was done by using SPSS program, version 22.

3.10 Ethical Consideration

This study was performed on patients. The research proposal was submitted and approved by Institutional Review Board (IRB) of Faculty of Medicine, Chulalongkorn University [APPENDIX B].

Belmont report

Respect for persons

Respect for free and informed consent: the patient who participates in this research can decide whether he/she participates in this study or not after obtain the information.

Respect for confidential: the patient data will be for academic objective only, conceal to the public and no patient's name reveal according to the law.

Beneficence

The patient participated in this research will be informed the effective dose from myocardial perfusion SPECT/CT procedures after completion of the research.

Justice

Selection of subjects for this research has clear inclusion and exclusion criteria, non-bias.

3.11 Expected benefits

Factors evaluated from this study are effective dose from myocardial perfusion SPECT/CT in Thai patients and biokinetics data of ^{99m}Tc MIBI. These values could be used as the reference of the Asian population for determination of radiation doses from myocardial perfusion imaging. Furthermore, the parameters influenced the radiation dose from myocardial perfusion SPECT/CT could be determined.

The effective dose was expressed in relation with background radiation so that patients could better understand the radiation risk of undergoing myocardial perfusion SPECT/CT scan.

CHAPTER 4

RESULTS

4.1 Quality Control of SPECT/CT system

The results of quality control from August, 2016 to March, 2017 are shown in APPENDIX E.

4.2 Biokinetics data and radiation dose from ^{99m}Tc-MIBI

4.2.1 Biokinetics data of ^{99m}Tc-MIBI

The anterior and posterior whole-body planar images at 15 min, 2 h, 4 h and 24 h after injection are shown in figure 4.1. The fractional distribution of ^{99m}Tc-MIBI in various organs at different time measurements for rest and stress studies is summarized in Table 4.1. ^{99m}Tc-MIBI was taken up by the myocardium and muscle tissue in proportion to the regional blood flow. Immediately after injection, the highest fractional distribution of ^{99m}Tc-MIBI was found in liver, intestine, muscles and kidneys in both rest and stress studies. The uptake and retention of the activity in these organs showed individual variation. Hepatic activity decreased more rapidly due to excretion into the biliary system. At 2 h after injection, the half of its initial activity was cleared by the liver. Activity from the gall bladder appeared in the intestines within two hours of injection. The major pathway for clearance of ^{99m}Tc-MIBI was the hepatobiliary system and some of the substance was eliminated through the urinary tract. The time-activity curves for ^{99m}Tc-MIBI are presented in figure 4.2. Table 4.2 summarized the biokinetics data of ^{99m}Tc MIBI in rest and stress studies of MPI estimated from the present study.
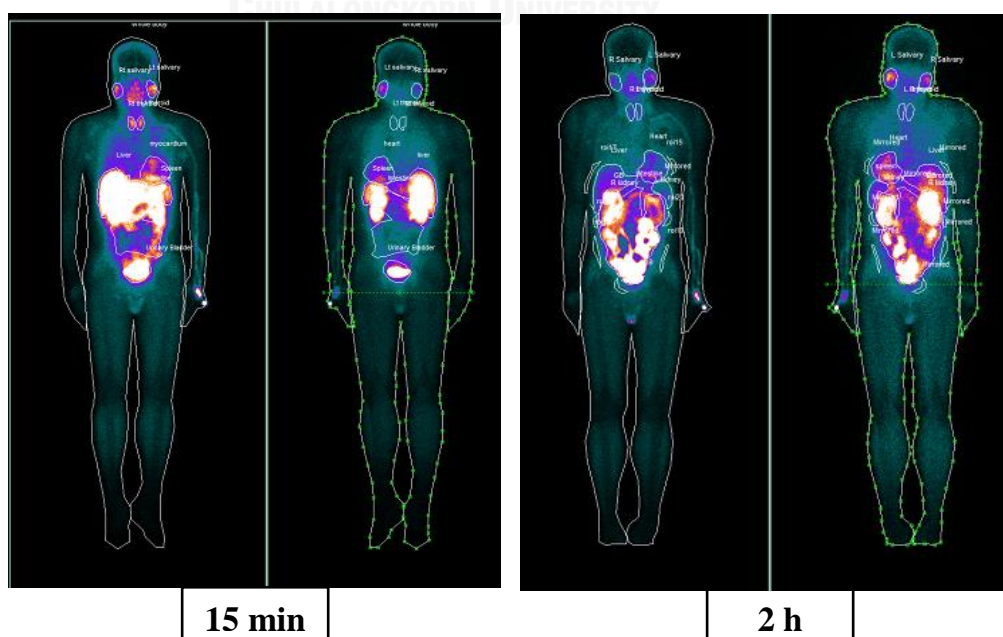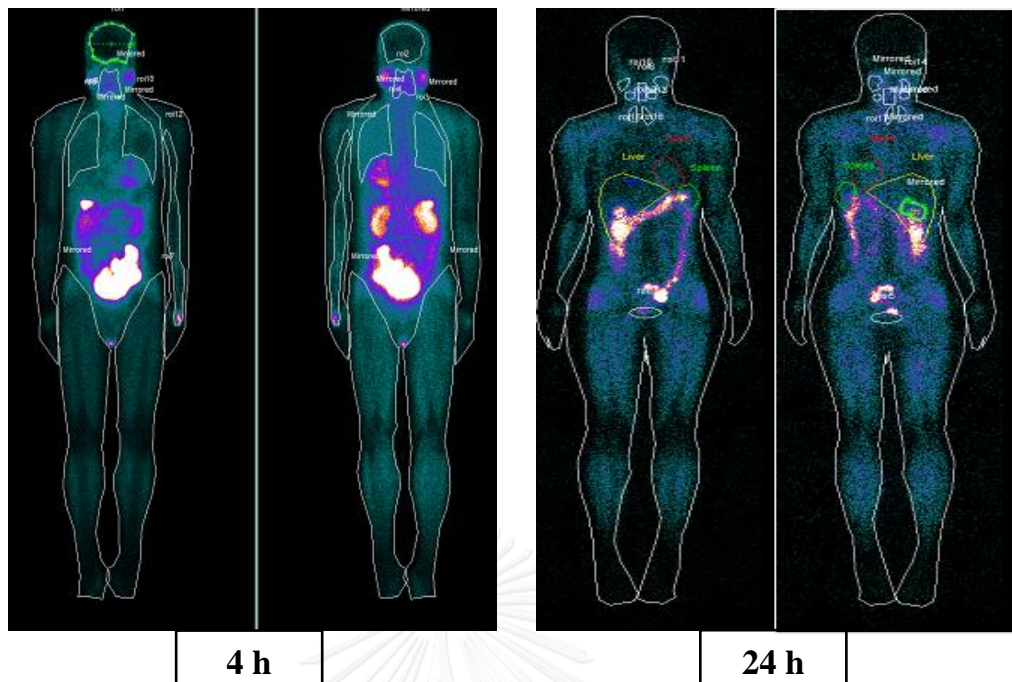
| 15 min | 2 h |

Figure 4.1 Anterior and posterior whole-body planar images at 15 min, 2 h, 4 h and 24 h after injection of ^{99m}Tc-MIBI (rest)
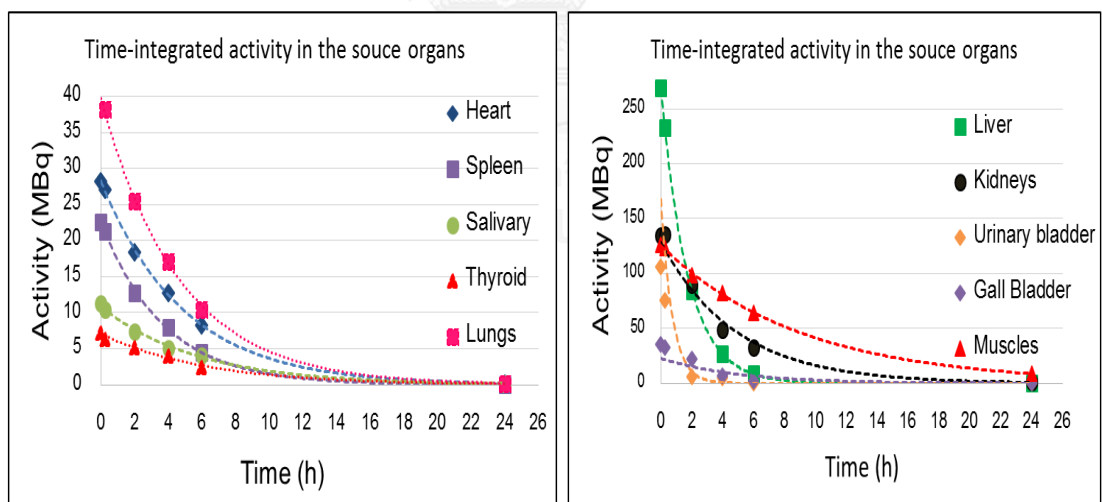
Figure 4.2 Time-activity curves for ^{99m}Tc-MIBI in various source organs

Table 4.1 The fractional distribution of MIBI (% of injected activity) at different time measurements in various organs at stress and rest studies

Fraction distribution of ^{99m}Tc-MIBI in the source organs (% of injected activity)						
Organ	**15 min**		**2 h**		**4 h**		**24 h**
	Rest	**Stress**	**Rest**	**Stress**	**Rest**	**Stress**	**Rest**
Heart	2.2 ±0.2	3.5±1.0	1.6±0.2	2.0±0.8	1.0±0.1	1.4±0.6	0.003± 0.00
Liver	17.5 ±2.7	19.1±3	6.0±1.8	7.5±2.5	3.5±1.8	3.5±1.2	0.001± 0.00
Intestine	15.0 ±2.3	18.0±2.3	27.0±4.0	24.0±6.0	24.0±4.2	22.0±5.5	0.009± 0.00
Salivary glands	0.9 ±0.2	1.5±0.5	0.7±0.1	1.0±0.2	0.4±0.1	0.7±0.1	0.0002± 0.00
Thyroid	0.7 ±0.1	0.9±0.3	0.5±0.1	0.8±0.4	0.3±0.1	0.4±0.1	0.0002± 0.00
Kidneys	11.0 ±1.5	9.0±5.0	5.7±1.6	7.0±2.0	3.9±1.3	4.0±1.2	0.001± 0.00
Spleen	1.9 ±1.0	2.5±0.7	0.9±0.5	1.0±0.3	0.5±0.3	0.6±0.3	0.0002± 0.00
Gall bladder	3.0 ±1.8	3.7±1.1	2.3±1.1	2.8±1.0	1.6±1.0	1.0±0.5	0.0003± 0.00
Urinary bladder	4.2 ±2.0	6.3±2.1	0.9±0.8	1.6±0.6	0.3±0.1	0.4±0.1	0.0001± 0.00
Brain	0.9 ±1.0	1.1±0.1	0.5±0.1	0.7±0.1	0.4±0.1	0.4±0.1	0.0002± 0.00
Lungs	4.5 ±1.0	5.0±0.6	2.8±0.7	3.4±0.7	2.0±0.4	2.4±0.4	0.001± 0.00
Muscles	21.0 ±2.5	17.0±3.4	17.0±1.8	14.2±3.4	13.7±1.6	1.4±0.6	0.015± 0.01
Whole body	96.6±0.6	97.0±0.4	72.0±4.0	71.6±3.0	58.0±4.0	55.0±3.0	0.03± 0.01
Decay (washout)	3.4±0.7 Physical	3.0±0.4	28.0±4.0 28.5 ±1.4 Physical + biological		42.0±4.0 44.0±2.7 Physical + biological		96.73±0.1 Physical +biological

Data were expressed in terms of mean±SD.

Table 4.2 The biokinetics data of ^{99m}Tc-sestamibi

Organs	Fs (%)		$T_{1/2}$ (h)		ã (r_S, T_D) (h)	
	Rest	**Stress**	**Rest**	**Stress**	**Rest**	**Stress**
Heart	2.00±0.40	3.50±0.50	3.50±0.40	3.60±0.60	0.12±0.01	0.14±0.02
Gall bladder	2.50±0.80	3.00±1.00	-	-	0.15±0.05	0.14±0.03
Thyroid	0.60±0.10	0.80±0.30	2.80±0.50	2.70±0.50	0.03±0.01	0.04±0.01
Salivary glands	1.00±0.20	1.50±0.30	3.30±0.60	2.80±0.50	0.05±0.01	0.06±0.02
Liver	10.00±2.50	12.00±3.00	1.50±0.80	1.20±0.20	0.47±0.05	0.44±0.09
Intestine	35.00±6.00	32.00±5.00	-	-	2.69±0.40	2.37±0.18
Muscle	22.00±4.50	20.00±4.00	7.50±1.40	8.00±1.50	2.06±0.30	1.86±0.16
Kidneys	8.50±1.50	8.50±3.00	2.90±1.30	2.40±0.40	0.48±0.08	0.37±0.01
Spleen	1.50±0.70	1.60±0.50	2.30±1.00	2.30±1.00	0.10±0.01	0.07±0.02
Urinary bladder	2.00±1.00	3.00±1.00	-	-	0.07±0.03	0.08±0.02
Lungs	4.50±0.70	4.40±1.00	3.00±0.50	3.00±0.50	0.21±0.05	0.24±0.05

Fs- Fractional distribution of ^{99m}Tc-MIBI

$T_{1/2}$- Effective Half-time of radionuclide in each organ

ã (r_S, T_D) – Time-integrated activity coefficient (TIAC) or residence time

4.2.1.1 Time-integrated activity coefficient (TIAC) or residence time

The time-integrated activity coefficient (TIAC) or residence time is related to the characteristics of both physical and biological removal of the radiopharmaceuticals from the source organs. It represents the total number of disintegrations which have occurred during an integration time per unit administered activity. Ideally, integration was performed from the time of administration to infinity, dose-integration period.

In this study, 10 patients at rest and 10 patients under stress study were collected to investigate the mean residence time in various source organs. The highest residence time of ^{99m}Tc-MIBI was seen in muscles and intestine in both rest and stress studies. The mean residence time of ^{99m}Tc-MIBI in 11 source organs, heart, liver, gall bladder, intestine, thyroid, salivary glands, muscle, kidneys, spleen, urinary bladder and lungs are presented in table 4.4 and table 4.5 for rest and stress studies.

4.2.2 Radiation doses from ^{99m}Tc-MIBI

4.2.2.1 Absorbed doses to target organs

The absorbed doses to 23 target organs (adrenals, bone surface, brain, breasts, gall bladder, heart, kidneys, liver, lower large intestine, lungs, muscles, pancreas, red marrow, skin, small intestine, spleen, stomach wall, thymus, thyroid, upper large intestine, urinary bladder, gonads and other remaining organs) were calculated irradiated from 11 source organs (heart, liver, intestine, salivary glands, thyroid, kidneys, spleen, gall bladder, urinary bladder, lungs and muscles).

The result showed that gall bladder was the organ that received the highest mean absorbed dose for examination with ^{99m}Tc-MIBI, 35.8±6.0 μGy/MBq (mean±SD), ranged from 26 to 44 μGy/MBq at rest and 34.8±7.3 μGy/MBq, and ranged from 25.8 to 48.1 μGy/MBq at stress study. The organs involved in the excretory pathway of MIBI (upper large intestine, lower large intestine, kidneys and liver) also received the high absorbed dose. There was also specific uptake in thyroid and salivary glands and therefore thyroid glands received relatively high absorbed dose. The mean absorbed doses in 23 target organs were calculated in 10 patients at rest and 10 patients under stress as summarized in figure 4.2, table 4.3 and detail in table 4.6 for rest study and table 4.7 for stress study of each patient.

Figure 4.3 The mean absorbed dose (μGy/MBq) to 23 target organs between rest and stress studies from ^{99m}Tc-MIBI
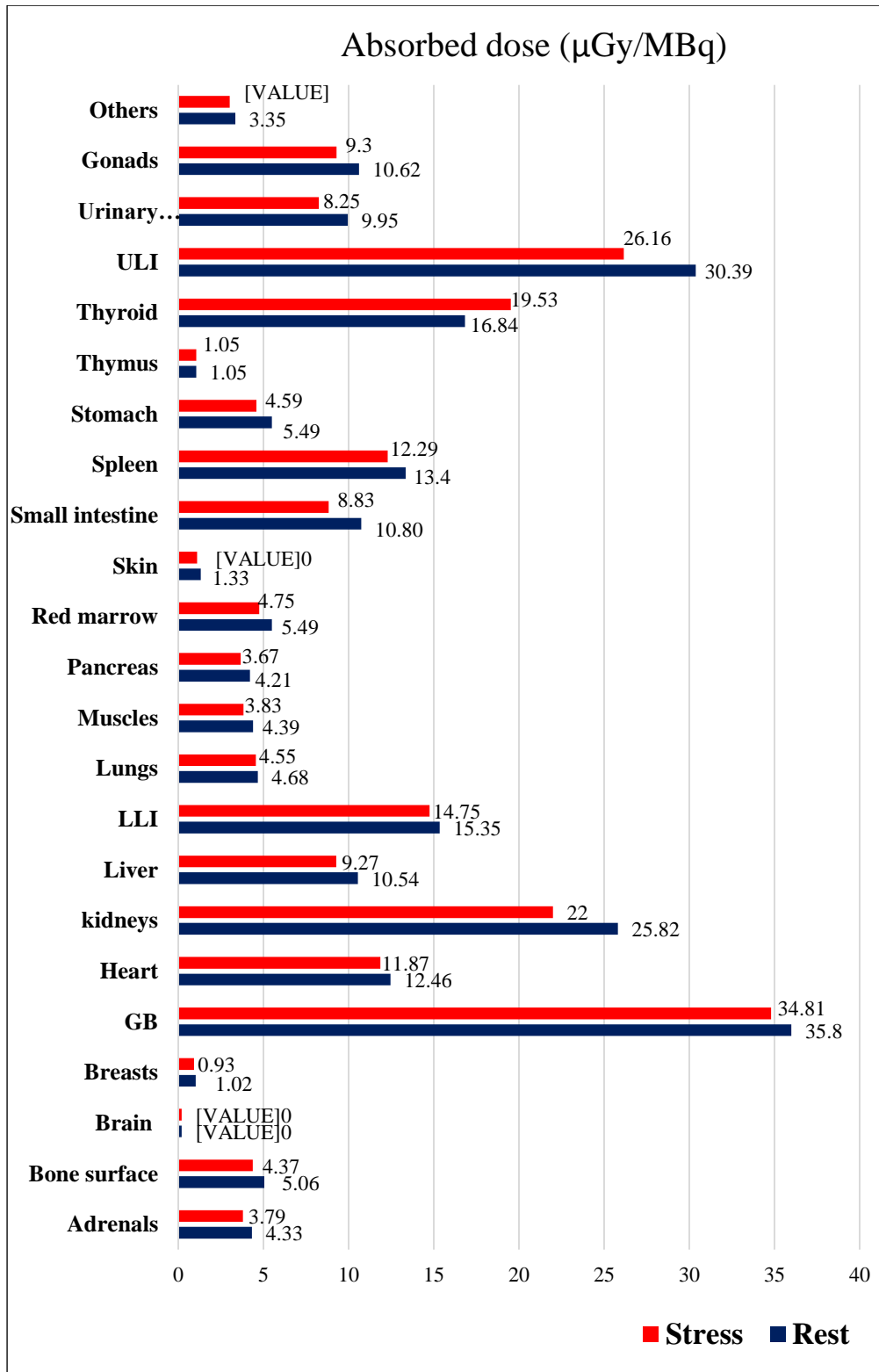
GB-gall bladder, LLI-lower large intestine, ULI-upper large intestine

Table 4.3 Absorbed doses in 23 target organs between rest and stress studies
(µGy/MBq)

Target organs	Max		Min		Mean±SD	
	Rest	Stress	Rest	Stress	Rest	Stress
Adrenals	5.41	4.24	3.34	3.20	4.33±0.60	3.79±0.30
Bone surface	5.74	5.07	4.14	3.33	5.06±0.60	4.37±0.50
Brain	0.26	0.28	0.15	0.12	0.2±0.03	0.20±0.04
Breasts	1.15	0.98	0.75	0.88	1.02±0.14	0.93±0.05
Gall bladder	44.43	48.10	25.61	25.81	35.8±6.00	34.81±7.33
Heart	17.85	18.93	7.83	7.00	12.46±2.85	11.87±3.10
kidneys	33.85	29.14	17.81	13.02	25.82±6.22	22.00±5.00
Liver	11.73	10.73	8.46	5.61	10.54±1.05	9.27±1.50
LLI	19.65	17.20	12.22	10.99	15.35±3.09	14.75±1.82
Lungs	5.99	5.33	2.99	3.75	4.68±0.91	4.55±0.60
Muscles	5.34	4.49	3.54	3.06	4.40±0.48	3.83±0.43
Pancreas	5.08	4.05	3.38	2.85	4.21±0.45	3.67±0.32
Red marrow	6.32	5.33	4.63	3.73	5.50±0.59	4.75±0.50
Skin	1.83	1.30	1.03	0.83	1.33±0.22	1.10±0.15
Small intestine	17.58	9.98	8.56	6.99	10.8±2.52	8.83±0.99
Spleen	20.73	17.25	8.61	7.70	13.35±4.12	12.29±3.17
Stomach	7.18	5.25	4.42	3.50	5.48±0.75	4.59±0.50
Thymus	1.19	1.70	0.75	0.81	1.05±0.12	1.05±0.25
Thyroid	16.78	20.97	14.34	17.72	16.84±3.24	19.53±1.20
ULI	35.55	30.58	24.59	19.19	30.40±3.64	26.16±3.32
Urinary bladder	16.68	10.37	5.11	5.66	9.95±3.60	8.25±1.50
Gonads	12.69	10.59	8.94	7.71	10.62±1.39	9.30±0.90
Others	3.76	3.39	2.67	2.73	3.35±0.35	3.02±0.25

LLI- lower large intestine, ULI- upper large intestine

Table 4.4 Time-integrated activity coefficient (TIAC) or residence time (h) of ^{99m}Tc-MIBI in 11 source organs at rest study

Patient No	Time-integrated activity coefficient or residence time (h)										
	Heart	Liver	Intestine	Salivary glands	Thyroid	Kidneys	Spleen	Gall bladder	Urinary bladder	Lungs	Muscles
1	0.1134	0.4529	2.5741	0.0572	0.0439	0.4078	0.0927	0.1611	0.071	0.1651	2.573
2	0.1212	0.5102	2.9668	0.0514	0.0255	0.5837	0.1242	0.2551	0.047	0.236	1.6742
3	0.1255	0.3959	2.8054	0.0394	0.0231	0.5035	0.0815	0.2305	0.1962	0.3036	2.2276
4	0.1	0.451	2.9455	0.0471	0.0421	0.5836	0.109	0.1006	0.0249	0.1826	2.4309
5	0.1162	0.4707	3.0351	0.0361	0.0215	0.5604	0.081	0.0785	0.021	0.1894	1.8862
6	0.1251	0.4862	2.7632	0.0496	0.0384	0.4377	0.0851	0.173	0.0763	0.1773	2.762
7	0.1032	0.3723	2.2525	0.0576	0.0242	0.3234	0.0919	0.1606	0.0698	0.1194	1.5987
8	0.1192	0.5446	2.0936	0.0551	0.0364	0.4798	0.1092	0.1027	0.0595	0.2357	2.095
9	0.1238	0.4944	2.5651	0.0517	0.0294	0.4637	0.0885	0.1377	0.09	0.2094	1.833
10	0.1271	0.564	2.1498	0.0543	0.0362	0.4835	0.099	0.1202	0.0616	0.2387	2.0637
Mean	0.1174	0.4742	2.6852	0.0499	0.0321	0.4827	0.0962	0.1521	0.0717	0.2057	2.0561
SD	0.0089	0.0569	0.3996	0.0068	0.0078	0.0776	0.0133	0.0539	0.0463	0.0481	0.3071

Table 4.5 Time-integrated activity coefficient (TIAC) or residence time (h) of ^{99m}Tc-MIBI in 11 source organs under stress study

Patient No	Heart	Liver	Intestine	Salivary glands	Thyroid	Kidneys	Spleen	Gall Bladder	Urinary Bladder	Lungs	Muscles
				Time-integrated activity coefficient or residence time (h)							
1	0.1548	0.2251	2.0864	0.0725	0.0314	0.3790	0.0406	0.1158	0.0809	0.2518	1.8151
2	0.1527	0.4960	2.5528	0.0552	0.0496	0.5336	0.0594	0.1014	0.0977	0.3013	1.7714
3	0.1150	0.4221	2.2265	0.0692	0.0310	0.4871	0.0826	0.1755	0.0590	0.2574	1.8311
4	0.1108	0.5197	2.6422	0.0641	0.0356	0.3099	0.0322	0.0955	0.0722	0.2673	1.6605
5	0.1311	0.4044	2.4167	0.0803	0.0266	0.2418	0.1097	0.1834	0.0979	0.1511	2.0709
6	0.1270	0.3880	2.4182	0.0652	0.0320	0.3038	0.0727	0.1595	0.0799	0.1705	2.0872
7	0.1508	0.3853	2.2003	0.0344	0.0348	0.3852	0.0551	0.1008	0.0940	0.2566	1.6507
8	0.1700	0.5318	2.5859	0.0481	0.0599	0.3903	0.1097	0.1834	0.0514	0.3024	2.0650
9	0.1250	0.4817	2.3918	0.0398	0.0535	0.3620	0.0765	0.1408	0.0923	0.2075	1.8549
10	0.1221	0.5151	2.1625	0.0798	0.0277	0.2908	0.0836	0.1426	0.0687	0.1862	1.7557
Mean	0.1359	0.4369	2.3683	0.0609	0.0382	0.3684	0.0722	0.1399	0.0794	0.2352	1.8562
SD	0.0187	0.0887	0.1822	0.0152	0.0111	0.0848	0.0247	0.0332	0.0156	0.0506	0.1559

Table 4.6.1 Absorbed doses to 23 target organs of each patient at rest study

Target organs	Absorbed dose (μGy/MBq) Patient number									
	1	2	3	4	5	6	7	8	9	10
Adrenals	4.51	5.41	4.65	4.55	4.60	4.64	3.34	3.95	3.69	3.99
Bone surface	5.15	5.03	5.75	4.47	5.49	6.04	4.14	4.84	4.84	4.87
Brain	0.19	0.17	0.21	0.21	0.18	0.27	0.15	0.21	0.18	0.20
Breasts	-	1.13	1.15	-	0.98	1.13	0.75	-	0.97	-
Gall bladder	36.15	40.09	43.95	30.53	25.61	44.43	39.65	28.89	36.22	32.61
Heart	11.75	17.85	12.36	7.83	11.29	12.35	9.64	15.25	11.70	14.63
Kidneys	28.23	31.21	30.89	30.85	33.85	27.55	20.43	18.55	17.81	18.83
Liver	11.43	11.73	10.06	9.19	10.56	11.11	8.45	11.02	10.47	11.39
LLI	15.07	14.34	18.60	12.22	19.65	18.34	14.48	13.91	16.57	14.23
Lungs	5.75	5.18	5.99	3.36	4.32	4.46	2.99	5.11	4.51	5.14
Muscles	4.58	4.19	4.98	4.12	4.67	5.34	3.54	4.21	4.16	4.23
Pancreas	4.39	5.08	4.54	4.05	4.41	4.52	3.38	3.99	3.72	4.02
Red marrow	5.49	5.55	6.26	5.08	6.25	6.32	4.63	4.99	5.30	5.06

Table 4.6.2 Absorbed doses to 23 target organs of each patient at rest study

Target organs	Absorbed dose (µGy/MBq)									
	Patient number									
	1	2	3	4	5	6	7	8	9	10
Skin	1.83	1.255	1.44	1.11	1.36	1.55	1.03	1.24	1.21	1.25
Small intestine	10.27	9.49	11.37	17.58	11.60	11.24	8.74	8.56	9.87	8.77
Spleen	12.62	20.73	10.31	16.12	13.83	9.45	8.75	17.17	8.62	15.98
Stomach	7.18	5.76	5.87	4.89	5.86	5.90	4.41	4.96	4.97	5.01
Thymus	1.03	1.11	1.13	1.08	0.96	1.19	0.76	1.13	0.96	1.12
Thyroid	16.13	15.15	16.00	16.78	14.33	15.83	16.19	14.24	16.66	14.13
ULI	31.33	34.40	32.84	33.22	34.53	32.37	25.97	24.59	29.42	25.26
Urinary bladder	12.38	6.75	16.69	5.10	15.52	9.90	7.95	7.61	9.76	7.78
Gonads	10.53	9.15	12.25	11.95	12.69	11.77	9.19	8.93	10.55	9.13
Others	3.57	3.27	3.65	3.74	3.56	3.76	2.67	3.05	3.10	3.08
Weight (kg)	73.00	60.00	55.00	73.00	70.00	60.00	53.50	49.00	54.00	52.00
Activity(MBq)	991.23	976.8	969.4	821.4	987.53	983.83	920.56	829.91	939.8	916.49

Table 4.7.1 Absorbed doses to 23 target organs of each patient under stress study

Target organs	Absorbed dose (µGy/MBq)									
	Patient number									
	1	2	3	4	5	6	7	8	9	10
Adrenals	3.20	4.24	3.96	3.75	3.74	3.74	3.72	4.11	3.82	3.71
Bone surface	3.33	3.97	4.13	4.73	5.07	4.93	4.46	4.26	4.36	4.48
Brain	0.16	0.17	0.12	0.16	0.21	0.20	0.17	0.28	0.17	0.17
Breasts	0.00	0.00	0.88	0.98	0.00	0.00	0.98	0.00	0.88	0.00
Gall bladder	25.81	26.64	33.93	31.17	48.10	43.19	30.65	38.88	30.50	39.51
Heart	9.50	10.58	11.28	10.82	13.25	11.87	13.25	18.93	12.25	7.00
Kidneys	20.23	28.13	29.14	20.18	16.83	19.89	23.72	13.02	23.72	19.01
Liver	5.61	9.54	9.49	10.73	9.33	9.03	8.71	10.53	9.13	10.57
LLI	13.44	17.20	14.15	16.81	16.00	15.86	14.35	10.99	14.49	14.13
Lungs	3.75	4.50	4.94	5.23	3.82	4.00	5.07	5.33	4.57	4.18
Muscles	3.06	3.52	3.39	3.97	4.49	4.32	3.80	4.07	3.80	3.86
Pancreas	2.85	3.65	3.85	3.67	4.05	3.87	3.59	3.83	3.59	3.76
Red marrow	3.73	4.63	4.76	5.31	5.33	5.27	4.87	4.06	4.76	4.80

Table 4.7.2 Absorbed doses to 23 target organs of each patient under stress study

Target organs	Absorbed dose (µGy/MBq) Patient number									
	1	2	3	4	5	6	7	8	9	10
Skin	0.83	0.97	1.01	1.16	1.30	1.25	1.12	1.14	1.11	1.13
Small intestine	7.84	9.98	8.74	9.91	9.72	9.60	8.66	6.99	8.26	8.65
Spleen	7.70	10.53	14.22	7.95	17.25	12.89	10.75	16.00	11.75	13.89
Stomach	3.50	4.37	4.72	4.93	5.25	5.07	4.64	4.15	4.58	4.72
Thymus	1.00	1.08	0.81	0.93	1.03	1.00	0.98	1.70	0.99	0.93
Thyroid	17.72	20.51	20.34	20.49	18.07	18.41	20.97	20.32	19.97	18.54
ULI	23.66	30.58	25.83	29.98	28.23	28.08	25.40	19.19	25.40	25.25
Urinary bladder	6.49	7.78	7.05	8.61	10.37	9.19	9.44	5.66	9.54	7.98
Gonads	10.29	9.27	8.92	10.59	10.25	8.53	9.22	7.71	9.12	9.04
Others	2.76	3.39	2.73	3.07	3.19	3.11	2.85	3.39	2.82	2.87
Weight (kg)	50.00	57.00	65.00	56.00	70.00	62.50	54.00	57.00	57.00	62.00
Activity(MBq)	853.96	916.00	954.60	916.49	993.00	932.40	899.10	902.43	917.60	577.20

4.2.2.2 Effective dose from ^{99m}Tc-sestamibi

      The summary of patient information, effective dose coefficient (μSv/MBq), effective dose (mSv) from ^{99m}Tc-MIBI are shown in table 4.8.1 and 4.8.2 for rest study and table 4.9.1 and 4.9.2 for stress study.

Table 4.8.1 Dose coefficients (Γ_E^{MIBI}) for ^{99m}Tc-MIBI and effective dose (mSv) at rest study

Pt No	Gender	Age (yr)	Weight (kg)	Activity (MBq)	Γ_E^{MIBI} (μSv/MBq)	Effective dose (mSv)
1	M	59	73.00	991.23	12.40	12.29
2	F	62	60.00	976.80	12.30	12.01
3	F	26	55.00	969.40	11.40	11.03
4	M	53	73.00	821.40	10.30	8.45
5	F	57	70.00	987.53	12.50	12.21
6	F	70	60.00	983.83	12.20	12.02
7	F	65	53.50	920.56	10.90	9.95
8	M	70	49.00	829.91	11.80	9.75
9	F	70	54.00	939.80	11.60	10.90
10	M	68	52.00	916.49	11.00	9.89

Table 4.8.2 Summary of effective dose (mSv) from ^{99m}Tc-MIBI and patient characteristics at rest study

	Max	Min	Mean±SD
Age (yr)	70.00	26.00	60.00±13.00
Body weight (kg)	70.00	49.00	60.00±8.50
^{99m}Tc-MIBI activity (MBq)	993.00	821.00	935.00±60.00
Dose coefficient (μSv/MBq)	12.40	10.30	11.64±0.70
Effective Dose (mSv)	12.29	8.45	10.85±1.24

Table 4.9.1 Dose coefficients (Γ_E^{MIBI}) for ^{99m}Tc-MIBI and effective dose (mSv) under stress study

Pt No	Gender	Age (yr)	Weight (kg)	Activity (MBq)	Γ_E^{MIBI} (μSv/MBq)	Effective dose (mSv)
1	F	64	50.00	853.96	9.80	8.30
2	M	54	57.00	916.00	10.20	9.34
3	F	52	65.00	954.60	10.70	10.17
4	F	50	56.00	916.49	10.20	9.35
5	M	70	70.00	993.00	10.20	10.23
6	M	51	62.50	932.40	10.50	9.84
7	F	47	54.00	899.10	10.70	9.60
8	M	68	57.00	902.43	9.30	8.40
9	F	58	57.00	917.60	9.90	9.13
10	M	64	62.00	577.20	10.30	5.73

Table 4.9.2 Summary of effective dose (mSv) from ^{99m}Tc-MIBI and patient characteristics under stress study

	Max	Min	Mean±SD
Age (yr)	70.00	47.00	57.80±7.75
Body weight(kg)	70.00	50.00	59.00±5.50
^{99m}Tc-MIBI activity (MBq)	993.00	577.20	886.28±108.60
Dose coefficient (μSv/MBq)	10.70	9.30	10.18±0.40
Effective Dose (mSv)	10.23	5.73	9.01±1.25

4.2.2.3 The correlation between effective dose and influenced parameters

The correlation between effective dose and characteristics for myocardial perfusion examination has been investigated. Figure 4.3 represents the scatter diagrams showing the correlation between effective dose and influenced parameters. The y-axis represents the patient effective dose in mSv. The x-axis represents the factors affecting the effective dose. Table 4.10 shows the relationship by Pearsons' correlation. The results show;

- A significant strong linear relationship between the effective dose and injected activity
  ($r = 0.922$, $p = 0.000$) for rest study and ($r = 0.928$, $p = 0.005$) for stress study.
- A significant strong linear relationship between the effective dose and body weight
  ($r = 0.749$, $p = 0.013$) for rest study and ($r = 0.800$, $p = 0.01$) for stress study.
- Not significant weak linear relationship between the effective dose and patient age
  ($r = -0.022$, $p = 0.951$) for rest study and ($r = -0.426$, $p = 0.220$) for stress study.

Table 4.10 The correlations between effective dose and patient characteristics of myocardial perfusion examination

Characteristics	Correlation coefficient (r)		*p-value*	
	Rest	Stress	Rest	Stress
Injected activity	0.922	0.928	0.000*	0.005*
Body weight	0.749	0.800	0.013**	0.01*
BMI	0.626	0.455	0.053	0.305
Age	-0.022	-0.426	0.951	0.220

*Correlation is significant at the 0.01 level (2-tailed).
**Correlation is significant at the 0.05 level (2-tailed).

(a)

(b)
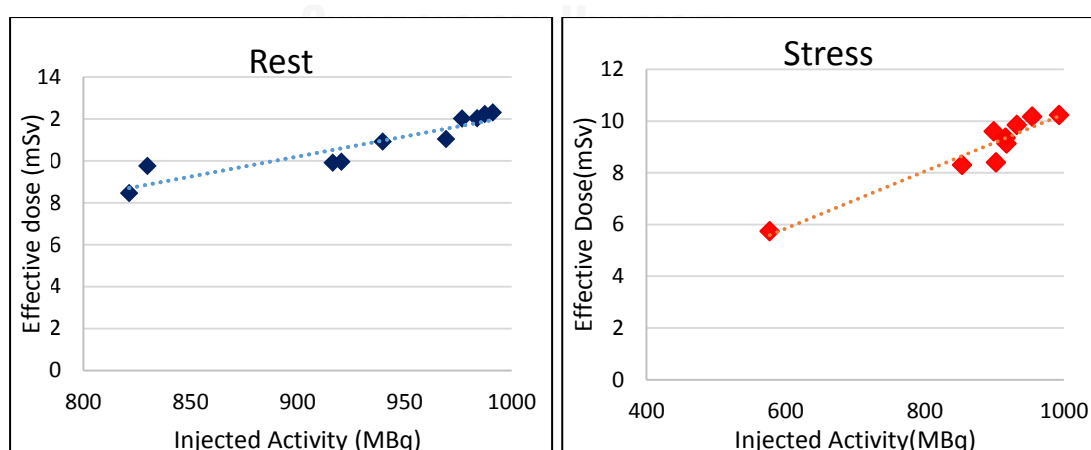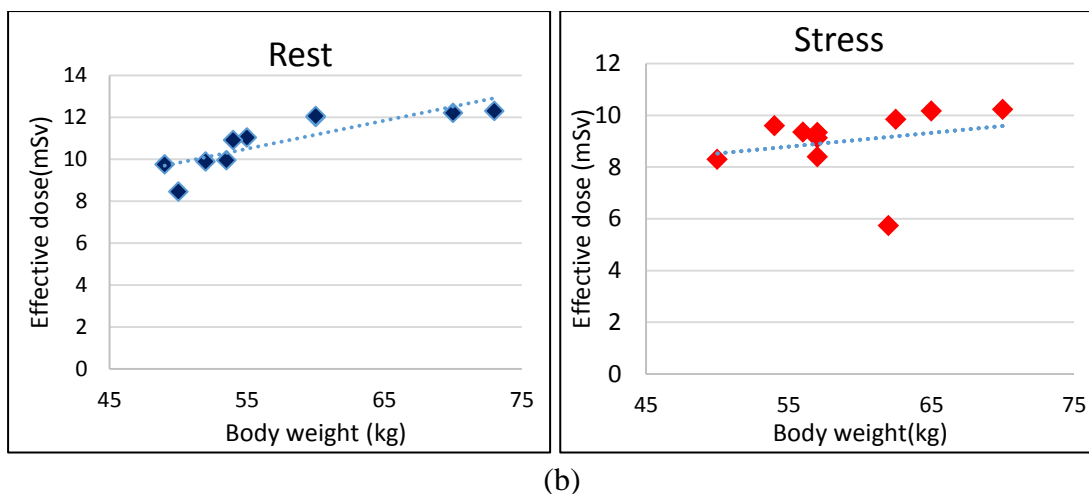
Figure 4.4 Scatter plots of correlations between the effective doses and; (a) injected activity, (b) patient's body weight

4.3. Radiation doses from CT

4.3.1 Measurement of computed tomography dose index

The CTDI measurement in air and body phantom for the measurement values are shown in table 4.11. The CTDI value in air indicated 26.9 mGy/100mAs and CTDI values in the body phantom of 32 cm diameter indicated that 6.20 mGy/100mAs at the center and 11.98 mGy/100mAs at the periphery. There were no published data of CTDI measurements for GE BrightSpeed E-Lite 16 in ImPACT spread sheet. Therefore, CTDI measurements in air and in body phantom measurements have been entered into the spread sheet manually.

Table 4.11 Computed Tomography Dose Index in air and body phantom

CTDI	Measured value (mGy/100mAs)
air	26.9
center	6.20
periphery	11.98
$CTDI_w$	10.21

4.3.2 Mean absorbed dose and effective dose from CT of myocardial perfusion imaging by Monte Carlo simulation program, ImPACT scan

The mean absorbed doses and effective doses with tissue weighting factors for calculation by Monte Carlo examination are shown in table 4.2 for rest and table 4.3 for stress study. The summary of effective doses from CT scan for rest and stress study was presented in table 4.12 and table 4.13. The effective dose from CT scan ranged from 0.90 mSv to 1.30 mSv (mean±SD, 1.14±0.11 mSv) for rest study and ranged from 0.90 mSv to 1.13 mSv (mean±SD, 1.12±0.13 mSv) for stress study.

Table 4.12 The absorbed dose and effective dose from CT by Monte Carlo simulation technique for rest study

Organs	Tissue weighting factor(W_T)	Absorbed dose(D_T)	Effective Dose ($D_T.W_T$)
Gonads	0.08	0.01±0.00	0.01±0.00
Bone Marrow	0.12	0.67±0.05	0.08±0.01
Colon	0.12	0.04±0.00	0.01±0.00
Lung	0.12	2.73±0.19	0.33±0.02
Stomach	0.12	0.89±0.01	0.11±0.01
Bladder	0.04	0.01±0.00	0.00±0.00
Breast	0.12	3.29±0.08	0.39±0.01
Liver	0.04	1.40±0.00	0.06±0.00
Esophagus	0.04	2.14±0.50	0.09±0.02
Thyroid	0.04	0.08±0.02	0.01±0.00
Skin	0.01	0.53±0.03	0.01±0.00
Bone Surface	0.01	1.31±0.09	0.01±0.00
Brain	0.01	0.01±0.00	0.00±0.00
Salivary Glands	0.01	0.01±0.00	0.00±0.00
Remainder**	0.12	0.85±0.06	0.10±0.01
Effective Dose (mSv)			1.14±0.11

**Remainder organs

Adrenals	1.82±0.04
Small Intestine	0.05±0.00
Kidney	0.30±0.01
Pancreas	1.09±0.03
Spleen	1.20±0.00
Thymus	2.14±0.50
Muscle	0.48±0.03
Gall Bladder	0.34±0.01
Heart	3.04±0.08

Table 4.13 The absorbed dose and effective dose from CT by Monte Carlo simulation technique for stress study

Organs	Tissue weighting factor(W_T)	Absorbed dose(D_T)	Effective Dose ($D_T.W_T$)
Gonads	0.08	0.01±0.00	0.01±0.00
Bone Marrow	0.12	0.65±0.06	0.08±0.01
Colon	0.12	0.04±0.00	0.01±0.00
Lung	0.12	2.65±0.22	0.32±0.03
Stomach	0.12	0.889±0.01	0.11±0.01
Bladder	0.04	0.003±0	0.00±0.00
Breast	0.12	3.21±0.1	0.39±0.01
Liver	0.04	1.4±0	0.06±0.00
Esophagus	0.04	1.95±0.6	0.08±0.02
Thyroid	0.04	0.074±0.017	0.01±0.00
Skin	0.01	0.513±0.04	0.01±0.00
Bone Surface	0.01	1.28±0.11	0.01±0.00
Brain	0.01	0.004±0	0.00±0.00
Salivary Glands	0.01	0.0039±0.0007	0.00±0.00
Remainder**	0.12	0.83±0.057	0.09±0.01
Effective Dose (mSv)			1.12±0.13

**Remainder organs

Adrenals	1.82±0.04
Small Intestine	0.05±0.00
Kidney	0.30±0.01
Pancreas	1.08±0.04
Spleen	1.20±0.00
Thymus	1.95±0.60
Muscle	0.47±0.04
Gall Bladder	0.34±0.00
Heart	3.01±0.08

Table 4.14 Summary of patient data with the effective dose from CT scan using
Monte Carlo simulation for rest study

	Max	Min	Mean±SD
Body weight(kg)	70.00	49.00	60.00±8.50
Patient height (cm)	167.00	152.00	160.00±6.70
Scan Length (cm)	20.00	16.00	18.65±1.25
Effective Dose (mSv)	1.30	0.90	1.14±0.11

Table 4.15 Summary of patient data with the effective dose from CT scan using
Monte Carlo simulation for stress study

	Max	Min	Mean±SD
Body weight(kg)	70.00	50.00	59.00±5.50
Patient height (cm)	178.00	150.00	159.40±8.30
Scan Length (cm)	20.50	16.00	18.30±1.40
Effective Dose (mSv)	1.34	0.90	1.12±0.13

4.3.3. The correlations between effective doses and influenced parameters

The correlation between effective dose from CT and characteristics for myocardial perfusion examination has been investigated. Figure 4.4 demonstrates the scatter diagrams showing the correlation between effective dose and influenced parameters. The y-axis represents the patient effective dose in mSv. The x-axis shows the factors affecting the effective dose. Table 4 shows the relationship by Pearson's correlation. The results show;

- A significant strong linear relationship between the effective dose from CT and scan length ($r = 0.968$, $p = 0.000$) for rest study and ($r = 0.987$, $p = 0.000$) for stress study.

- A significant strong linear relationship between the effective dose and patient's height
($r = 0.847$, $p = 0.002$) for rest study and ($r = 0.881$, $p = 0.001$) for stress study.

- Not significant weak linear relationship between the effective dose and patient age
($r = -0.226$, $p = 0.529$) for rest study and   ($r = 0.445$, $p = 0.269$) for stress study.

Table 4.16 The correlations between effective dose from CT and patient
characteristics of myocardial perfusion examination

Characteristics	Correlation coefficient (r)		*p-value*	
	Rest	Stress	Rest	Stress
Scan length	0.968	0.987	0.000*	0.000*
Patient's height	0.847	0.881	0.002*	0.001*
Age	-0.226	0.445	0.529	0.269

*Correlation is significant at the 0.01 level (2-tailed).
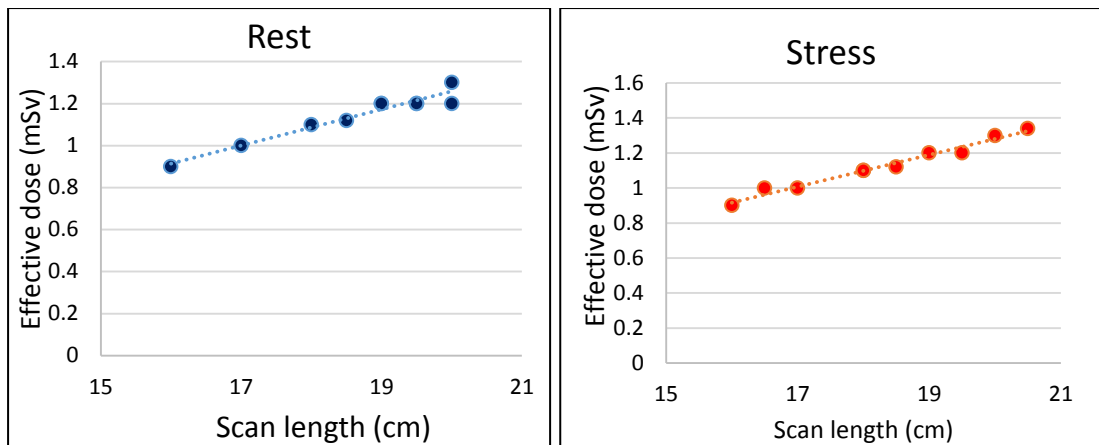
(a)
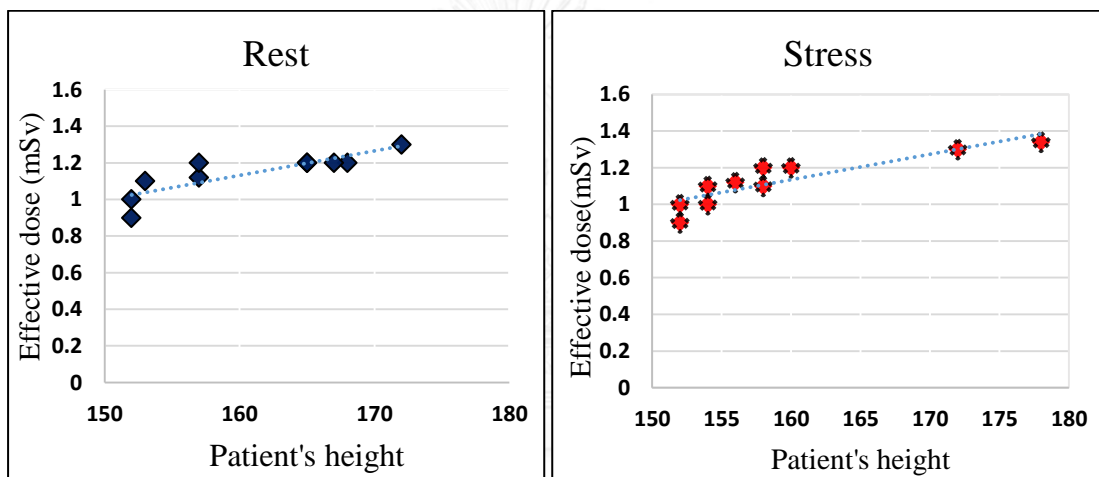
(b)

Figure 4.5 Scatter plots of correlations between the effective doses and; (a) scan length, (b) patient's height

4.4. Effective doses from myocardial perfusion SPECT/CT and related BERT

The summary of effective dose from myocardial perfusion SPECT/CT is presented in table 4.17 for rest and table 4.18 for stress study. The results showed that the mean effective dose from rest study of myocardial perfusion SPECT/CT was 11.99±1.20 mSv, ranged from 9.75 mSv to 13.49 mSv and its related mean BERT was 3.99±0.40 years, ranged from 3.25 years to 4.50 years. The mean effective dose from stress study of myocardial perfusion SPECT/CT was 10.35±1.20 mSv, ranged from 6.83 mSv to 11.45 mSv and its related BERT was 3.50±0.20 years, ranged from 2.28 years to 3.82 years. Effective dose coefficient (Γ_E^{MIBI}) of ^{99m}Tc-MIBI from MPI are summarized in table 4.19.

Table 4.17.1 Patient Characteristics and effective dose from myocardial perfusion SPECT/CT (rest)

Pt No.	Age	Weight (kg)	Height (cm)	Activity (MBq)	Effective dose(mSv)			BERT (years)
					MIBI	CT	Total	
1	59	73.00	165.00	991.23	12.29	1.20	13.49	4.50
2	62	60.00	153.00	976.80	12.01	1.10	13.11	4.37
3	26	55.00	157.00	969.40	11.03	1.12	12.15	4.05
4	53	73.00	172.00	821.40	8.45	1.30	9.75	3.25
5	57	70.00	165.00	987.53	12.21	1.20	13.41	4.47
6	70	60.00	152.00	983.83	12.02	1.00	13.02	4.34
7	65	53.5.00	168.00	920.56	9.95	1.20	11.15	3.72
8	70	49.00	157.00	829.91	9.75	1.20	10.95	3.65
9	70	54.00	152.00	939.80	10.9	0.90	11.80	3.93
10	68	52.00	167.00	916.49	9.89	1.20	11.09	3.70

Table 4.17.2 Summary of effective dose from myocardial perfusion SPECT/CT (rest)

	Max	Min	Mean±SD
Effective dose from MIBI	12.29	8.45	10.85±1.20
Effective dose from CT	1.30	0.90	1.14±0.10
Total effective dose from MPI	13.49	9.75	11.99±1.20
BERT	4.50	3.25	3.99±0.40

Table 4.18.1 Patient Characteristics and effective dose from myocardial perfusion
SPECT/CT (stress)

Pt No.	Age	Weight (kg)	Height (cm)	Activity (MBq)	Effective dose(mSv)			BERT (years)
					MIBI	CT	Total	
1	64	50.00	154	853.96	8.30	1.10	9.40	3.13
2	54	57.00	156	916.00	9.34	1.12	10.24	3.41
3	52	65.00	158	954.60	10.17	1.20	11.08	3.69
4	50	56.00	152	916.49	9.35	0.90	9.98	3.33
5	70	70.00	172	993.00	10.23	1.30	11.45	3.82
6	51	62.50	178	932.40	9.84	1.34	10.82	3.61
7	47	54.00	152	899.10	9.60	1.00	10.20	3.40
8	68	57.00	160	902.43	8.40	1.20	9.60	3.20
9	58	57.00	154	917.60	9.13	1.00	10.13	3.38
10	64	62.00	158	577.20	5.73	1.10	6.83	2.28

Table 4.18.2 Summary of effective dose from myocardial perfusion SPECT/CT
(stress)

	Max	Min	Mean±SD
Effective dose from MIBI	10.23	5.73	9.01±1.25
Effective dose from CT	1.34	0.90	1.13±0.10
Total effective dose from MPI	11.45	6.83	10.35±1.20
BERT	3.82	2.28	3.50±0.20

Table 4.19 Effective dose coefficient (Γ_E^{MIBI}) from myocardial perfusion SPECT/CT

	Effective dose coefficient (µSv/MBq)		
	Max	Min	Mean±SD
Rest	12.40	10.30	11.64±0.70
stress	10.70	9.30	10.18±0.60

CHAPTER 5

DISCUSSION AND CONCLUSIONS

5.1 Discussion

As myocardial perfusion SPECT/CT has been increasingly used in the diagnostic assessment of cardiovascular diseases, the estimation of patient dose received greater importance as the projected risk of late radiation effects, particularly cancer does not have any threshold [18, 26]. The estimated radiation dose from nuclear medicine examination is dependent on various factors such as scanner setting parameters, diagnostic protocols used, patient geometry and physiology. Therefore, studies on patient dose estimation should critically address these issues for more realistic dose calculation. Studies on organ absorbed dose based on human biokinetic data required for internal dose calculation were reported [21, 27]. In addition, biokinetic data, absorbed dose and dose coefficient of ^{99m}Tc MIBI were provided by ICRP publication 80 and 128 [28, 29]. Conversely, in the present study, the patient doses were calculated based on the biokinetics data obtained in humans, Thai patients and organ masses from Asian reference man [24].

5.1.1 Comparison of fractional distribution of ^{99m}Tc-MIBI with published data

The fractional distribution of ^{99m}Tc-MIBI in various organs in this study was comparable with Leide et al study between rest and stress studies. The fractional uptake of injected activity of MIBI by muscle and intestine showed significant difference, nearly doubled between rest and stress in Leide et al study because stress condition was achieved by means of the real exercise, bicycle ergometer which make increased blood flow to the extremity muscles in Leide et al study. Whereas, adenosine was intravenously injected for the purpose of stress condition instead according to routine protocol in the present study. Figure 5.1 shows the fractional distribution of ^{99m}Tc-MIBI in various organs between this study and Leide et al study.
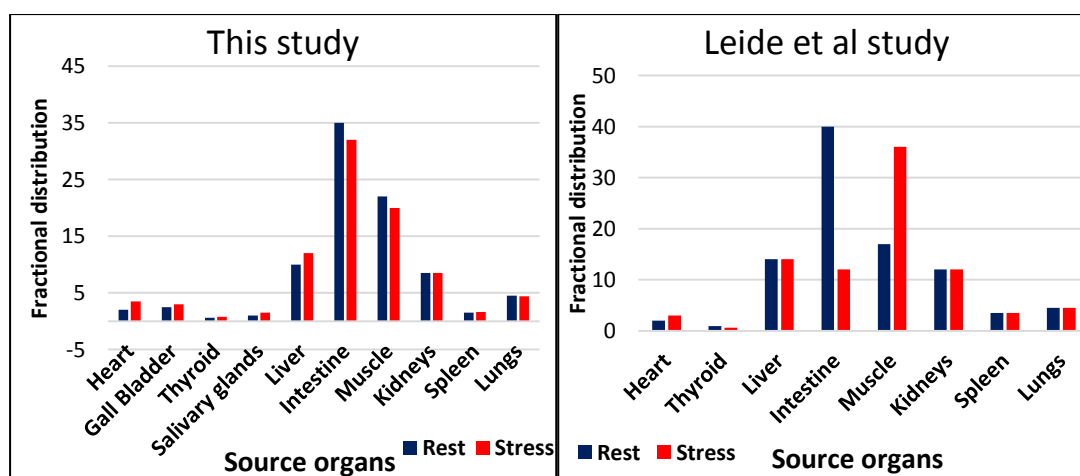
Figure 5.1 The fractional distribution of ^{99m}Tc-MIBI in various organs between this study and Leide et al study

5.1.2. Comparison of time-integrated activity coefficient or residence time with published data

The time-integrated activity coefficient or residence time in 11 source organs were calculated by the measurement of organ activity at 15 min, 2 h and 4 h after injection of ^{99m}Tc-MIBI, fitted the time-activity curve by using the exponential equation and normalized with injected activity. The results agree with residence time of the published data with minimal difference because of different biodistribution among each individual based on individual physiology and different types of stress condition (exercise and pharmacologic stress). The residence time of muscles showed significant difference between the present study and published data because of different fractional distribution of MIBI in muscles between the studies. The comparison of time-integrated activity coefficient in 11 source organs with other studies was summarized in table 5.1.

Table 5.1 Comparison of time-integrated activity coefficient or time in 11 source organs of this study to other published data

| Organs | Time-integrated activity coefficient, TIAC (h) | | | | | |
| | This study | | Leide et al [21] | | ICRP 128 [29] | |
	Rest	Stress	Rest	Stress	Rest	Stress
Heart	0.12±0.01	0.14±0.02	0.13	0.15	0.07	0.09
Gall Bladder	0.15±0.05	0.14±0.03	-	-	0.25	0.20
Thyroid	0.03±0.01	0.04±0.01	0.04	0.03	0.01	0.01
Salivary glands	0.05±0.01	0.06±0.02	-	-	-	-
Liver	0.47±0.05	0.44±0.09	0.33	0.33	0.68	0.53
Intestine	2.69±0.4	2.37±0.18	2.86	2.08	-	-
Muscle	2.06±0.30	1.86±0.16	1.50	3.20	1.40	2.80
Kidneys	0.48±0.08	0.37±0.01	0.47	0.47	0.60	0.47
Spleen	0.10±0.01	0.07±0.02	0.12	0.12	-	-
Urinary bladder	0.07±0.03	0.08±0.02	0.03	0.03	0.10	0.15
Lungs	0.21±0.05	0.24±0.05	0.25	0.25	-	-

5.1.3. Comparison of time-integrated activity coefficient or residence time with Dosimetry Toolkit

Dosimetry Toolkit is provided by SPECT/CT, GE Discovery NM/CT 670. Verification of toolkit was performed by comparing with the residence time resulted from the present study. Multi whole-body planar datasets were used for quantifying changes in radiopharmaceutical uptake over time and calculating residence time per organ in Dosimetry Toolkit. Time-activity curves were fitted to an exponential function by using least square fit. The accuracy of the Dosimetry Toolkit results depends heavily on user provided quantitative input, i.e. consecutive activity measurements, ROI drawing based on the operator experience

and registering of serial WB planar images. The time-integrated activity coefficients by manual integration of this study was comparable with Dosimetry Toolkit as good agreement (within 20%) for data measurements at 15 min, 2 h, 4 h and 24 h. However, for the data measurements at 15 min, 2 h and 4 h, the residence time resulted from Dosimetry Toolkit were lower than the manual integration because that toolkit has not taken into account the data between the injection time and first measurement and also beyond last measurement point. The comparison of residence time in 11 source organs with Dosimetry Toolkit was presented in table 5.2 for subject with last 24 h data and subject with last 4 h data.

Table 5.2 Comparison of residence time with calculated and Dosimetry Toolkit

For subject with 15 min, 2 h, 4 h and 24 h data measurements				For subject with 15 min, 2 h and 4 h data measurements			
Residence time ($\tilde{A}$/A0) (min)				Residence time ($\tilde{A}$/A0) (min)			
Organ	Cal:	Dosi: Toolkit	Diff; (%)	Organ	Cal:	Dosi: Toolkit	Diff; (%)
Heart	7.0	6.0	14	Heart	7.5	5.4	28
Liver	24.0	24.0	0	Liver	29.0	16.0	44
Salivary	2.4	2.2	4	Salivary	3.0	2.4	19
Thyroid	1.4	1.2	14	Thyroid	2.3	1.8	22
Kidneys	30.0	29.0	3	Kidneys	26.0	19.8	25
Spleen	2.5	2.4	4	Spleen	2.0	1.8	15
Gall Bladder	13.8	13.2	4	Gall Bladder	11.0	13.2	-27
Lungs	18.2	18.0	1	Lungs	10.0	4.8	55
Muscles	163.0	188.0	15	Muscles	166.0	88.8	46

Cal: calculated value, Dosi: Toolkit dosimetry toolkit, Diff: difference

Figure 5.2.1 shows the integration of area under the time-activity curve in residence time calculation for subject with 15 min, 2 h, 4 h and 24 h activity measurements . In that curve, data between measurements were interpolated by using an exponential equation. Therefore the area under the curve were integrated from time of injection to 24 h (dose-integration period).

Figure 5.2.2 shows the integration of area under the time-activity curve in residence time calculation for subject with 15 min, 2 h and 4 h activity measurements. In that curve, data between measurements (shaded red area) from 15 min to 4 h were interpolated by using an exponential equation but (a) the data between the injection time and first measurement and (b) the data beyond the last measurement were not taken into account. Therefore dosimetry toolkit would result in underestimation of residence time. Therefore Dosimetry Toolkit should be used when the measurement points would be covered three to four half-lives to avoid underestimation of residence time.
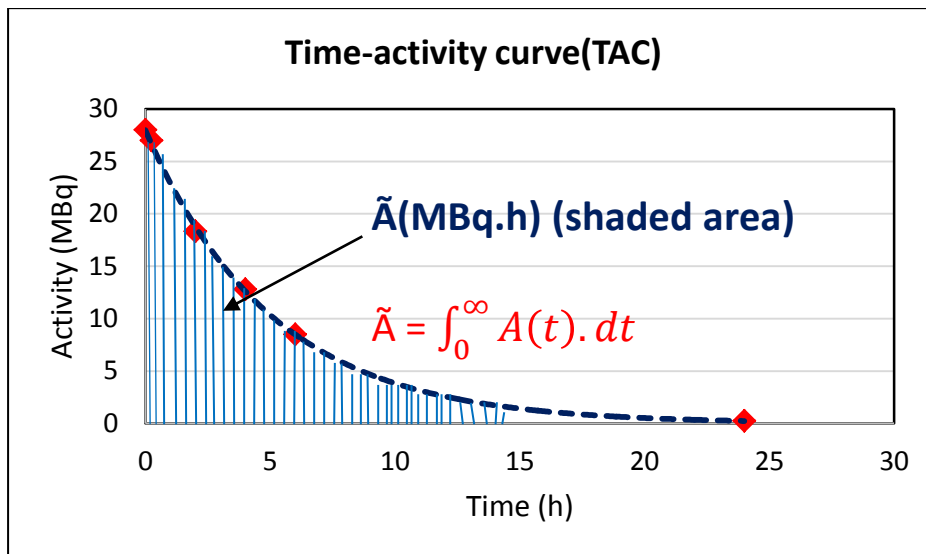
Figure 5.2.1 Integration of area under the curve in Dosimetry Toolkit calculation of residence time for subject with 15 min, 2 h, 4 h and 24 h activity measurements
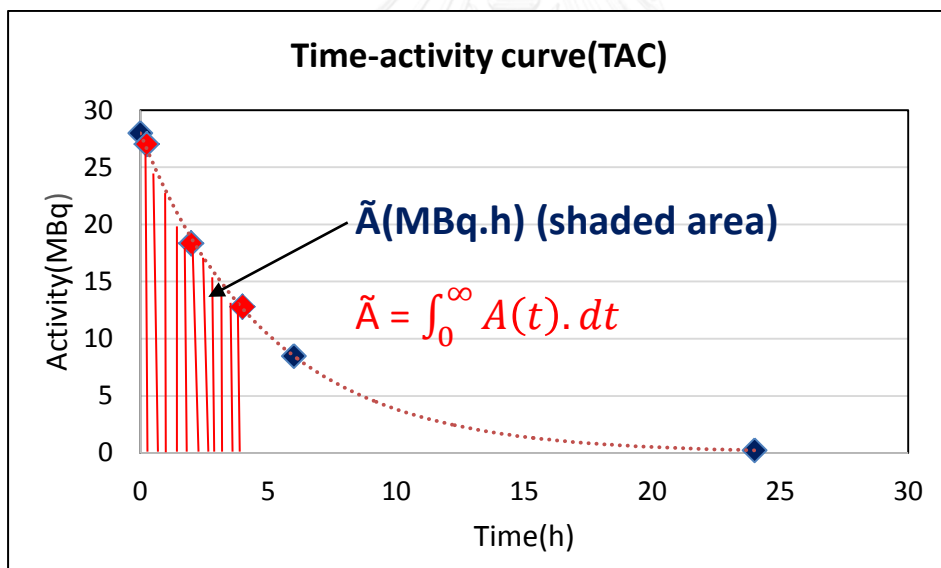
Figure 5.2.2 Integration of area under the curve in Dosimetry Toolkit calculation of residence time for subject with 15 min, 2 h, and 4 h activity measurements

5.1.4. Comparison of effective dose coefficient of MIBI of this study with published data

The comparison of effective dose coefficient (effective dose/injected activity) of MIBI between this study and ICRP publication 128 was summarized in table 5.3. In the present study, the effective doses were calculated based on organ masses of the Asian reference man [24] whereas the effective dose coefficient from ICRP publication 128 were estimated based on organ masses of Cristy and Eckerman phantom [30]. The difference between the body weight of Cristy and Eckerman

phantom and Asian reference man is 20 percent. The dose coefficient from ^{99m}Tc-MIBI in this study was higher than that of ICRP publication 128 around 20 percent in both rest and stress studies due to smaller organ masses of Asian reference man.

Table 5.3 Comparison of mean dose coefficient from ^{99m}Tc-MIBI of this study with ICRP publication 128

		This study	ICRP128 (2015)	Difference (%)
Reference man (kg)		60.0	73.7	-23.0
Mean dose coefficient(μSv/MBq)	Rest	11.6	9.0	22.0
	Stress	10.0	7.9	21.0

5.1.5. Comparison of effective dose from CT of this study with published data

In the present study, the effective dose from CT was calculated by using ImPACT program, Monte Carlo dose simulation tools for reference human phantoms. The results demonstrated that the effective dose from CT of myocardial perfusion SPECT/CT ranged from 0.9 mSv to 1.3 mSv (mean±SD, 1.14±0.11 mSv) for rest study and ranged from 0.9 mSv to 1.134 mSv (mean±SD, 1.12±0.13 mSv) for stress study. The comparison of effective dose, type of scanner and dose measurement methods between the present study and literatures was summarized in the Table 5.4.

Table 5.4 Comparison of effective dose from CT of this study with published data

Studies	Scanner	Mean effective dose (mSv)	Measurement methods	Number of Cases
This study	GE-Bright Speed (ELite)	1.14	Monte Carlo	20
Tootell A K et al. (BJR, 2015) [20]	GE Infinia Hawkeye (single slice)	1.90	TLD	Phantom
	GE Infinia Hawkeye (Four slice)	2.50	TLD	Phantom
	Siemens Symbia™ T6	1.80	TLD	Phantom
	Philips Precedence	3.00	TLD	Phantom
Montes C et al. (Annals of nuclear medicine, (2013) [22]	Siemens Symbia T2 Emotion Duo	1.20	DLP×k-factor	145

TLD-Thermoluminescent dosimeter, N/A Not applicable

5.1.6. Comparison of effective dose from myocardial perfusion SPECT/CT and related parameters with the published data

Table 5.5 summarized the comparison of effective doses from myocardial perfusion SPECT/CT and related parameters between the present study and published data. The mean effective doses from ^{99m}Tc-MIBI in this study were higher than that of the literature because of the higher injected activity in the present study. The weight based injected dose of 0.5 mCi/kg or 18.5 MBq/kg [31] were applied in the present study. Tootell et al. study followed the procedure guidelines and injected activity for myocardial perfusion imaging adopted by the British Cardiac Society, the British Nuclear Cardiology Society and the British Nuclear Medicine Society [32]. In this procedure guideline, the maximum allowable dose for myocardial perfusion scan was a total of 1600 MBq (divided as 400 MBq and 1200 MBq) for one-day stress/rest protocol or 800 MBq on each day of two-day protocol. The latest guideline for SPECT nuclear cardiology had been updated by American Society of Nuclear Cardiology (ASNC) on 25 February 2016 [11]. They recommend that 8-12 mCi (296-444 MBq) of injected dose for each rest and stress study of two-day protocol and suggested that for high-efficiency cameras, newer technology reduced-dose protocols of 4-6 mCi (148-222 MBq) of injected dose for each rest and stress study for two-day protocol should be studied for optimization of myocardial perfusion imaging.

Moreover, since S-values in this study were modified based on organ masses of Asian reference man, the smaller the organ masses, the higher the dose. Therefore the mean absorbed doses to the target organs are relatively higher than the literature that based on organ masses of ICRP reference man [20].

It was found that the lower tube current and tube rotation time in the present study were applied rather than the other studies. All of the CT acquisition parameters were fixed for all myocardial perfusion SPECT/CT except scan length with patient's height. The effective doses from CT in this study were lower than that of the literature.

5.1.7. BERT in relation with effective dose from myocardial perfusion imaging

As the effective dose is not a magnitude that is easily understood by patients and the population in general, it was compared with the background radiation level to provide an equivalent BERT estimate. Three mSv is considered to be the worldwide average annual background radiation exposure. The equivalent for effective dose from rest study of MPI was ranged from 3.25 years to 4.50 years of background radiation exposure, and that for stress study ranged between 2.28 and 3.82 years of background radiation exposure. American College of Radiologists (ACR) and Radiological Society of North American (RSNA) have been updated qualitative risk levels in relation to background equivalent radiation time (BERT) [Appendix H]. As this recommendation, each rest and stress study involve low risk (1 in 10000 to 1 in 1000) and both studies were associated with moderate risk (1 in 500 to 1 in 1000). To maintain the benefit-risk balance, protocols for myocardial perfusion imaging should be optimized as recommendations.

5.1.8. Factors affecting effective doses from myocardial perfusion SPECT/CT

The results showed that the significant correlation between the effective doses from ^{99m}Tc-MIBI and injected activity, r=0.922 for rest and r=0.928 for stress (p-value<0.01), also patient's body weight, r= 0.749 for rest and r= 0.800 for stress study (p-value< 0.01). Therefore, for the optimization of myocardial perfusion SPECT/CT, the injected activity should be maintained as low as reasonably achievable but high enough to obtain the desired diagnostic information while maintaining the benefit-risk-balance.

For the effective dose from CT, the effective doses increase with increasing the scan length with good correlation r=0.968 for rest and r=0.987 for stress study (p-value<0.01). The correlation between effective doses and patient's height were good, r=0.847 for rest and r=0.881 for stress study. Other fixed parameters such as tube voltage (kVp), tube current (mA), tube rotation time, pitch, and slice collimation had not been investigated for correlation with effective dose. Applying an AEC method in the CT scan is benefit to small patient size such as Asian people for the optimization of myocardial perfusion imaging in aspect of CT. This technique not only reduces the patient dose, but also preserves the image quality.

Table 5.5 Comparison of effective dose from myocardial perfusion SPECT/CT and related parameters with the published data

MPI	This study		Leide et al [21]		Tootell el al [20]	
	SPECT/CT		SPECT		SPECT/CT	
	Rest	Stress	Rest	Stress	Rest	Stress
Injected activity (MBq)	935±60	886±109	700	500	800	800
S-value	Asian reference man (60kg)		ICRP reference man (70kg)		Cristy and Eckerman (73kg)	
Γ_E^{MIBI} (µSv/MBq)	11.64±0.7	10.18±0.4	12	9.8	9.5 (ICRP 80)	7.9 (ICRP 80)
^{99m}Tc-MIBI effective dose (mSv)	10.85±1.2	9.01±1.3	8.4	4.9	7.2	6.4
CT parameters	20 mAs 5mm slice thickness 0.8sec	20mAs 5mm slice thickness 0.8sec	N/A	N/A	30 mAs 5mm slice thickness 1.5sec	30 mAs 5mm slice thickness 1.5 sec
CT effective dose (mSv)	1.14±0.11	1.12±0.13	N/A	N/A	3	3
Total effective dose (mSv)	11.99±1.2	10.35±1.2	8.4	4.9	10.2	9.4

Note: Γ_E^{MIBI} dose coefficient, N/A - Not applicable

5.2 Conclusions

Though the patient radiation dose computed by various techniques from SPECT/CT examination reported estimates of the exposure level, the dosimetry using patient-specific biokinetics data and parameters can provide more realistic biological consequences to the patients. The organ and effective dose estimated in this study would be worthwhile in estimating risk of radiation-induced cancer from myocardial perfusion SPECT/CT.

From 10 patients who underwent rest study of myocardial perfusion SPECT/CT examinations at King Chulalongkorn Memorial Hospital, the mean effective dose was 11.99±1.2 mSv, ranged from 9.75 mSv to 13.49 mSv and related mean BERT was 3.99±0.4 years, ranged from 3.25 years to 4.50 years. From 10 patients who underwent stress study of myocardial perfusion SPECT/CT was 10.35±1. 2mSv, ranged from 6.83mSv to 11.45 mSv and related BERT was 3.5±0.2 years, ranged from 2.28 years to 3.82 years respectively. The mean effective dose coefficient of ^{99m}Tc-MIBI in rest study was 11.64±0.7 μSv/MBq, ranged from 10.3 μSv/MBq to 12.4 μSv/MBq. The mean effective dose coefficient of ^{99m}Tc-MIBI in stress study was 10.18±0.6 μSv/MBq, ranged from 9.3 μSv/MBq to 10.7 μSv/MBq. These dose coefficients of ^{99m}Tc-MIBI in this study can be used as the reference for the Asian population for determination of patient radiation dose from myocardial perfusion imaging. Furthermore, the specific dosimetric information in the present study assists in the justification of risk and optimization of myocardial perfusion imaging.

According to ACR and RSNA recommendation, each rest and stress of this study was associated with low risk (1 per 1000 to 10,000 of investigated patients may have risk of radiation-induced cancer) and both rest and stress studies were associated with moderate risk (1 per 500 to 1000 of investigated patients may have risk of radiation-induced cancer).

In conclusion, the effective dose received from non-invasive imaging of ^{99m}Tc-MIBI SPECT/CT should be accepted for the patient benefit in an urgent management of cardiovascular disease rather than the cancer risk occurs at the later age.

5.3 Recommendations

For the optimization of myocardial perfusion SPECT/CT

- The injected activity should be maintained as low as reasonably achievable but high enough to obtain the desired diagnostic information while maintaining the benefit-risk-balance. The optimal range of injected activity with desired image quality should be investigated for the Asian population in the future studies.
- Methods for accelerated excretion such as laxatives, hydration and frequent voiding of the urinary bladder should be encouraged if possible to reduce the radiation dose to the patients.
- In the aspect of CT, the reduction of the radiation dose can be done by adjusting the acquisition parameters such as kVp, mA, tube rotation time, pitch, and slice thickness as well as the routine use with AEC. The low-dose CT protocol for the myocardial perfusion imaging should be investigated for the further study in order to reduce the patient dose substantially.

REFERENCES

[1]   Mozaffarian D, Benjamin EJ, Go AS, Arnett DK, Blaha MJ, Cushman M, et al. Heart disease and stroke statistics-2015 update: a report from the American Heart Association. Circulation 2015;131:e29-322.

[2]   Kaufmann PA. Cardiac hybrid imaging: state-of-the-art. Ann Nucl Med 2009;23:325-31.

[3]   Nguyen PK, Wu JC. Radiation exposure from imaging tests: is there an increased cancer risk? Expert Rev Cardiovasc Ther 2011;9:177-83.

[4]   Radiation exposure from x-ray examinations. Available at : http://www.radiologyinfo.org/en/safety/index.cfm?pg=sfty_xray. [cited August 26, 2010].

[5]   Hall EJ. Radiobiology for the radiologist . Hagerstown, Md. :Medical Dept., Harper & Row,1973.

[6]   Radiation exposure from x-ray examinations. Available at : https://www.radiologyinfo.org/en/pdf/safety-hiw_07.pdf [cited August 26, 2010].

[7]   Health Physics Society. Radiation term and definitions. Available at : http://hps.org/publicinformation/radterms/ [cited November 28, 2005].

[8]   Douglas LM, Douglas PZ, Peter L, Robert OB. Heart disease : a textbook of cardiovascular medicine: Tenth edition. Philadelphia, PA : Elsevier/Saunders, [2015] ©2015; 2015.

[9]   Zaret BL, Beller GA. Clinical Nuclear Cardiology: State of the Art and Future Directions, fourth ed: ELSEVIER; 2010.

[10]   Dvorak RA, Brown RK, Corbett JR. Interpretation of SPECT/CT myocardial perfusion images: common artifacts and quality control techniques. Radiographics 2011;31:2041-57.

[11]   Henzlova MJ, Duvall WL, Einstein AJ, Travin MI, Verberne HJ. ASNC imaging guidelines for SPECT nuclear cardiology procedures: Stress, protocols, and tracers. J Nucl Cardiol 2016;23:606-39.

[12]   Berne RM. The role of adenosine in the regulation of coronary blood flow. Circ Res 1980;47:807-13.

[13]   Hwang BH, Kim MH, Chang K. Molecular imaging of high-risk atherosclerotic plaques: is it clinically translatable? Korean Circ J 2011;41:497-502.

[14]   Bolch WE, Eckerman KF, Sgouros G, Thomas SR. MIRD pamphlet No. 21: a generalized schema for radiopharmaceutical dosimetry--standardization of nomenclature. J Nucl Med 2009;50:477-84.

[15]   Stabin MG, Siegel JA. Physical models and dose factors for use in internal dose assessment. Health Phys 2003;85:294-310.

[16]   Snyder WS, Ford MR, Warner GG, Watson SB. MIRD Pamphlet No.11: S, Absorbed Dose per Unit Cumulated Activity for Selected Radionuclides and Organs (PART 2). Society of Nuclear Medicine 1975.

[17]   Snyder WS, Fisher HL, Jr., Ford MR, Warner GG. Estimates of absorbed fractions for monoenergetic photon sources uniformly distributed in various organs of a heterogeneous phantom. J Nucl Med 1969:Suppl 3:7-52.

[18]   Icrp. 1990 Recommendations of the International Commission on Radiological Protection. ICRP Publication 60. Ann ICRP 1991b;21:1-3.

[19]   GE Healthcare.Organ Dose estimates for Radio-Isotope Therapy treatment planning purposes. 2011.

[20]   Tootell AK, Szczepura K, Hogg P. Comparison of effective dose and lifetime risk of cancer incidence of CT attenuation correction acquisitions and radiopharmaceutical administration for myocardial perfusion imaging. Br J Radiol 2014;87:20140110.

[21]   Leide S, Diemer H, Ahlgren L, Mattsson S. In vivo distribution and dosimetry of Tc-99m MIBI in man. In: S-Stelson A, Watson EE, editors. Fifth International Radiopharmaceutical Dosimetry Symposium: CONF-910529. Oak Ridge, TN: Oak Ridge Associated Universities; 1992. p. 483-97.

[22]   Montes C, Tamayo P, Hernandez J, Gomez-Caminero F, Garcia S, Martin C, et al. Estimation of the total effective dose from low-dose CT scans and radiopharmaceutical administrations delivered to patients undergoing SPECT/CT explorations. Ann Nucl Med 2013;27:610-7.

[23]   Radiation Dose Assessment Resource (RADAR). Available at :http://www.doseinfo-radar.com [cited December 17, 2011].

[24]   Tanaka G, Kawamura H. Reference man models based on normal data from human populations. Available at : http://www.irpa.net/irpa10/cdrom/00602.pdf 2011 [cited 2011 24 June].

[25]   ICRP. The 2007 Recommendations of the International Commission on Radiological Protection. ICRP publication 103. Ann ICRP 2007;37:1-332.

[26]   National Research Council Committee on Health Effects of Exposure to Low Levels of Ionizing R. Health Effects of Exposure to Low Levels of Ionizing Radiations: Time for Reassessment? Washington (DC): National Academies

Press (US)Copyright 1998 by the National Academy of Sciences. All rights reserved.; 1998.

[27]   Wackers FJ, Berman DS, Maddahi J, Watson DD, Beller GA, Strauss HW, et al. Technetium-99m hexakis 2-methoxyisobutyl isonitrile: human biodistribution, dosimetry, safety, and preliminary comparison to thallium-201 for myocardial perfusion imaging. J Nucl Med 1989;30:301-11.

[28]   Radiation dose to patients from radiopharmaceuticals (addendum 2 to ICRP publication 53). Ann ICRP 1998;80:1-126.

[29]   Mattsson S, Johansson L, Leide Svegborn S, Liniecki J, Nosske D, Riklund KA, et al. Radiation Dose to Patients from Radiopharmaceuticals: a Compendium of Current Information Related to Frequently Used Substances. Ann ICRP 2015;44:7-321.

[30]   Cristy M, Eckerman KF. Specific absorbed fractions of energy at various ages from internal photons sources Oak Ridge National Lab., TN (USA)1987.

[31]   Treves ST, Davis RT, Fahey FH. Administered radiopharmaceutical doses in children: a survey of 13 pediatric hospitals in North America. J Nucl Med 2008;49:1024-7.

[32]   Arumugam P, Harbinson M, Reyes E, Sabharwal N, Tonge C, SR U. Procedure guidelines for radionuclide myocardial perfusion imaging with single-photon emission computed tomography (SPECT) 2012 [cited 2014 22 July].

APPENDICES

APPENDIX A

Table A.1: Masses of the target organs and tissues (unit: gram)

Organ	Organ masses of Asian Reference man
Adrenals[2]	14
Bone	4500
Brain	1470
Breasts[2]	300
Gall Bladder	8
Heart	380
Kidneys[2]	320
Liver	1600
LLI	150
Lungs[2]	1200
Muscles (skeletal)	25000
Salivary	72
Pancreas	130
Red marrow	1000
Skin	2400
Small intestine	590
Spleen	140
Stomach	140
Thymus	30
Thyroid[2]	19
ULI	180
Urinary Bladder	40
Uterus	70
Prostate	12

APPENDIX B

Certificate of approval from Institutional Review Board (IRB) of Faculty of Medicine, Chulalongkorn University, Bangkok, Thailand

COA No. 577/2016

IRB No. 299/59

INSTITUTIONAL REVIEW BOARD

Faculty of Medicine, Chulalongkorn University

1873 Rama 4 Road, Patumwan, Bangkok 10330, Thailand, Tel 662-256-4493

Certificate of Approval

The Institutional Review Board of the Faculty of Medicine, Chulalongkorn University, Bangkok, Thailand, has approved the following study which is to be carried out in compliance with the International guidelines for human research protection as Declaration of Helsinki, The Belmont Report, CIOMS Guideline and International Conference on Harmonization in Good Clinical Practice (ICH-GCP)

Study Title : Estimation of Effective Dose to Patients Undergoing Myocardial Perfusion SPECT/CT.

Study Code : -

Principal Investigator : Miss Hnin Nitar

Affiliation of PI : Department of Radiology, Faculty of Medicine, Chulalongkorn University.

Review Method : Expedited

Continuing Report : At least once annually or submit the final report if finished.

Document Reviewed :

1. THESIS PROPOSAL Version 2.0 Date 11 July 2016
2. Protocol Synopsis Version 2.0 Date 11 July 2016
3. Information sheet for research participant Version 2.0 Date 11 July 2016
4. Informed Consent Form Version 2.0 Date 11 July 2016
5. Case Record form Version 1.0 Date 1 April 2016
6. Principle investigator's CV Version 1.0 Date 1 April 2016
7. GCP Training

Signature:... Signature:...

(Emeritus Professor Tada Sueblinvong MD)   (Assistant Professor Prapapan Rajatapiti MD, PhD)

Chairperson   Member and Secretary

The Institutional Review Board   The Institutional Review Board

Date of Approval : July 27, 2016

Approval Expire Date : July 26, 2017

Approval granted is subject to the following conditions: (see back of this Certificate)

APPENDIX C

Case record form of myocardial perfusion SPECT/CT

Date of Exam:

Patient No: ………………

Type of exam (rest/stress): …………..

Age: ……………… (Years)

Sex: ……………

Height: ……… (cm)   Weight: ………………… (kg)

Body Mass Index: ………… (kg/m^2)

Injected Activity: ………… (MBq)   Injection time:..…………

Start scan time: ……………   Finish scan time: …………..

Scan Length: ………………… (cm)

CTDI$_{vol}$:…………………….(mGy)   DLP …………… (mGy.cm)

APPENDIX D

Patient Consent Form

การวิจัยเรื่อง..การประเมินปริมาณรังสียังผลในผู้ป่วยจากการตรวจกล้ามเนื้อหัวใจด้วยเครื่องสเปก-ซีที (SPECT-CT)

....

วันให้คำยินยอม วันที่.............เดือน.......................................พ.ศ..

        ข้าพเจ้า นาย/นาง/นางสาว...ที่

อยู่...ได้อ่านรายละเอียดจากเอกสารข้อมูล

สำหรับผู้เข้าร่วมโครงการวิจัยวิจัยที่แนบมาฉบับวันที่.................................. และข้าพเจ้ายินยอมเข้าร่วมโครงการวิจัยโดยสมัครใจ

        ข้าพเจ้าได้รับสำเนาเอกสารแสดงความยินยอมเข้าร่วมในโครงการวิจัยที่ข้าพเจ้าได้ลงนาม และ วันที่ พร้อมด้วยเอกสารข้อมูล สำหรับผู้เข้าร่วมโครงการวิจัย ทั้งนี้ก่อนที่จะลงนามในใบยินยอมให้ทำการวิจัยนี้ ข้าพเจ้าได้รับการอธิบายจากผู้วิจัยถึงวัตถุประสงค์ของ การวิจัย ระยะเวลาของการทำวิจัย วิธีการวิจัย อันตราย หรืออาการที่อาจเกิดขึ้นจากการวิจัย หรือจากยาที่ใช้รวมทั้งประโยชน์ที่จะ เกิดขึ้นจากการวิจัยและแนวทางรักษาโดยวิธีอื่นอย่างละเอียด ข้าพเจ้ามีเวลาและโอกาสเพียงพอในการซักถามข้อสงสัยจนมีความเข้าใจ อย่างดีแล้ว โดยผู้วิจัยได้ตอบคำถามต่าง ๆ ด้วยความเต็มใจไม่ปิดบังซ่อนเร้นจนข้าพเจ้าพอใจ

        ข้าพเจ้ารับทราบจากผู้วิจัยว่าหากเกิดอันตรายใด ๆ จากการวิจัยดังกล่าว ข้าพเจ้าจะได้รับการรักษาพยาบาลโดยไม่เสีย ค่าใช้จ่าย และจะได้รับการชดเชยจากผู้สนับสนุนการวิจัย

        ข้าพเจ้ามีสิทธิที่จะบอกเลิกเข้าร่วมในโครงการวิจัยเมื่อใดก็ได้ โดยไม่จำเป็นต้องแจ้งเหตุผล และการบอกเลิกการเข้าร่วมการ วิจัยนี้ จะไม่มีผลต่อการรักษาโรคหรือสิทธิอื่น ๆ ที่ข้าพเจ้าจะพึงได้รับต่อไป

        ผู้วิจัยรับรองว่าจะเก็บข้อมูลส่วนตัวของข้าพเจ้าเป็นความลับ และจะเปิดเผยได้เฉพาะเมื่อได้รับการยินยอมจากข้าพเจ้า เท่านั้น บุคคลอื่นในนามของบริษัทผู้สนับสนุนการวิจัย คณะกรรมการพิจารณาจริยธรรมการวิจัยในคน สำนักงานคณะกรรมการอาหาร และยาอาจได้รับอนุญาตให้เข้ามาตรวจและประมวลข้อมูลของข้าพเจ้า ทั้งนี้จะต้องกระทำไปเพื่อวัตถุประสงค์เพื่อตรวจสอบความ ถูกต้องของข้อมูลเท่านั้น โดยการตกลงที่จะเข้าร่วมการศึกษานี้ข้าพเจ้าได้ให้คำยินยอมที่จะให้มีการตรวจสอบข้อมูลประวัติทาง การแพทย์ของข้าพเจ้าได้

        ผู้วิจัยรับรองว่าจะไม่มีการเก็บข้อมูลใด ๆ เพิ่มเติม หลังจากที่ข้าพเจ้าขอยกเลิกการเข้าร่วมโครงการวิจัยและต้องการให้ ทำลายเอกสารและ/หรือ ตัวอย่างที่ใช้ตรวจสอบทั้งหมดที่สามารถสืบค้นถึงตัวข้าพเจ้าได้

        ข้าพเจ้าเข้าใจว่า ข้าพเจ้ามีสิทธิที่จะตรวจสอบหรือแก้ไขข้อมูลส่วนตัวของข้าพเจ้าและสามารถยกเลิกการให้สิทธิในการใช้ ข้อมูลส่วนตัวของข้าพเจ้าได้ โดยต้องแจ้งให้ผู้วิจัยรับทราบ

        ข้าพเจ้าได้ตระหนักว่าข้อมูลในการวิจัยรวมถึงข้อมูลทางการแพทย์ของข้าพเจ้าที่ไม่มีการเปิดเผยชื่อ จะผ่านกระบวนการต่าง ๆ เช่น การเก็บข้อมูล การบันทึกข้อมูลในแบบบันทึกและในคอมพิวเตอร์ การตรวจสอบ การวิเคราะห์ และการรายงานข้อมูลเพื่อ วัตถุประสงค์ทางวิชาการ รวมทั้งการใช้ข้อมูลทางการแพทย์ในอนาคตหรือการวิจัยทางด้านเภสัชภัณฑ์ เท่านั้น

        ข้าพเจ้าได้อ่านข้อความข้างต้นและมีความเข้าใจดีทุกประการแล้ว ยินดีเข้าร่วมในการวิจัยด้วยความเต็มใจ จึงได้ลงนามใน เอกสารแสดงความยินยอมนี้

                ....ลงนามผู้ให้ความยินยอม

                (..) ชื่อผู้ยินยอมตัวบรรจง

                วันที่ ....เดือน...................................พ.ศ..........................

        ข้าพเจ้าได้อธิบายถึงวัตถุประสงค์ของการวิจัย วิธีการวิจัย อันตราย หรืออาการไม่พึงประสงค์หรือความเสี่ยงที่อาจเกิดขึ้น
จากการวิจัย หรือจากยาที่ใช้ รวมทั้งประโยชน์ที่จะเกิดขึ้นจากการวิจัยอย่างละเอียด ให้ผู้เข้าร่วมในโครงการวิจัยตามนามข้างต้นได้
ทราบและมีความเข้าใจดีแล้ว พร้อมลงนามลงในเอกสารแสดงความยินยอมด้วยความเต็มใจ

        ....ลงนามผู้ทำวิจัย

        (..) ชื่อผู้ทำวิจัย ตัวบรรจง

        วันที่ ....เดือน..................................พ.ศ...........................

        ....ลงนามพยาน

        (..) ชื่อพยาน ตัวบรรจง

        วันที่ ....เดือน..................................พ.ศ...........................

        ....

APPENDIX E

Quality Control of research equipment

Daily Quality Control

1.1 Part of SPECT

The daily quality control for SPECT and CT was regularly performed. For SPECT system, background count rate, energy peak, extrinsic energy resolution and extrinsic uniformity were evaluated as daily QC tests. The weekly QC is center of rotation (COR) test which must be accurately aligned with the center of the acquisition matrix in the computer. The x-ray CT tube warm-up and fast calibration were performed daily. The results of daily quality control from August, 2016 to March, 2017 are presented from Table E.1 to Table E.8.

Background count rate check

Purpose: To check the background radiation activity before starting QC tests.

Methods: It was sure that there are no radioactive sources (including the daily QC source) or injected patients in the scan room and acquired with 60sec acquisition time and 256x256 matrices.

Tolerance: Count rate < 1.5 kcts/sec.

Results: The results for background count rate check are summarized in report of daily quality control from August 2016 to March 2017.

Comment: PASS

Energy window check (Peaking)

Purpose: To check the correct energy setting (i.e. a photo peak in the center of the energy window).

Materials: [57]Cobalt sheet source
           Flood holder

Methods: With the detectors in H-mode, the flood holder was placed on the lower detector so that the legs straddle the contour mechanism.[57] Cobalt flood source was placed on the holder. Both detectors tested simultaneously with LEHR collimators, energy session of Co-57   and start position of H QC D1D2. Check the energy spectrum and ensure that a 15-20% energy window is peaked on the main photopeak at 122keV. Verify that persistence image and energy graph are acceptable. The results of energy window check test were assessed automatically.

Tolerance: Energy peak, [keV] - 122±3

Figure E.1: Image quality test by using ^{57}Co Flood source

Results: The results for energy window check (peaking) are summarized in report of daily quality control from August 2016 to March 2017.
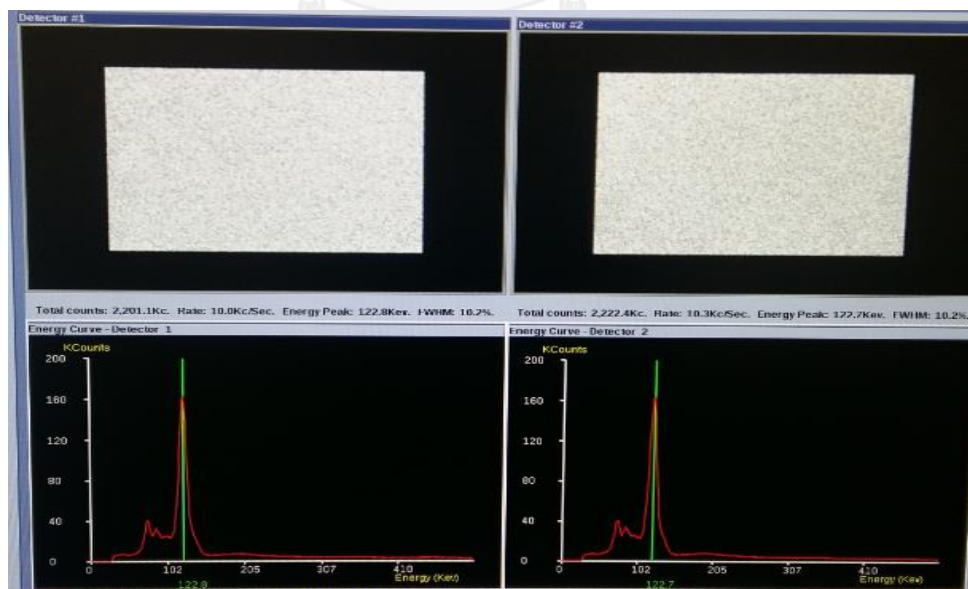
Figure E.2: Energy Spectrum of Co-57

Comment: PASS.

Extrinsic energy resolution

Purpose: To test the system energy resolution.

Methods: Set up the ^{57}Co flood source and acquisition parameters as energy window check (peaking). The results of energy resolution test were assessed automatically.

Tolerance: Energy Resolution, FWHM, [%] $\leq$ 12.0.

Results: The results for energy window check (peaking) are summarized in report of daily quality control from August 2016 to March 2017.
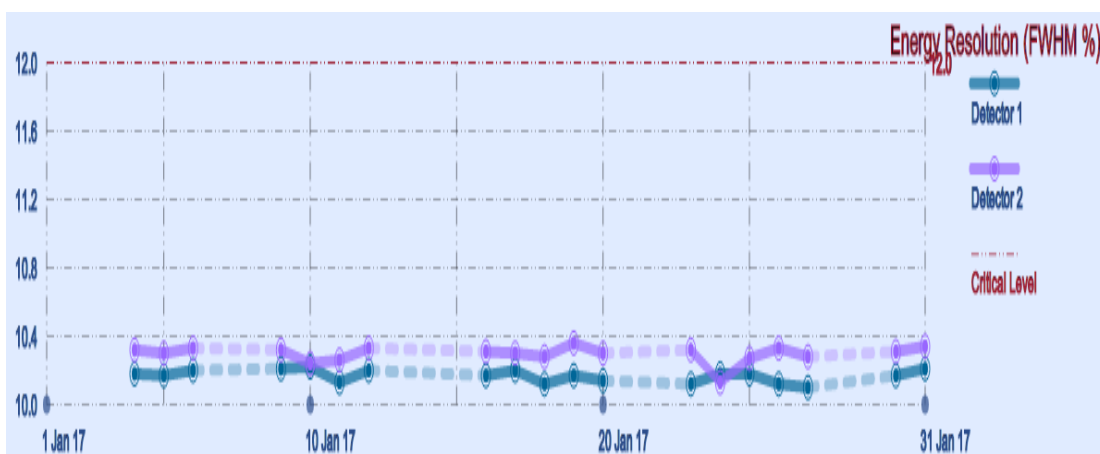
Figure E.3: Report for extrinsic energy resolution (FWHM) on January, 2017

Comment: PASS

Extrinsic uniformity

Purpose: To check the flood field uniformity of scintillation camera

Methods: Set up the ^{57}Co flood source and acquisition parameters as energy window check (peaking). The results of uniformity test were assessed automatically.

Tolerance: Uniformity @ CFOV, [%] $\leq$ 5.0

Uniformity @ UFOV, [%] $\leq$ 5.5

Results: The results for energy window check (peaking) are summarized in report of daily quality control from August 2016 to February 2017.
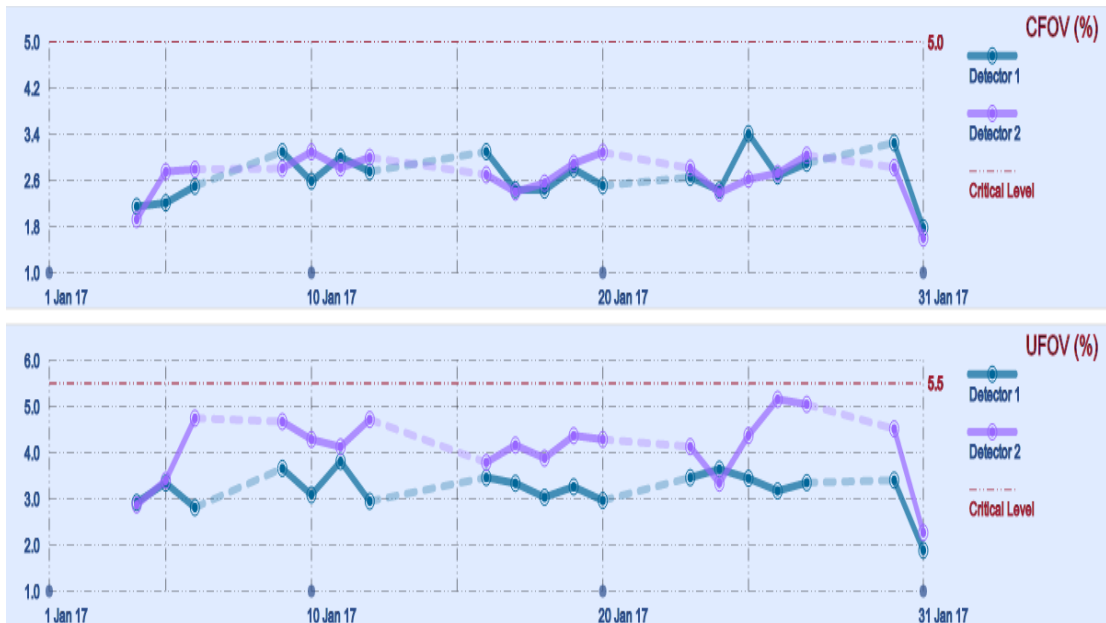
Figure E.4: Report for extrinsic energy resolution (FWHM) on January, 2017

Comment: PASS

1.2 Part of CT

X-ray Tube Warm up
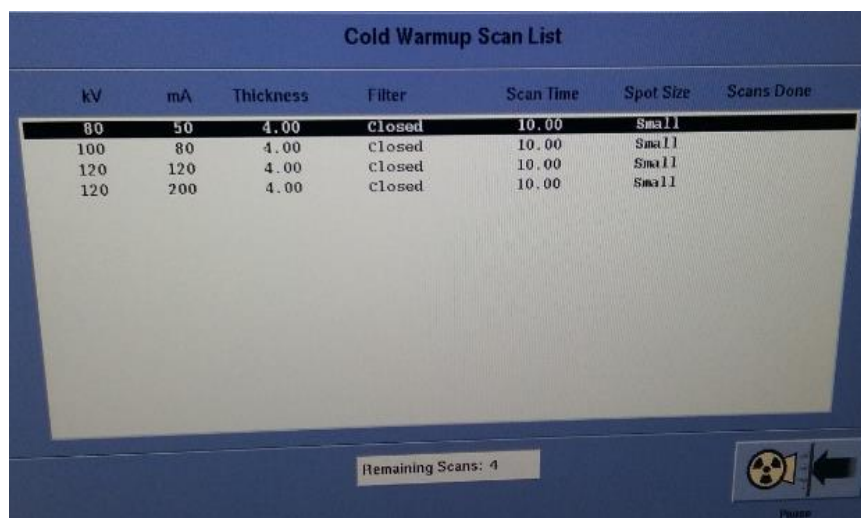
Warm-up provides an automated group of low technique exposures designed to safely bring the X-Ray tube to operating temperature before you start to scan for the day. Warm-up increase tube life and help produce more consistent, quality images.

Purpose: To warm up the CT tube in order to obtain optimal image quality and long tube life prior to quality control or calibration procedures.

Method: Make sure gantry area is clear of all objects and personnel. System up and running. Position the gantry to 0 degree tilt. Perform an x-ray tube warm up if the x-ray tube has not been used for more than two hours, before Fast cal, before Cal check and before system calibration

Tolerance: if no error messages received, the system is ready for CT scanning.

Comment: PASS

Figure E.5: X-ray tube warm-up
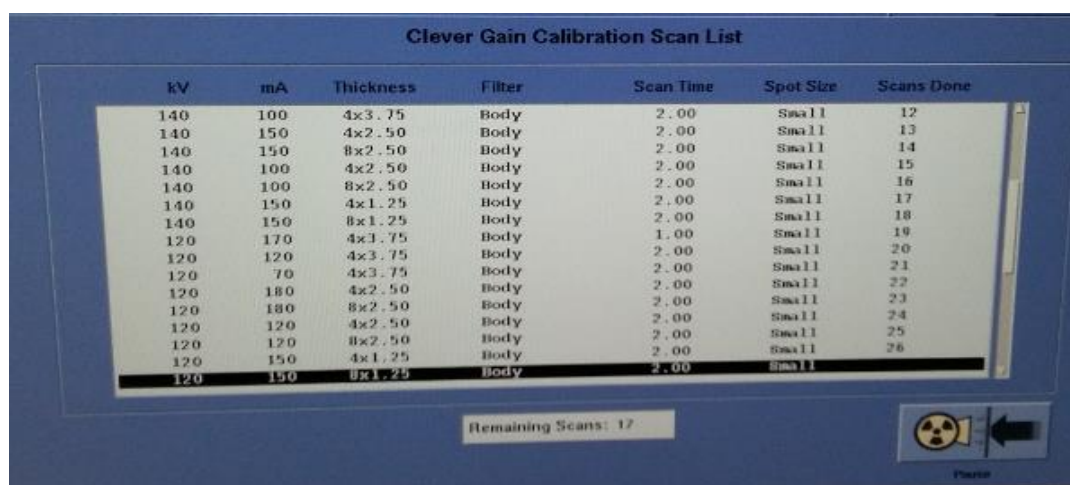
CT air calibration (Fast calibration)

Purpose: To ensure consistent image quality and radiation exposure

Method: Raise the table above the patient loading level. After tube warm up have been completed, CT air calibration (Fast calibration) was performed with every possible combination of kV, detector row thickness, focal spot size, and scan field of view. After pressing <Start Scan>, the system automatically selects the Auto Scan function and runs the following sequence of scans: (a) Mylar Window Check (b) Cold Warm-up (c) Warm-up 1 (d) Warm-up 2 (d) Collimation Cal (e) FPA Check Scans (f) Clever gain calibration and (g) Fast calibration. The system instructions were followed to initiate the first scan, and the system acquired the rest of the scan set.

Tolerance: if no error messages received, the system is ready for CT scanning.

Comment: PASS

Figure E.6: CT air calibration (Fast calibration

2. Report of daily quality control of research equipment

Table E.1: The results of quality control on August, 2016

Date	CT		Background (kc/s)		Energy Peak (keV)		Energy Res. (FWHM %)	Uniformity Det 1 (%)		Uniformity Det 2 (%)		Comment	Temp (C)	Humd (%)
	Warm up	Fast cal	Det 1	Det 2	Det 1	Det 2	Det 1	CFOV	UFOV	CFOV	UFOV			
1/8/16	P	P	0.31	0.34	123.50	124.03	10.55	18.20	3.22	3.22	3.03	5.10	P	18.20	72.00
2/8/16	P	P	0.31	0.34	123.45	124.12	10.51	18.00	2.51	2.79	2.11	3.06	P	18.00	70.00
3/8/16	P	P	0.31	0.34	123.44	124.17	10.60	18.00	2.78	2.32	3.05	3.91	P	18.00	68.00
4/8/16	P	P	0.31	0.34	123.44	124.17	10.57	18.00	3.08	3.08	2.90	4.12	P	18.00	71.00
5/8/16	P	P	0.24	0.27	123.45	124.16	10.62	20.00	3.28	3.28	2.75	4.15	P	20.00	68.00
8/8/16	P	P	0.31	0.34	123.51	124.17	10.49	19.00	2.61	2.64	3.50	4.14	P	19.00	71.00
9/8/16	P	P	0.31	0.34	123.55	124.21	10.55	20.00	2.91	3.02	3.10	5.02	P	20.00	64.00
10/8/16	P	P	0.31	0.34	123.53	124.23	10.56	19.00	3.16	3.16	2.45	4.23	P	19.00	66.00
11/8/16	P	P	0.31	0.34	123.56	124.25	10.57	20.00	3.26	3.26	3.69	5.31	P	20.00	67.00
15/8/16	P	P	0.31	0.34	123.60	124.31	10.58	19.00	3.37	3.45	3.10	5.33	P	19.00	65.00
16/8/16	P	P	0.31	0.34	123.64	124.36	10.60	19.00	2.87	3.11	3.43	4.93	P	19.00	64.00
17/8/16	P	P	0.31	0.35	123.66	124.36	10.52	21.00	2.99	3.73	3.04	4.47	P	21.00	61.00
18/8/16	P	P	0.31	0.34	123.63	124.34	10.52	20.00	3.02	3.78	3.91	5.48	P	20.00	64.00
19/8/16	P	P	0.31	0.34	123.58	124.38	10.59	19.00	3.05	3.05	2.91	4.97	P	19.00	67.00
22/8/16	P	P	0.31	0.34	123.62	124.46	10.64	0.00	3.23	3.58	3.17	4.57	P	0.00	0.00
23/8/16	P	P	0.31	0.35	123.72	124.40	10.60	21.00	2.89	3.31	3.29	4.72	P	21.00	60.00
24/8/16	P	P	0.31	0.34	123.72	124.45	10.58	20.00	3.09	3.44	4.08	5.20	P	20.00	65.00
25/8/16	P	P	0.31	0.35	123.72	124.41	10.55	20.00	3.08	3.38	3.59	4.48	P	20.00	63.00
26/8/16	P	P	0.31	0.35	122.32	122.33	10.42	20.00	2.89	3.13	3.21	4.32	P	20.00	66.00
29/8/16	P	P	0.31	0.34	123.84	124.55	10.58	20.00	2.62	3.52	3.25	4.98	P	20.00	65.00
30/8/16	P	P	0.31	0.34	122.32	122.33	10.42	20.00	2.89	3.13	3.21	4.32	P	20.00	63.00
31/8/16	P	P	0.31	0.35	122.36	122.29	10.36	20.00	2.65	2.78	2.72	3.77	P	20.00	67.00

FWHM - full width at half maximum, Energy Res- Energy resolution, Det 1- detector1, Det 2- detector2, P- pass.
Comment: PASS

Table E.2: The results of quality control on September, 2016

Date	CT		Background (kc/s)		Energy Peak (keV)		Energy Res. (FWHM %)		Uniformity Det 1 (%)		Uniformity Det 2 (%)		Comment	Temp (C)	Humd (%)
	Warm up	Fast cal	Det 1	Det 2	Det 1	Det 2	Det 1	Det 2	CFOV	UFOV	CFOV	UFOV			
1/9/16	P	P	0.31	0.35	122.30	122.40	10.28	10.44	2.83	3.19	2.66	4.14	P	20.00	65.00
2/9/16	P	P	0.31	0.34	122.40	122.40	10.34	10.43	2.95	3.49	2.80	3.71	P	21.00	64.00
5/9/16	P	P	0.30	0.35	122.50	122.50	10.29	10.42	2.94	3.34	2.63	4.31	P	20.00	64.00
6/9/16	P	P	0.30	0.35	122.50	122.50	10.28	10.45	2.36	3.10	2.20	3.28	P	22.00	64.00
7/9/16	P	P	0.30	0.35	122.50	122.50	10.30	10.43	2.32	3.02	2.29	2.85	P	20.00	65.00
8/9/16	P	P	0.30	0.35	122.50	122.50	10.31	10.38	2.88	3.52	2.44	3.46	P	20.00	65.00
9/9/16	P	P	0.31	0.34	122.50	122.50	10.25	10.42	3.07	3.45	3.04	3.88	P	21.00	65.00
12/9/16	P	P	0.31	0.34	122.60	122.60	10.28	10.38	2.99	2.99	3.08	4.53	P	20.00	65.00
13/9/16	P	P	0.31	0.34	122.60	122.60	10.30	10.33	2.70	2.92	2.99	4.22	P	20.00	65.00
14/9/16	P	P	0.31	0.35	122.60	122.50	10.25	10.42	2.69	2.96	3.11	5.00	P	20.00	63.00
15/9/16	P	P	0.31	0.35	122.50	122.50	10.30	10.45	2.05	2.65	2.20	3.00	P	20.00	64.00
16/9/16	P	P	0.31	0.36	122.60	122.60	10.28	10.39	1.94	2.31	1.80	3.21	P	21.00	61.00
19/9/16	P	P	0.31	0.34	122.70	122.70	10.29	10.31	3.42	4.10	2.86	4.58	P	20.00	64.00
20/9/16	P	P	0.30	0.34	122.60	122.70	10.28	10.31	2.78	3.32	2.35	3.73	P	21.00	63.00
21/9/16	P	P	0.31	0.34	122.60	122.70	10.30	10.37	2.11	2.42	2.56	3.13	P	21.00	65.00
22/9/16	P	P	0.31	0.33	122.60	122.70	10.25	10.39	2.87	3.41	3.15	4.43	P	20.00	65.00
23/9/16	P	P	0.30	0.34	122.70	122.60	10.21	10.39	2.57	2.82	2.92	4.59	P	20.00	65.00
26/9/16	P	P	0.30	0.34	122.70	122.70	10.22	10.39	2.61	2.61	2.05	3.54	P	20.00	65.00
27/9/16	P	P	0.30	0.34	122.80	122.70	10.17	10.36	2.39	3.28	2.08	3.70	P	20.00	65.00
28/9/16	P	P	0.31	0.34	122.80	122.70	10.23	10.34	2.78	3.00	3.02	4.18	P	21.00	64.00

FWHM - full width at half maximum, Energy Res- Energy resolution, Det 1 - detector1, Det 2 - detector2, P - pass.
Comment: PASS

Table E.3: The results of quality control on October, 2016

Date	CT		Background (kc/s)		Energy Peak (keV)		Energy Res. (FWHM %)		Uniformity Det 1 (%)		Uniformity Det 2 (%)		Comment	Temp (C)	Humd (%)
	Warm up	Fast cal	Det 1	Det 2	Det 1	Det 2	Det 1	Det 2	CFOV	UFOV	CFOV	UFOV			
3/10/16	P	P	0.30	0.34	122.80	122.80	10.13	10.33	3.42	3.57	2.81	4.19	P	22.00	61.00
4/10/16	P	P	0.31	0.34	122.90	122.80	10.14	10.40	2.65	2.95	2.65	4.62	P	22.00	63.00
5/10/16	P	P	0.34	0.44	122.80	122.68	10.18	10.33	2.98	3.18	3.17	4.58	P	21.00	62.00
7/10/16	P	P	0.30	0.34	122.68	122.55	10.18	10.27	2.60	2.65	2.77	4.15	P	21.00	61.00
10/10/16	P	P	0.30	0.34	122.77	122.68	10.20	10.31	2.91	2.92	2.42	3.81	P	21.00	62.00
11/10/16	P	P	0.31	0.34	122.75	122.59	10.13	10.33	2.17	2.66	2.16	2.55	P	21.00	62.00
12/10/16	P	P	0.31	0.34	122.80	122.67	10.14	10.30	2.12	2.61	2.23	2.55	P	20.00	61.00
13/10/16	P	P	0.30	0.33	122.88	122.66	10.13	10.29	2.05	2.60	2.11	2.93	P	21.00	60.00
14/10/16	P	P	0.29	0.31	122.86	122.61	10.22	10.25	2.72	3.30	2.97	4.70	P	21.00	61.00
17/10/16	P	P	0.31	0.34	122.97	122.72	10.14	10.33	2.12	2.68	2.61	3.08	P	21.00	61.00
18/10/16	P	P	0.29	0.32	122.87	122.77	10.17	10.26	2.68	3.05	2.89	3.45	P	21.00	62.00
19/10/16	P	P	0.28	0.32	122.88	122.77	10.14	10.26	2.39	2.78	2.47	3.77	P	20.00	60.00
20/10/16	P	P	0.30	0.34	122.93	122.80	10.14	10.26	2.48	2.91	2.97	4.23	P	21.00	61.00
21/10/16	P	P	0.30	0.34	122.96	122.84	10.18	10.22	2.79	3.34	2.88	3.77	P	20.00	60.00
25/10/16	P	P	0.30	0.34	123.04	122.95	10.16	10.28	3.20	3.60	3.01	4.10	P	21.00	60.00
26/10/16	P	P	0.31	0.34	123.00	122.86	10.18	10.30	2.44	2.91	3.05	3.52	P	20.00	61.00
27/10/16	P	P	0.29	0.33	123.39	122.77	10.28	10.31	3.73	3.53	2.31	2.76	P	21.00	62.00

FWHM - full width at half maximum, Energy Res- Energy resolution, Det 1 - detector1, Det 2 - detector2, P- pass.

Comment: PASS

Table E.4: The results of quality control on November, 2016

Date	CT		Background (kc/s)		Energy Peak (keV)		Energy Res. (FWHM %)		Uniformity Det 1 (%)		Uniformity Det 2 (%)		Comment	Temp (C)	Humd (%)
	Warm up	Fast cal	Det 1	Det 2	Det 1	Det 2	Det 1	Det 2	CFOV	UFOV	CFOV	UFOV			
1/11/16	P	P	0.30	0.34	123.10	123.00	10.18	10.33	1.97	2.24	2.31	3.17	P	21.00	61.00
2/11/16	P	P	0.31	0.33	123.00	123.00	10.23	10.25	2.46	2.95	2.90	3.72	P	21.00	61.00
3/11/16	P	P	0.30	0.34	122.90	122.90	10.20	10.39	2.38	2.46	2.13	2.90	P	21.00	61.00
4/11/16	P	P	0.30	0.34	122.90	122.90	10.19	10.35	2.81	2.93	2.55	2.65	P	21.00	61.00
7/11/16	P	P	0.30	0.34	123.00	122.90	10.11	10.30	2.38	3.35	2.24	2.81	P	21.00	61.00
8/11/16	P	P	0.31	0.34	123.00	123.00	10.23	10.33	2.60	2.86	1.92	2.60	P	21.00	61.00
9/11/16	P	P	0.30	0.33	123.00	123.00	10.27	10.31	2.83	3.19	2.84	3.40	P	21.00	61.00
10/11/16	P	P	0.30	0.34	123.00	123.00	10.23	10.33	2.56	2.96	2.51	3.02	P	21.00	61.00
11/11/16	P	P	0.30	0.34	123.00	123.00	10.25	10.35	2.74	2.90	2.15	2.95	P	21.00	61.00
14/11/16	P	P	0.24	0.27	123.20	123.10	10.19	10.34	2.33	2.65	2.26	2.57	P	21.00	62.00
15/11/16	P	P	0.30	0.34	123.10	123.10	10.29	10.30	2.74	3.27	2.62	3.78	P	21.00	61.00
16/11/16	P	P	0.31	0.34	123.10	123.00	10.28	10.22	3.31	3.37	2.81	3.77	P	21.00	61.00
17/11/16	P	P	0.31	0.34	123.00	123.00	10.26	10.37	2.17	2.70	2.01	2.95	P	21.00	61.00
18/11/16	P	P	0.30	0.34	122.67	122.60	10.21	10.36	2.73	3.27	1.83	3.25	P	20.00	59.00
21/11/16	P	P	0.31	0.34	122.80	122.70	10.27	10.32	3.02	3.50	2.77	4.68	P	19.00	59.00
22/11/16	P	P	0.31	0.34	122.76	122.72	10.28	10.30	3.06	3.20	2.56	5.38	P	19.00	59.00
23/11/16	P	P	0.31	0.34	122.78	122.77	10.28	10.29	2.66	3.23	2.31	4.11	P	19.00	58.00
24/11/16	P	P	0.30	0.34	122.80	122.76	10.25	10.26	2.84	3.61	2.92	4.52	P	19.00	59.00
25/11/16	P	P	0.30	0.34	122.68	122.68	10.22	10.34	2.46	3.02	2.76	3.83	P	19.00	58.00
28/11/16	P	P	0.30	0.34	122.76	122.78	10.24	10.37	2.51	2.97	2.77	3.71	P	19.00	58.00
29/11/16	P	P	0.28	0.32	122.75	122.67	10.28	10.34	2.86	3.92	3.10	4.37	P	19.00	58.00
30/11/16	P	P	0.30	0.34	122.70	122.68	10.28	10.38	2.82	3.03	2.76	3.80	P	20.00	57.00

FWHM - full width at half maximum, Energy Res- Energy resolution, Det 1 - detector1, Det 2- detector2, P- pass.

Comment: PASS

Table E.5: The results of quality control on December, 2016

Date	CT Warm up	Fast cal	Background (kc/s) Det 1	Det 2	Energy Peak (keV) Det 1	Det 2	Energy Res. (FWHM %) Det 1	Det 2	Uniformity Det 1 (%) CFOV	UFOV	Uniformity Det 2 (%) CFOV	UFOV	Comment	Temp (C)	Humd (%)
1/12/16	P	P	0.31	0.35	122.42	122.19	10.27	10.41	2.34	3.08	1.96	3.56	P	19.00	59.00
2/12/16	P	P	0.31	0.34	122.46	122.15	10.29	10.44	2.09	3.15	1.98	3.00	P	19.00	59.00
6/12/16	P	P	0.31	0.34	122.64	122.34	10.20	10.33	2.53	3.45	2.11	3.43	P	19.00	60.00
7/12/16	P	P	0.31	0.34	122.53	122.30	10.25	10.41	2.38	3.10	2.34	2.89	P	19.00	60.00
8/12/16	P	P	0.31	0.35	122.51	122.31	10.24	10.41	2.37	2.56	2.27	3.05	P	19.00	59.00
9/12/16	P	P	0.31	0.35	122.52	122.28	10.27	10.40	3.21	3.54	2.70	4.48	P	19.00	58.00
13/12/16	P	P	0.31	0.36	122.65	122.34	10.24	10.39	2.27	2.30	2.19	2.85	P	19.00	59.00
14/12/16	P	P	0.32	0.35	122.62	122.40	10.27	10.40	2.89	3.86	2.87	3.90	P	19.00	59.00
15/12/16	P	P	0.31	0.35	122.62	122.39	10.24	10.36	2.70	3.09	2.52	3.79	P	19.00	60.00
16/12/16	P	P	0.31	0.35	122.68	122.44	10.22	10.38	2.87	3.43	2.86	4.88	P	19.00	60.00
19/12/16	P	P	0.31	0.35	122.74	122.53	10.15	10.34	2.75	3.06	2.60	4.80	P	19.00	59.00
20/12/16	P	P	0.32	0.35	122.69	122.47	10.17	10.36	2.42	2.75	2.39	3.07	P	19.00	58.00
21/12/16	P	P	0.32	0.35	122.70	122.50	10.17	10.37	0.00	0.00	0.00	0.00	P	19.00	60.00
22/12/16	P	P	0.32	0.35	122.68	122.48	10.20	10.34	2.77	3.23	2.40	4.21	P	19.00	60.00
23/12/16	P	P	0.32	0.35	122.67	122.47	10.25	10.27	3.19	3.36	3.18	4.66	P	18.00	64.00
26/12/16	P	P	0.31	0.35	122.70	122.50	10.09	10.38	2.07	2.74	1.93	3.12	P	18.00	67.00
27/12/16	P	P	0.28	0.32	122.70	122.53	10.17	10.34	3.00	3.29	2.72	4.15	P	19.00	58.00
28/12/16	P	P	0.31	0.35	122.69	122.53	10.22	10.38	2.17	3.05	2.53	2.90	P	19.00	59.00
29/12/16	P	P	0.31	0.35	122.68	122.53	10.22	10.37	2.77	3.35	2.55	4.02	P	19.00	57.00
30/12/16	P	P	0.31	0.35	122.72	122.55	10.19	10.33	2.64	3.37	2.71	3.66	P	18.00	57.00

FWHM - full width at half maximum, Energy Res- Energy resolution, Det 1- detector1, Det 2- detector2, P- pass.
Comment: PASS

Table E.6: The results of quality control on January, 2017

Date	CT Warm up	Fast cal	Background (kc/s) Det 1	Det 2	Energy Peak (keV) Det 1	Det 2	Energy Res. (FWHM %) Det 1	Det 2	Uniformity Det 1 (%) CFOV	UFOV	Uniformity Det 2 (%) CFOV	UFOV	Comment	Temp (C)	Humd (%)
4/1/17	P	P	0.24	0.28	122.86	122.61	10.18	10.32	2.15	2.92	1.92	2.87	P	19.00	62.00
5/1/17	P	P	0.24	0.27	122.78	122.64	10.17	10.30	2.21	3.34	2.75	3.40	P	19.00	62.00
6/1/17	P	P	0.31	0.35	122.77	122.58	10.20	10.33	2.50	2.81	2.79	4.75	P	19.00	61.00
9/1/17	P	P	0.24	0.27	122.84	122.64	10.21	10.32	3.10	3.66	2.81	4.67	P	19.00	60.00
10/1/17	P	P	0.24	0.27	122.82	122.67	10.22	10.24	2.59	3.09	3.09	4.29	P	19.00	60.00
11/1/17	P	P	0.24	0.27	122.87	122.69	10.13	10.26	3.00	3.81	2.82	4.13	P	20.00	61.00
12/1/17	P	P	0.24	0.27	122.85	122.67	10.20	10.33	2.75	2.95	3.00	4.72	P	20.00	61.00
16/1/17	P	P	0.32	0.35	122.97	122.68	10.17	10.31	3.10	3.46	2.70	3.79	P	19.00	60.00
17/1/17	P	P	0.32	0.35	122.94	122.68	10.20	10.30	2.44	3.34	2.40	4.16	P	19.00	59.00
18/1/17	P	P	0.31	0.35	122.94	122.68	10.12	10.28	2.43	3.03	2.55	3.88	P	19.00	59.00
19/1/17	P	P	0.31	0.34	122.97	122.70	10.17	10.36	2.80	3.26	2.89	4.37	P	19.00	58.00
20/1/17	P	P	0.31	0.34	122.94	122.64	10.14	10.30	2.51	2.96	3.09	4.29	P	19.50	59.00
23/1/17	P	P	0.24	0.27	122.94	122.64	10.12	10.32	2.65	3.46	2.81	4.13	P	20.00	55.00
24/1/17	P	P	0.24	0.28	122.99	122.72	10.18	10.13	2.43	3.64	2.38	3.34	P	20.00	57.00
25/1/17	P	P	0.32	0.35	122.95	122.70	10.18	10.27	3.41	3.44	2.62	4.37	P	19.00	57.00
26/1/17	P	P	0.31	0.35	123.00	122.71	10.12	10.33	2.68	3.17	2.72	5.16	P	20.00	57.00
27/1/17	P	P	0.31	0.35	123.08	122.72	10.10	10.28	2.90	3.35	3.04	5.05	P	20.00	57.00
30/1/17	P	P	0.32	0.35	123.12	122.80	10.17	10.31	3.25	3.40	2.82	4.52	P	21.00	58.00
31/1/17	P	P	0.31	0.35	122.54	122.47	10.21	10.34	1.78	1.88	1.60	2.27	P	20.00	57.00

FWHM - full width at half maximum, Energy Res- Energy resolution, Det 1 - detector1, Det 2 - detector2, P- pass.

Comment: PASS

Table E.7: The results of quality control on February, 2017

Date	CT		Background (kc/s)		Energy Peak (keV)		Energy Res. (FWHM %)		Uniformity Det 1 (%)		Uniformity Det 2 (%)		Comment	Temp (C)	Humd (%)
	Warm up	Fast cal	Det 1	Det 2	Det 1	Det 2	Det 1	Det 2	CFOV	UFOV	CFOV	UFOV			
1/2/17	P	P	0.32	0.35	122.53	122.44	10.20	10.38	1.71	1.76	1.44	2.25	P	21.00	55.00
2/2/17	P	P	0.32	0.35	122.54	122.42	10.18	10.35	1.87	1.87	1.81	1.81	P	20.00	58.00
3/2/17	P	P	0.32	0.35	122.59	122.47	10.10	10.30	2.03	2.03	1.72	2.06	P	20.00	57.00
6/2/17	P	P	0.31	0.34	122.57	122.58	10.33	10.31	2.72	2.84	2.41	3.06	P	20.00	57.00
7/2/17	P	P	0.32	0.35	122.50	122.54	10.21	10.30	2.42	2.99	2.49	3.26	P	21.00	58.00
8/2/17	P	P	0.31	0.35	122.47	122.57	10.21	10.28	2.37	2.81	2.93	3.14	P	20.00	58.00
9/2/17	P	P	0.31	0.34	122.54	122.54	10.19	10.32	1.74	2.07	1.87	1.91	P	20.00	58.00
10/2/17	P	P	0.31	0.35	122.61	122.59	10.16	10.32	2.07	2.07	1.65	1.75	P	21.00	57.00
14/2/17	P	P	0.31	0.35	122.54	122.61	10.27	10.28	2.25	2.97	2.23	3.08	P	18.30	57.00
15/2/17	P	P	0.29	0.32	122.61	122.68	10.26	10.24	2.74	3.07	2.85	3.37	P	18.50	58.00
16/2/17	P	P	0.32	0.36	122.55	122.66	10.22	10.28	2.44	3.43	2.83	3.56	P	18.70	58.00
20/2/17	P	P	0.32	0.37	122.66	122.69	10.20	10.28	2.43	3.28	2.49	3.06	P	19.40	57.00
21/2/17	P	P	0.34	0.34	122.69	122.72	10.20	10.26	2.32	2.68	2.35	2.91	P	19.50	58.00
22/2/17	P	P	0.31	0.39	122.56	122.64	10.24	10.21	2.34	2.74	2.54	2.98	P	19.40	55.00
23/2/17	P	P	0.35	0.34	122.78	122.73	10.18	10.22	2.49	3.02	2.92	3.66	P	19.50	56.00
24/2/17	P	P	0.31	0.34	122.81	122.68	10.11	10.19	2.71	3.17	2.47	2.99	P	20.40	55.00
27/2/17	P	P	0.31	0.34	122.82	122.70	10.10	10.25	2.81	3.09	2.46	3.21	P	20.00	57.00
28/2/17	P	P	0.31	0.34	122.84	122.73	10.18	10.19	3.09	3.70	2.96	3.61	P	21.00	60.00

FWHM - full width at half maximum, Energy Res- Energy resolution, Det 1- detector1, Det 2- detector2, P- pass.

Comment: PASS

Table E.8: The results of quality control on March, 2017

Date	CT Warm up	Fast cal	Background (kc/s) Det 1	Det 2	Energy Peak (keV) Det 1	Det 2	Energy Res. (FWHM %) Det 1	Det 2	Uniformity Det 1 (%) CFOV	UFOV	Uniformity Det 2 (%) CFOV	UFOV	Comment	Temp (C)	Humd (%)
1/3/17	P	P	0.311	0.342	122.84	122.75	10.16	10.26	2.422	2.623	2.312	2.756	P	20.0	56.0
2/3/17	P	P	0.306	0.337	122.79	122.73	10.12	10.29	2.635	2.805	2.547	3.025	P	20.0	56.0
3/3/17	P	P	0.306	0.344	122.76	122.74	10.16	10.23	2.344	3.077	2.764	3.405	P	20.0	53.0
6/3/17	P	P	0.309	0.346	122.78	122.75	10.13	10.3	3.374	3.647	2.881	3.348	P	19.0	57.0
7/3/17	P	P	0.313	0.345	122.78	122.7	10.1	10.27	2.52	3.188	2.769	3.275	P	19.0	60.0
8/3/17	P	P	0.31	0.339	122.81	122.73	10.13	10.27	2.564	3.5	2.309	2.772	P	19.0	59.0
9/3/17	P	P	0.311	0.337	122.81	122.76	10.13	10.3	2.847	3.189	2.632	2.868	P	19.0	59.0
10/3/17	P	P	0.289	0.309	122.8	122.73	10.17	10.3	2.618	3.081	2.577	3.254	P	19.0	59.0
13/3/17	P	P	0.313	0.343	122.82	122.74	10.18	10.29	2.194	3.005	2.24	2.938	P	19.0	58.0
14/3/17	P	P	0.309	0.339	122.89	122.08	10.16	10.26	1.673	2.044	1.834	2.449	P	19.0	61.0
15/3/17	P	P	0.31	0.345	122.81	122.8	10.25	10.25	2.29	2.374	2.46	3.088	P	19.0	62.0
16/3/17	P	P	0.307	0.341	122.79	122.77	10.16	10.29	1.543	1.99	2.202	2.358	P	19.0	59.0
17/3/17	P	P	0.241	0.271	122.71	122.86	10.16	10.3	2.635	3.223	2.727	2.972	P	19.0	59.0
20/3/17	P	P	0.31	0.341	122.81	122.92	10.12	10.26	1.587	2.366	1.91	2.149	P	19.0	62.0
21/3/17	P	P	0.312	0.339	122.79	122.91	10.1	10.3	2.658	3.45	2.881	3.354	P	19.0	62.0
22/3/17	P	P	0.315	0.341	122.75	122.94	10.14	10.26	2.583	2.782	2.678	3.432	P	19.0	59.0
23/3/17	P	P	0.294	0.329	122.85	122.92	10.06	10.28	2.411	2.941	2.441	3.227	P	19.0	56.0
27/3/17	P	P	0.307	0.342	122.85	122.98	10.15	10.3	1.555	1.963	1.543	2.263	P	19.0	56.0
28/3/17	P	P	0.308	0.34	122.83	122.97	10.15	10.31	2.487	2.806	2.887	3.595	P	19.0	59.0
29/3/17	P	P	0.306	0.339	122.84	122.99	10.1	10.31	1.887	1.887	1.579	2.337	P	19.0	58.0
30/3/17	P	P	0.311	0.337	122.85	123.01	10.12	10.24	1.631	1.929	1.96	2.496	P	20.0	58.0
31/3/17	P	P	0.31	0.336	122.85	122.98	10.14	10.24	2.584	3.158	2.399	3.16	P	19.0	61.0

FWHM - full width at half maximum, Energy Res- Energy resolution, Det 1- detector1, Det 2- detector2, P- pass.

Comment: PASS

3. Center of Rotation

Purpose: To check the center of rotation offset, alignment of the camera Y-axis and head tilt with respect to the axis of rotation.

Materials: ^{99m}Tc point source activity (0.8 -1 mCi)

Methods: The source holder is positioned on the edge of the couch and placed the source on the source holder.

The source holder and the table height were adjusted until the source images are inside the two ROI circles on the persistence image.

The acquisitions were started for both H-mode and L-mode of gantry mode with Tc-99m energy session, rotation parameters of 720 total angular range, 6 angular steps and clockwise direction and 256x256 matrices.

Tolerance: The values must be < 0.55 mm for:

Delta X - Detector 1

Delta Y - Detector 1

Delta X - Detector 2

Delta Y - Detector 2

(a) H-mode   (b) L-mode

Figure E.7: Center of rotation check in (a) H-mode and (b) L-mode

Results: The results of center of rotation are summarized in table E.9.

Table E.9: Center of rotation check from August 2016 to March 2017

Date	COR Det 1 (mm)		COR Det 2 (mm)		Comment
	Δx	Δy	Δx	Δy	
1/8/16	0.35	0.23	0.00	-0.15	P
15/8/16	-0.17	0.00	0.34	0.04	P
22/8/16	-0.04	0.00	0.28	-0.17	P
29/8/16	-0.07	0.00	0.30	-0.08	P
5/9/16	0.08	0.00	0.20	0.08	P
12/9/16	0.10	0.00	0.23	0.15	P
19/9/16	-0.27	0.00	0.36	0.17	P
27/9/16	-0.26	0.00	0.33	0.10	P
3/10/16	-0.29	0.00	0.30	0.05	P
10/10/16	-0.34	0.00	0.31	0.14	P
15/11/16	-0.43	0.00	0.37	0.13	P
28/11/16	-0.46	0.00	0.25	0.11	P
6/12/16	0.00	0.00	0.01	0.19	P
26/12/16	0.05	0.00	0.03	0.16	P
9/1/17	0.05	0.00	0.16	0.07	P
16/1/17	0.00	0.00	0.20	0.02	P
23/1/17	0.03	0.00	0.15	0.14	P
30/1/17	0.00	0.00	0.17	0.02	P
6/2/17	0.08	0.00	0.13	0.20	P
20/2/17	-0.03	0.00	0.04	0.13	P
27/2/17	-0.05	0.00	0.17	0.19	P
6/3/17	0.06	0.00	0.15	0.19	P
13/3/17	0.00	0.00	0.14	0.14	P
20/3/17	0.05	0.00	0.08	0.18	P

Comment: PASS

4. System Planar Sensitivity

Purpose: To test the count rate response of a scintillation camera to a radionuclide source of known radioactivity.

Materials: A petri dish with 10 cm diameter

A foam with 10 cm height

Methods: Fill water 25 cc and 99mTc activity 106.93 MBq into the petri dish.

Place the foam on the center of detector and put on petri dish on top.

Acquire counts for three minutes with LEHR collimator, matrices 256x256, zoom 1 and no uniformity correction.

Background counts were also acquired three minutes for background correction.

Perform the acquisition with both detectors and record the total counts for each detector.

Tolerance: The results must be agreeable with specification.

Figure E.8: System planar sensitivity

Results: The results of system planar sensitivity for LEHR collimator are summarized in table E.10.

Table E.10.1: The results of system planar sensitivity test

	Detector 1	Detector 2	Specification
Counts/3min	1429207	1469441	
Bg/3min	5540	6070	
Net counts/3min	1423667	1463371	
cps/mCi	2811.68	2812.51	
cpm/µCi	168.71	168.75	160.00

TableE.10.2: The results of system planar sensitivity test on February 2016

	Detector 1	Detector 2	Specification
cpm/µCi	179.82	180.00	160.00

Comment: Difference between sensitivity of acceptance testing and current study is -6% in both detector because acceptance testing and current study use different dose calibrators. However, the results are within NEMA specification.

 PASS

6. Quality Control of CT

Alignment of Table to Gantry

Purpose: To ensure that long axis of the table is horizontally aligned with a vertical line passing through the rotational axis of the scanner.

Method: Locate the table midline using a ruler and mark it on a tape affixed to the table. With the gantry untilted, extend the table top into gantry to tape position. Measure the horizontal deviation between the gantry aperture center and the table midline.

Tolerance: The deviation should be within 5 mm.

Table E.12: The results of alignment of table to gantry

	Table	Bore
Distance from Right to Center (mm)	19.9	34.8
Distance from Center to Left (mm)	20.1	35.2
Measured Deviation* (mm)	0.1	0.2

Measured deviation = (Distance from right to center – Distance from center to left)/2

Comment: PASS

Table Increment Accuracy

Purpose: To determine accuracy and reproducibility of table longitudinal motion.

Method: Tape a measuring tape at the foot end of the table. Place a paper clip at the center of the tape to function as an indicator. Load the table uniformly with 150 lbs. From the initial position move the table 300, 400 and 500 mm into the gantry under software control. Record the relative displacement of the pointer on the ruler. Reverse the direction of motion and repeat. Repeat the measurements four times.

Tolerance: Positional errors should be less than 3 mm at 300 mm position.

Results

Table E.13: The results of table increment accuracy

Indicated	Measured	Deviation
100	100	0
200	200	0
300	299.9	0.1
-100	-99.95	0.05
-200	-199.95	0.05
-300	-300	0

Deviation = [Indicated-Measured]

Comment: 400 and 500 mm cannot be set because of couch limit.

Verification of Computed Tomography Dose Index (CTDI)

$CTDI_{100}$ in air

Purpose: To verify the measured CTDI in air values with system manual

Methods: CTDI in air measurement was performed at the isocenter by placing the 100mm active length ionization chamber in air with the support stem. Then, it was connected with the Raysafe Xi base unit for dose reading and scanned three times for head and body protocol. The acquisition parameters are 100mA tube current, 1 sec scan time for all measurement settings at tube voltage setting 80, 100, 120 and 140kVp.

Tolerance: Measured CT dose index should be within ±40% from system manual.

Results:

Table E.14: The measured $CTDI_{100}$ in air for head protocol at each kVp compared with system manual

kVp	Measured (mGy/100mAs)	System Manual(mGy/mAs)	Difference (%)
80	13.5	N/A	-
100	22.6	N/A	-
120	32.9	29.35	10.8
140	44.7	N/A	-

% Difference = [(Measured – System manual)/Measured] x 100

Table E.15: The measured $CTDI_{100}$ in air for body protocol at each kVp compared with system manual

kVp	Measured (mGy/100mAs)	System Manual(mGy/mAs)	Difference (%)
80	9.8	8.62	12
100	17.5	16.12	7.9
120	26.9	24.58	8.6
140	37.7	33.88	10

% Difference = [(Measured – System manual)/Measured] x 100

Comment: PASS

CTDI$_{100}$ in head phantom at each kVp compared with system manual

Methods: The CTDI$_{100}$ in head phantom was determined by using a 100 mm pencil ionization chamber placed in each hole of 16 cm diameter PMMA phantom. The acquisition parameters were 100 mA, 1 sec rotation time and small FOV 250mm for all measurements at kVp 80, 100, 120, and 140 respectively.

Tolerance: Measured CT dose index should be within ±40% from system manual.

Results:

Table E.16: The measured CTDI$_{100}$ at each position of 16 cm head phantom for each kVp and CTDI$_w$ compared with system manual

kVp	CTDI$_{100}$ in head phantom (mGy)					Calculated CTDI$_w$ (mGy/100 mAs)	System manual CTDI$_w$ (mGy/100mAs)	Diff (%)
	At center	At peripheral						
		North	East	South	West			
80	6.82	7.49	7.39	7.59	7.07	7.19	7.74	-7.65
100	12.91	13.41	13.12	12.95	12.98	13.04	13.84	-6.14
120	20.03	20.25	20.19	20.15	20.04	19.78	20.88	-5.56
140	28.36	28.53	28.92	28.20	28.53	28.87	29.32	-1.56

% Difference = [(Measured – System manual)/Measured] x 100

Comment: PASS

CTDI$_{100}$ in body phantom at each kVp compared with system manual

Methods: The CTDI100 in head phantom was determined by using a 100 mm pencil ionization chamber placed in each hole of 16 cm diameter PMMA phantom. The acquisition parameters were 100 mA, 1 sec rotation time and small FOV 250mm for all measurements at kVp 80, 100, 120, and 140 respectively.

Tolerance: Measured CT dose index should be within ±40% from system manual.

Results:

Table E.17: The measured $CTDI_{100}$ at each position of 32cm body phantom for each kVp and $CTDI_w$ compared with system manual

kVp	$CTDI_{100}$ in body phantom (mGy)					Calculated CTDIw (mGy/100 mAs)	System manual CTDIw (mGy/100mAs)	Diff (%)
	At center	At peripheral						
		North	East	South	West			
80	1.60	4.08	4.05	3.95	4.03	3.22	3.39	-5.28
100	3.61	7.75	7.75	7.55	7.60	6.31	6.43	-1.90
120	6.17	11.68	12.22	11.94	12.08	10.21	10.67	-4.50
140	9.25	18.08	17.36	17.08	17.21	14.70	14.69	0.07

Comment: PASS

Verification of $CTDI_{vol}$ on monitor and calculated values

Methods: Determine the $CTDI_w$ by using the results in Table E.16 and E.17. The $CTDI_{vol}$ displayed on CT monitor were recorded and compared with the calculated values in percent difference as shown in table 5 for $CTDI_{vol}$ in head phantom and table 4.6 for $CTDI_{vol}$ in body phantom.

Tolerance: The percent difference between the displayed $CTDI_{vol}$ on CT monitor and calculated $CTDI_{vol}$ should be less the than 10%

Results:

Table E.18: $CTDI_{vol}$ displayed on monitor and calculated $CTDI_{vol}$ using head techniques

kVp	$CTDI_{vol}$ in head phantom (mGy)		% Difference
	Calculated	Displayed	
80	7.19	7.73	-7.51
100	13.04	13.81	-5.90
120	19.78	21.46	-8.49
140	28.87	29.25	-1.32

% Difference = [(calculated – displayed)/calculated] x 100

CTDI$_{vol}$ displayed on monitor and calculated using head technique with each kVp is plotted in figure E.11 and E.12.
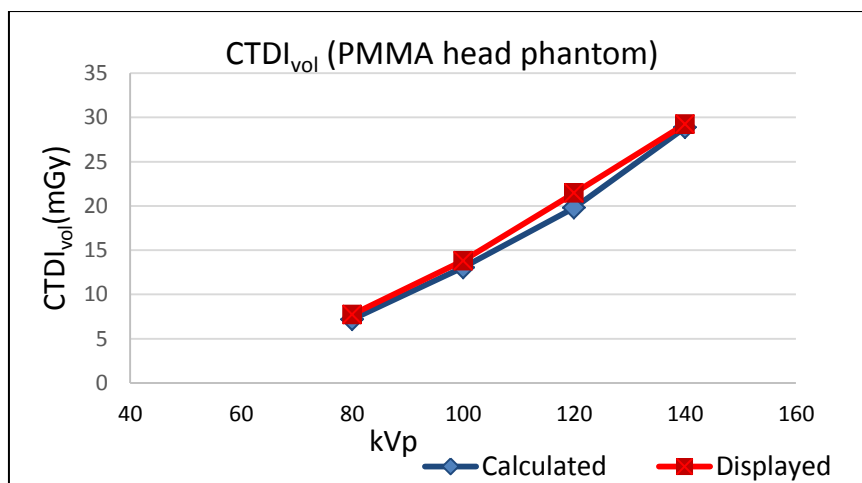
Figure E.11 Displayed and calculated CTDI$_{vol}$ as function of kVp in 16cm PMMA head phantom

Table E.19: CTDI$_{vol}$ displayed on monitor and calculated CTDI$_{vol}$ using body techniques

kVp	CTDI$_{vol}$ in body phantom (mGy)		% Difference
	Calculated	Displayed	
80	3.22	3.39	-5.28
100	6.31	6.42	-1.74
120	10.21	10.56	-3.43
140	14.70	14.66	0.27

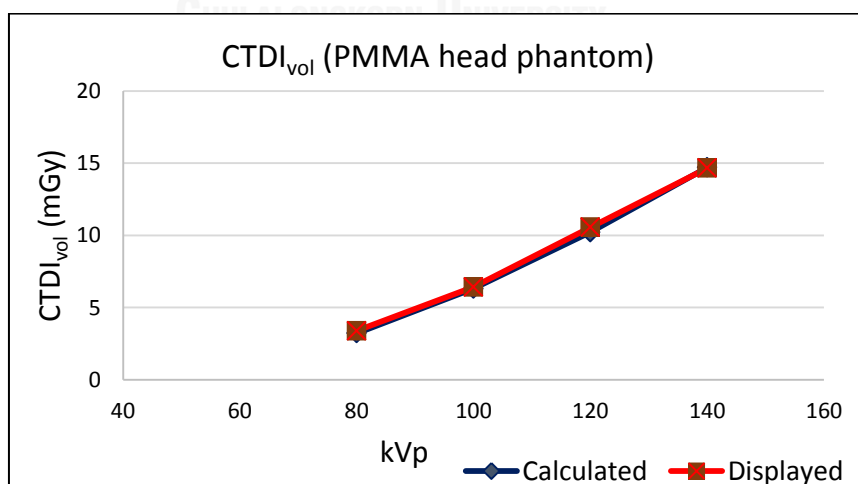**% Difference = [(calculated – displayed)/calculated] x 100**

Figure E.12: Displayed and calculated CTDI$_{vol}$ as function of kVp in 32cm PMMA body phantom

Comment: PASS

Characteristics of image quality in Catphan® 700 phantom

The Catphan ® 700 was used to study image quality which includes slice width measurement, linearity and reproducibility of CT number, image uniformity, high contrast resolution and low contrast detectability. The CTP682, Sensitometry module was used to study slice width measurement and linearity of CT number. The CTP714, High resolution module with 1 to 30 line pair per cm gauges, was used to study the high contrast resolution and CTP515, low contrast module with supra-slice and sub-slice contrast targets, was used to study low contrast detectability. The CTP712, Image uniformity module, was used to study image uniformity and reproducibility of CT numbers.

Slice thickness accuracy

Purpose: To assess the accuracy of slice thickness.

Methods: Set up the catphan phantom as described in beam alignment. Select the section containing the accuracy of slice thickness test object (CTP682). Choose 120kVp, 320mAs and perform scan with different slice thickness under auto control. Calculate the real slice thickness following Catphan manual.

Technique: 120kVp, 320mA, 1sec and 250mm FOV

Tolerance: The deviation should be less than 1.

Results:

Table E.20: Slice thickness accuracy in CTP682 of Catphan® 700 phantom

Slice thickness in mm	Measured thickness in mm	Deviation
1.25	1.13	0.12
5	4.87	0.13
10	9.53	0.47

Deviation= (slice thickness- measured thickness)

Comment: PASS

Linearity of CT numbers

Method: Set up the catphan phantom as described in beam alignment. Select the section containing the test objects of different CT numbers. Select the head technique and perform a single transverse scan. Select a region of interest (ROI) of sufficient size to cover the test objects. Place the ROI in the middle of each test object and record the mean CT number.

Technique: 120 kVp, 320 mA, 1 sec, 250 mm SFOV, slice collimation 5 mm.

Tolerance: R-square between measured CT number and linear attenuation coefficient (μ) more than 0.9

Results:

Table E.21: The measured CT number and linear attenuation coefficients of materials in CTP 682 test object of Catphan® 700 phantom

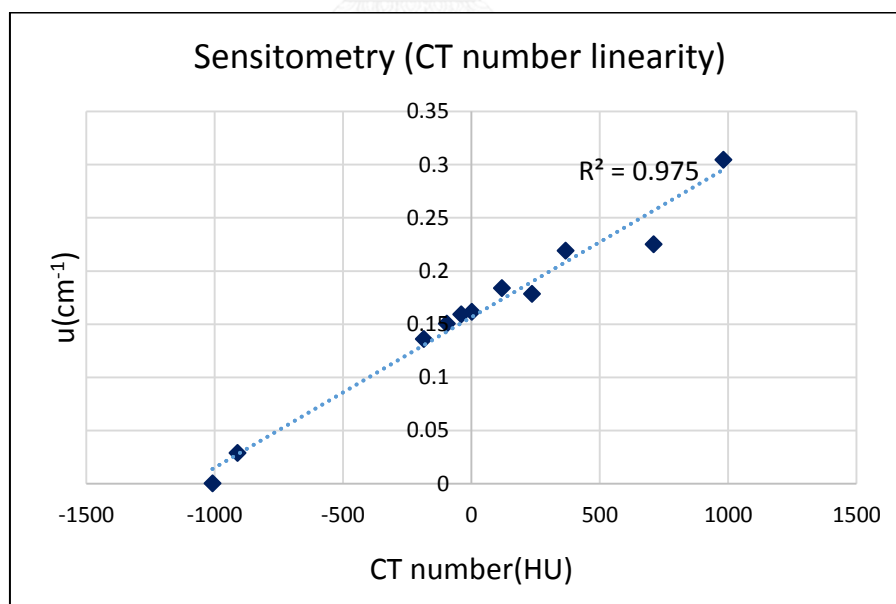| Material	Expected CT no. (HU)	Measured CT no. (HU)	μ (cm^{-1})
Air	-1000	-1008	0
Acrylic	120	119.23	0.184
Bone 50%	750	710	0.225
Bone 20%	240	237	0.178
Polystyrene	-35	-38.89	0.159
LDPE	-100	-95.6	0.151
PMP	-200	-184.39	0.136
Delrin	340	367.34	0.219
Teflon	990	982	0.305
Lungs	-867	-809	0.0287
Water	0	2	0.161

Figure E.13: The correlation between the measured CT number and linear attenuation coefficients

Comment: PASS

Position Dependence of CT numbers

Methods: Set up the Catphan phantom as described in beam alignment. Select the head technique and perform a single transverse scan. Select a circular region of interest of approximately 400mm.sq. And record the mean CT number and standard deviation for each of the position 1 through 5.

Technique: 120kVp, 320mA, 1sec and 250mm FOV

Tolerance: The coefficient of variation of mean CT numbers of the four scans should be less than 0.2.

Results:

Table E.22: Position dependence of CT numbers in CTP712 of Catphan® 700 phantom

Position	Mean CT No.(HU)	SD	CV
1	10.09	1.08	0.11
2	10.85	1.38	0.13
3	10.64	1.08	0.10
4	10.75	1.59	0.15
5	10.79	2.15	0.19

CV= SD/Mean CT No.

Comment: PASS

Reproducibility of CT numbers

Method: Using the same technique and set up as position dependence, obtain four scans. Using the same ROI as position dependence in location 5, which is the center of the phantom, obtain mean CT numbers for each of the four scans.

Tolerance: The coefficient of variation of mean C.T. numbers of the four scans should be less than 0.002.

Results:

Run Number	1	2	3	4
Mean CT Number (HU)	10.75	10.79	10.79	10.89

Mean Global C.T. Number	10.81

Standard deviation	0.01

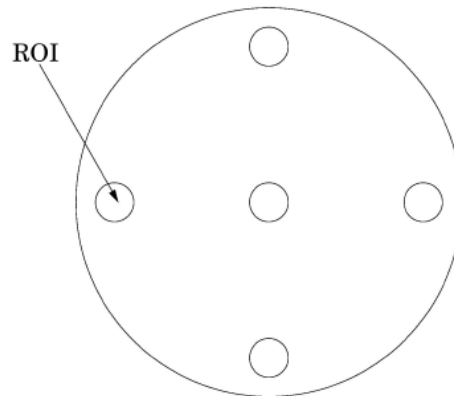| Coefficient of variation	0.001

Comment: PASS

Image uniformity (CTP 712)

Figure E.14: Image Uniformity

Method: Set up the catphan phantom as described in beam alignment. Select the section containing the image uniformity module. Select the head technique. Perform a single transverse scan. Measure the mean value and the corresponding standard deviations in CT numbers within a region of interest (ROI). These measurements are taken from different locations within the scan field.

Technique: 120kVp, 320 mA, 1.0 sec, 250 mm FOV.

Tolerance: 5 HU.

Results:

Table E.23: The results of image uniformity in CTP712 of Catphan® 700 phantom

Position	CT number (HU)	SD	Different (HU)
Center	10.85	3.6	0.95
3 o'clock	9.9	3.3	1.69
6 o'clock	9.16	3.22	1.96
9 o'clock	8.89	3.35	2.17
12 o'clock	8.68	3.64	0.95

Difference = (CT number$_{center}$- CT number$_{peripheral}$)

Comment: PASS

High Contrast Resolution

Method: Set up the catphan phantom as described in beam alignment. Select the section of CTP 714 containing the high resolution test objects. Select the head technique. Perform a single transverse scan. Select the area containing the high resolution test objects and zoom as necessary. Select appropriate window and level for the best visualization of the test objects. Record the smallest test object visualized on monitor.

Technique: 120 kVp, 320 mA, 1.0 sec, 250 mm FOV.
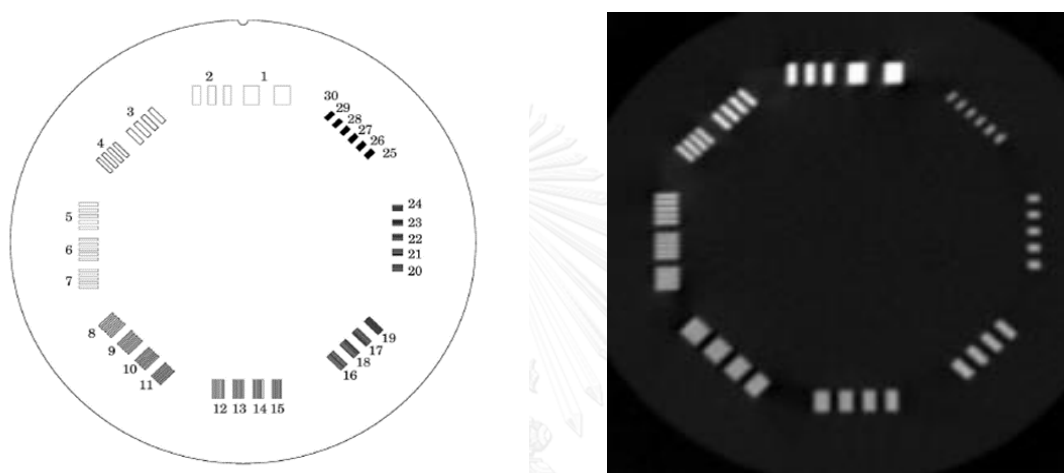
Figure E.15: High contrast resolution

Results:

Table E.24: The results of high contrast resolution in CTP714 of Catphan® 700 phantom

Slice thickness in mm	Resolution
6	16 line pair/cm with 0.083cm gap size

Comment: PASS

Low contrast detectability

Method: Select the section of CTP515 containing the low resolution test objects in the Catphan phantom. Perform a single transverse scan utilizing the same technique as high resolution. Select appropriate window and level for the best visualization of the test objects. Record the smallest test object visualized.

Technique: 120 kVp, 320 mA, 1.0 sec, 250 mm FOV, slice collimation 5 mm.

Tolerance: Should see 4 spokes at Supra-slice 0.5% nominal target contrast level.
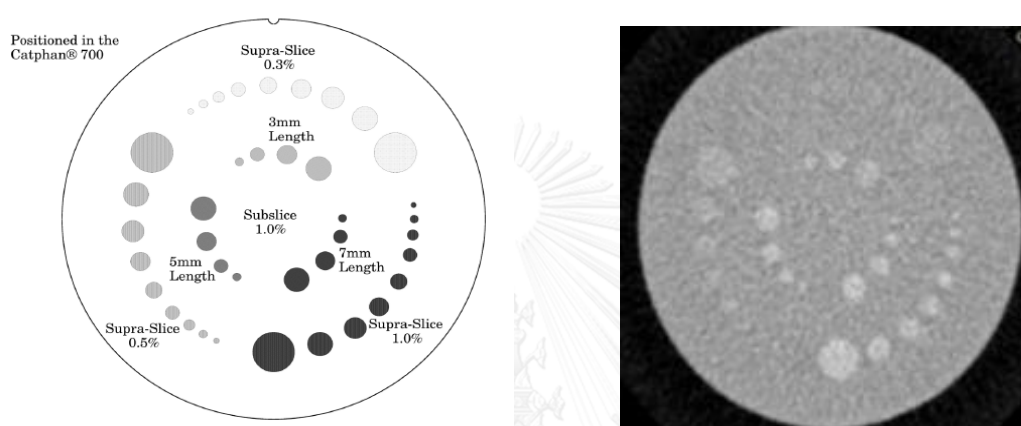
Figure E.16: Low contrast detectability

Results

Table E.25: The results of low contrast detectability in CTP515 of Catphan® 700 phantom

Supra-slice	Nominal target contrast levels	Hole	% contrast
	0.3%	5	1.8
	0.5%	8	1.5
	1%	9	2
Supra-slice	Nominal target contrast levels	Hole	% contrast
	3mm Length	3	2.25
	5mm Length	3	3.75
	7mm Length	4	7

Comment: PASS

APPENDIX F

Table F.1. S-values for calculation of absorbed doses to target organs based on organ masses of Asian reference man

Source organs	Target organs	S-values
Heart	Adrenals	3.08E-07
Heart	Brain	2.41E-09
Heart	Breasts	3.13E-07
Heart	GB wall	1.53E-07
Heart	LLI wall	5.24E-09
Heart	Small intestine	2.22E-08
Heart	Stomach wall	2.84E-07
Heart	ULI wall	3.11E-08
Heart	Heart wall	1.49E-05
Heart	kidneys	7.97E-08
Heart	Liver	2.62E-07
Heart	Lungs	3.65E-07
Heart	Muscles	1.10E-07
Heart	Pancreas	2.75E-07
Heart	Red marrow	1.67E-07
Heart	Bone surface	1.78E-07
Heart	Skin	3.99E-08
Heart	Spleen	2.15E-07
Heart	Thymus	4.92E-07
Heart	Thyroid	4.33E-08
Heart	Urinary Bladder wall	2.44E-09
Heart	Gonads	6.24E-09
Heart	Others	1.65E-07
Liver	Adrenals	4.69E-07
Liver	Brain	7.75E-10
Liver	Breasts	8.18E-08
Liver	GB wall	1.09E-06
Liver	LLI wall	1.54E-08
Liver	Small intestine	1.25E-07
Liver	Stomach wall	1.58E-07
Liver	ULI wall	2.19E-07
Liver	Heart wall	2.91E-07
Liver	kidneys	2.84E-07
Liver	Liver	3.56E-06
Liver	Lungs	1.73E-07
Liver	Muscles	9.02E-08
Liver	Pancreas	2.97E-07
Liver	Red marrow	1.25E-07
Liver	Bone surface	1.38E-07
Liver	Skin	3.91E-08
Liver	Spleen	9.31E-08

Source organs	Target organs	S-values
Liver	Thymus	3.97E-08
Liver	Thyroid	1.02E-08
Liver	Urinary Bladder wall	1.31E-08
Liver	Gonads	3.75E-08
Liver	Others	1.59E-07
Colon	Adrenals	8.06E-08
Colon	Brain	3.71E-11
Colon	Breasts	8.82E-09
Colon	GB wall	5.48E-07
Colon	LLI wall	6.33E-07
Colon	Small intestine	1.47E-06
Colon	Stomach wall	2.28E-07
Colon	ULI wall	4.94E-06
Colon	Heart wall	2.58E-08
Colon	kidneys	2.07E-07
Colon	Liver	1.31E-07
Colon	Lungs	1.12E-08
Colon	Muscles	1.34E-07
Colon	Pancreas	1.09E-07
Colon	Red marrow	2.69E-07
Colon	Bone surface	1.65E-07
Colon	Skin	3.25E-08
Colon	Spleen	1.30E-07
Colon	Thymus	3.12E-09
Colon	Thyroid	5.75E-10
Colon	Urinary Bladder wall	2.39E-07
Colon	Gonads	9.54E-07
Colon	Others	1.59E-07
Lungs	Adrenals	2.52E-07
Lungs	Brain	7.25E-09
Lungs	Breasts	2.80E-07
Lungs	GB wall	9.33E-08
Lungs	LLI wall	3.52E-09
Lungs	Small intestine	1.46E-08
Lungs	Stomach wall	1.27E-07
Lungs	ULI wall	2.12E-08
Lungs	Heart wall	5.50E-07
Lungs	kidneys	6.46E-08
Lungs	Liver	2.22E-07
Lungs	Lungs	2.96E-06
Lungs	Muscles	1.12E-07
Lungs	Pancreas	1.34E-07
Lungs	Red marrow	1.67E-07
Lungs	Bone surface	1.84E-07
Lungs	Skin	4.34E-08
Lungs	Spleen	2.12E-07

Source organs	Target organs	S-values
Lungs	Thymus	1.91E-07
Lungs	Thyroid	1.04E-07
Lungs	Urinary Bladder wall	1.50E-09
Lungs	Gonads	4.67E-09
Lungs	Others	1.44E-07
Thyroid	Adrenals	8.76E-09
Thyroid	Brain	1.28E-07
Thyroid	Breasts	3.61E-08
Thyroid	GB wall	3.30E-09
Thyroid	LLI wall	2.20E-10
Thyroid	Small intestine	5.26E-10
Thyroid	Stomach wall	3.97E-09
Thyroid	ULI wall	9.00E-10
Thyroid	Heart wall	5.41E-08
Thyroid	kidneys	2.86E-09
Thyroid	Liver	9.72E-09
Thyroid	Lungs	7.32E-08
Thyroid	Muscles	1.39E-07
Thyroid	Pancreas	5.61E-09
Thyroid	Red marrow	1.19E-07
Thyroid	Bone surface	2.19E-07
Thyroid	Skin	4.73E-08
Thyroid	Spleen	1.01E-08
Thyroid	Thymus	1.09E-07
Thyroid	Thyroid	1.76E-04
Thyroid	Urinary Bladder wall	1.09E-10
Thyroid	Gonads	2.44E-10
Thyroid	Others	1.49E-07
Kidneys	Adrenals	7.82E-07
Kidneys	Brain	1.50E-10
Kidneys	Breasts	2.39E-08
Kidneys	GB wall	5.11E-07
Kidneys	LLI wall	5.89E-08
Kidneys	Small intestine	2.30E-07
Kidneys	Stomach wall	2.71E-07
Kidneys	ULI wall	2.48E-07
Kidneys	Heart wall	1.03E-07
Kidneys	kidneys	1.28E-05
Kidneys	Liver	3.30E-07
Kidneys	Lungs	5.53E-08
Kidneys	Muscles	1.17E-07
Kidneys	Pancreas	3.83E-07
Kidneys	Red marrow	2.57E-07
Kidneys	Bone surface	1.80E-07
Kidneys	Skin	4.09E-08
Kidneys	Spleen	8.55E-07

Source organs	Target organs	S-values
Kidneys	Thymus	1.16E-08
Kidneys	Thyroid	3.48E-09
Kidneys	Urinary Bladder wall	2.10E-08
Kidneys	Gonads	7.32E-08
Kidneys	Others	1.58E-07
Spleen	Adrenals	4.95E-07
Spleen	Brain	4.93E-10
Spleen	Breasts	5.24E-08
Spleen	GB wall	1.69E-07
Spleen	LLI wall	4.98E-08
Spleen	Small intestine	1.09E-07
Spleen	Stomach wall	8.29E-07
Spleen	ULI wall	1.24E-07
Spleen	Heart wall	2.09E-07
Spleen	kidneys	6.43E-07
Spleen	Liver	8.12E-08
Spleen	Lungs	1.37E-07
Spleen	Muscles	1.24E-07
Spleen	Pancreas	9.86E-07
Spleen	Red marrow	1.26E-07
Spleen	Bone surface	1.40E-07
Spleen	Skin	3.77E-08
Spleen	Spleen	2.89E-05
Spleen	Thymus	2.61E-08
Spleen	Thyroid	9.24E-09
Spleen	Urinary Bladder wall	9.05E-09
Spleen	Gonads	2.93E-08
Spleen	Others	1.59E-07
Salivary	Adrenals	3.31E-08
Salivary	Brain	4.85E-07
Salivary	Breasts	1.37E-07
Salivary	GB wall	1.25E-08
Salivary	LLI wall	8.33E-10
Salivary	Small intestine	1.99E-09
Salivary	Stomach wall	1.50E-08
Salivary	ULI wall	3.40E-09
Salivary	Heart wall	2.05E-07
Salivary	kidneys	1.08E-08
Salivary	Liver	3.67E-08
Salivary	Lungs	2.77E-07
Salivary	Muscles	5.26E-07
Salivary	Pancreas	2.12E-08
Salivary	Red marrow	4.50E-07
Salivary	Bone surface	8.27E-07
Salivary	Skin	1.79E-07
Salivary	Spleen	3.82E-08

Source organs	Target organs	S-values
Salivary	Thymus	4.10E-07
Salivary	Thyroid	6.65E-04
Salivary	Urinary Bladder wall	4.10E-10
Salivary	Gonads	9.22E-10
Salivary	Others	5.63E-07
Gall Bladder	Adrenals	3.38E-07
Gall Bladder	Brain	1.42E-10
Gall Bladder	Breasts	4.00E-08
Gall Bladder	GB wall	4.21E-05
Gall Bladder	LLI wall	6.35E-08
Gall Bladder	Small intestine	4.95E-07
Gall Bladder	Stomach wall	3.14E-07
Gall Bladder	ULI wall	9.10E-07
Gall Bladder	Heart wall	1.30E-07
Gall Bladder	kidneys	3.77E-07
Gall Bladder	Liver	9.23E-07
Gall Bladder	Lungs	5.88E-08
Gall Bladder	Muscles	1.37E-07
Gall Bladder	Pancreas	5.20E-07
Gall Bladder	Red marrow	1.53E-07
Gall Bladder	Bone surface	1.27E-07
Gall Bladder	Skin	3.34E-08
Gall Bladder	Spleen	1.72E-07
Gall Bladder	Thymus	9.58E-09
Gall Bladder	Thyroid	2.89E-09
Gall Bladder	Urinary Bladder wall	4.75E-08
Gall Bladder	Gonads	1.32E-07
Gall Bladder	Others	1.36E-07
Urinary Bladder	Adrenals	9.08E-09
Urinary Bladder	Brain	5.64E-12
Urinary Bladder	Breasts	1.56E-09
Urinary Bladder	GB wall	4.31E-08
Urinary Bladder	LLI wall	6.18E-07
Urinary Bladder	Small intestine	2.42E-07
Urinary Bladder	Stomach wall	2.25E-08
Urinary Bladder	ULI wall	1.87E-07
Urinary Bladder	Heart wall	2.78E-09
Urinary Bladder	kidneys	1.94E-08
Urinary Bladder	Liver	1.32E-08
Urinary Bladder	Lungs	8.63E-10
Urinary Bladder	Muscles	1.56E-07
Urinary Bladder	Pancreas	1.06E-08
Urinary Bladder	Red marrow	1.20E-07
Urinary Bladder	Bone surface	1.17E-07
Urinary Bladder	Skin	4.21E-08
Urinary Bladder	Spleen	1.08E-08

Source organs	Target organs	S-values
Urinary Bladder	Thymus	5.40E-10
Urinary Bladder	Thyroid	1.13E-10
Urinary Bladder	Urinary Bladder wall	1.24E-05
Urinary Bladder	Gonads	1.41E-06
Urinary Bladder	Others	1.18E-07
Muscles	Adrenals	1.21E-07
Muscles	Brain	2.10E-08
Muscles	Breasts	5.10E-08
Muscles	GB wall	1.49E-07
Muscles	LLI wall	1.43E-07
Muscles	Small intestine	1.21E-07
Muscles	Stomach wall	1.17E-07
Muscles	ULI wall	1.29E-07
Muscles	Heart wall	1.15E-07
Muscles	kidneys	9.50E-08
Muscles	Liver	8.46E-08
Muscles	Lungs	7.77E-08
Muscles	Muscles	2.32E-07
Muscles	Pancreas	9.55E-08
Muscles	Red marrow	1.36E-07
Muscles	Bone surface	2.04E-07
Muscles	Skin	6.18E-08
Muscles	Spleen	1.33E-07
Muscles	Thymus	7.10E-08
Muscles	Thyroid	1.37E-07
Muscles	Urinary Bladder wall	1.58E-07
Muscles	Gonads	1.63E-07
Muscles	Others	1.33E-07

APPENDIX G

Steps for calculation the residence time from Dosimetry Toolkit

Preparation for Dosimetry Toolkit

- Multiple consecutive WB planar scans were created as input data (Dosimetry_Toolkit_Prep) for Dosimetry Toolkit by clicking the [WB Dosimetry Toolkit Prep] from the application list.

Registration of series of WB planar images

To adjust registration,
[Threshold slider](A) was used to set the ROI for registering WB planar images.

- Register WB planar images by clicking [Edit WBs/Std ROIs] (I).
- After WB registration, [Adjusted Selected WB] (B) tools were used to adjust the images.

  Tools to adjust registration:
  - Clockwise and counter-clockwise rotation of full scan
  - Left/Right/Up/Down shift of full scan
  - 0 buttons reset individual rotation/shifts to their original state.
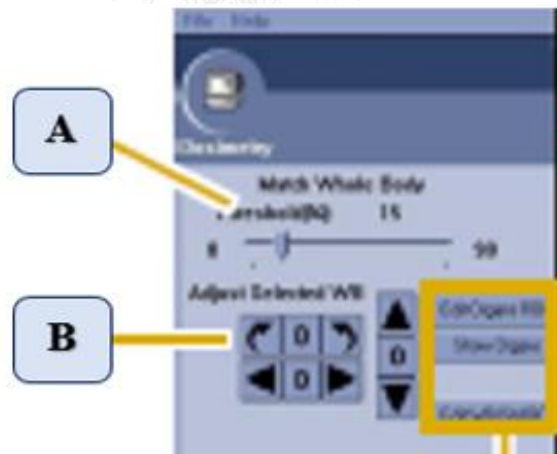
Figure H.1: Threshold and registration tools

Defining organs

- On one of the planar images, the organ ROI (C) was drawn using the ROI tool.
- For each organ ROI, select from **Organ Pick** list (D) and confirm by clicking (✔) (E).
- Organs ROIs were drawn for 11 source organs such as heart, liver, gall bladder, thyroid, salivary glands, lungs, spleen, intestine, kidneys, muscles and urinary bladder to calculate the residence time.

- If the defined organs do not exist in **Organ Pick** list, the name of that organs can be written down in the space and press 'save' (F) to save new or edited organs
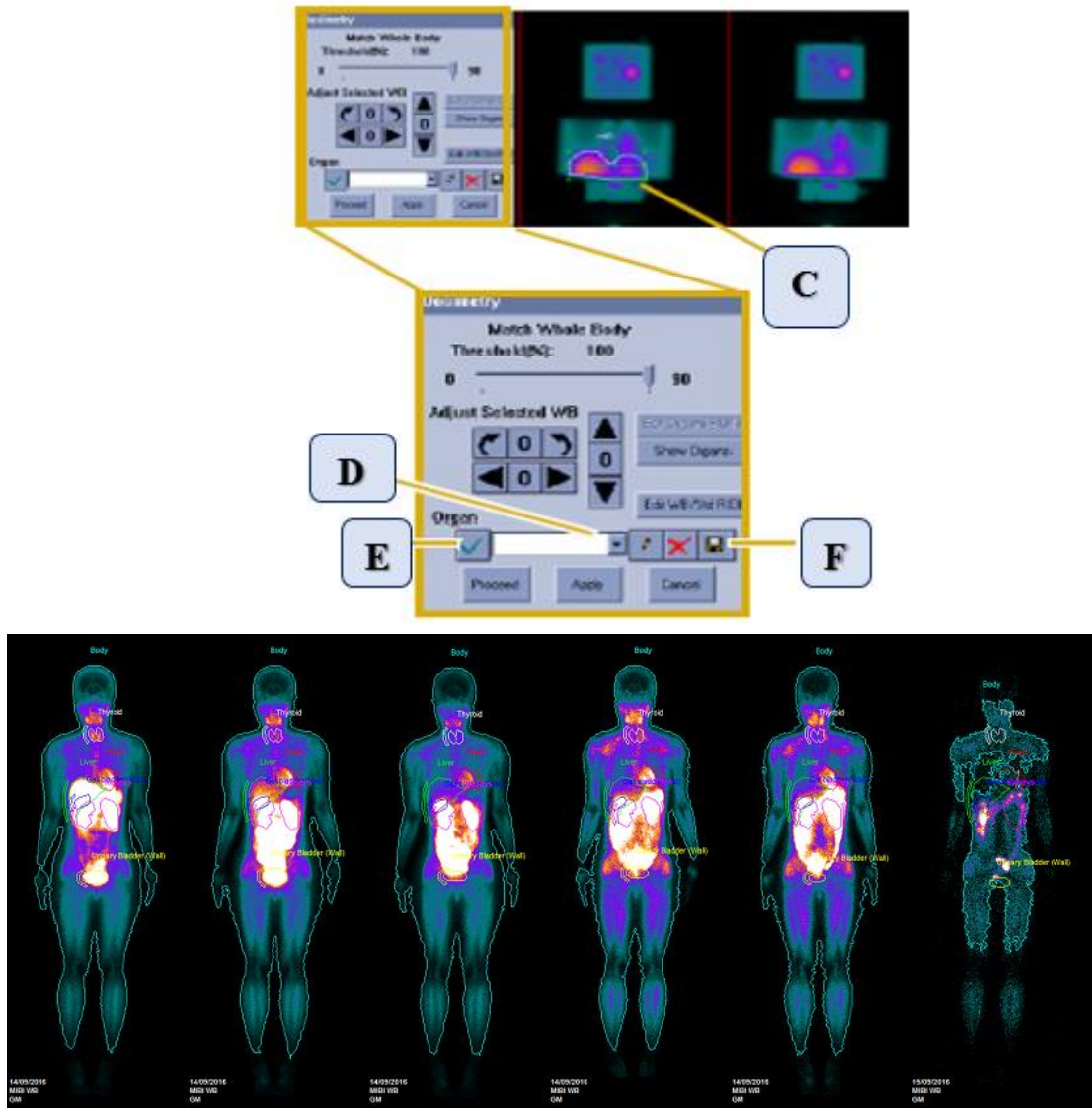

Figure H.2: Defining source organs in serial measurement images

Verify/Update organ definition and confirm organs on all time slots

- Because internal organs may be slightly mis-registered due to local shifts/rotation, organ ROIs was manually adjusted.

- [Edit Organ ROIs] (G) was used to enable selecting a ROI for editing which becomes active after an organ is picked.

- After editing ROI, [Confirm] (H) to revert to initial controls.

Figure H.3: Adjusting serial measurement images by using threshold and registration tools

For multiple segmented organs

For multiple segmented organs such as kidneys, lungs, thyroid and salivary, organ ROIs were drawn on both sides and defined organ and create background ROI per organ.
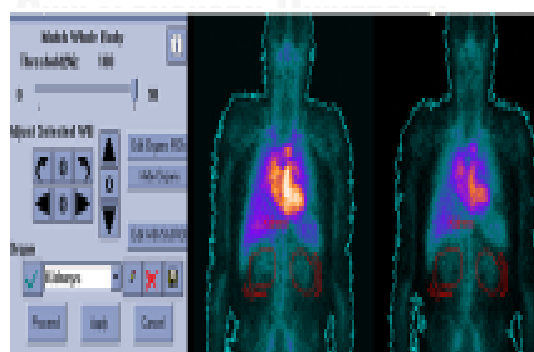
Figure H.4: Defining multiple segmented organs

Background Correction

- Background ROI (J) was created depending on the location of organ ROI center.

- Background ROI parameters were modified in the background ROI dialog (K).

- Because [Weight] is relative to surrounding body, it was set to close to 0 for small organs and close to 1 for large organs as recommended by Dosimetry Toolkit Technical publication.

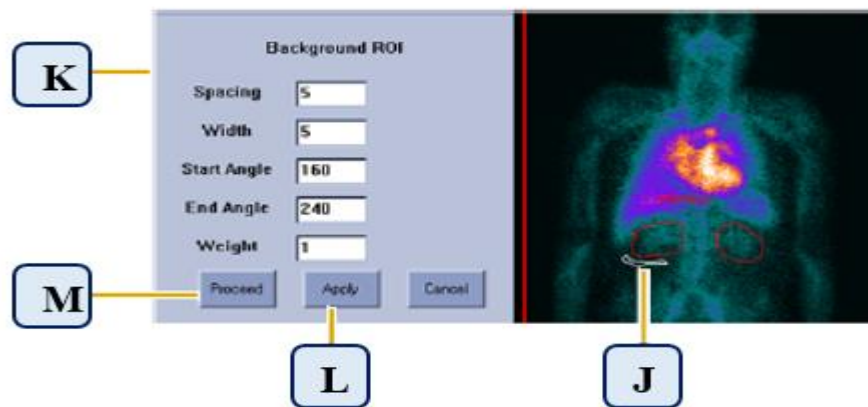- And then, click [**Apply**] (L) to apply modified setting, and then [Proceed] (M) to continue.

Figure H.5: Defining background ROIs for background correction

Calculation of radiopharmaceutical residence time per each organ

- Patient information (N) was filled.
- Tracer information (O) were entered as the following:

  - **Measured tracer activity**: Counts (MBq or mCi) of syringe pre-injection with time measured.

  - **Administered**: Time of injection

  - **Patient scanned with**: Time of acquisition alongside the decay corrected injected activity.

  - **Post injection measured**: Dose (MBq or mCi) of syringe post-injection with time measured.

  - **Calibration source**: optional: (***Hybrid Planar SPECT/CT scenario only***). * For planar WB scans, the activity of an organ is proportional to its counts, where the proportion factor is the WB activity to WB counts at the first scan time.
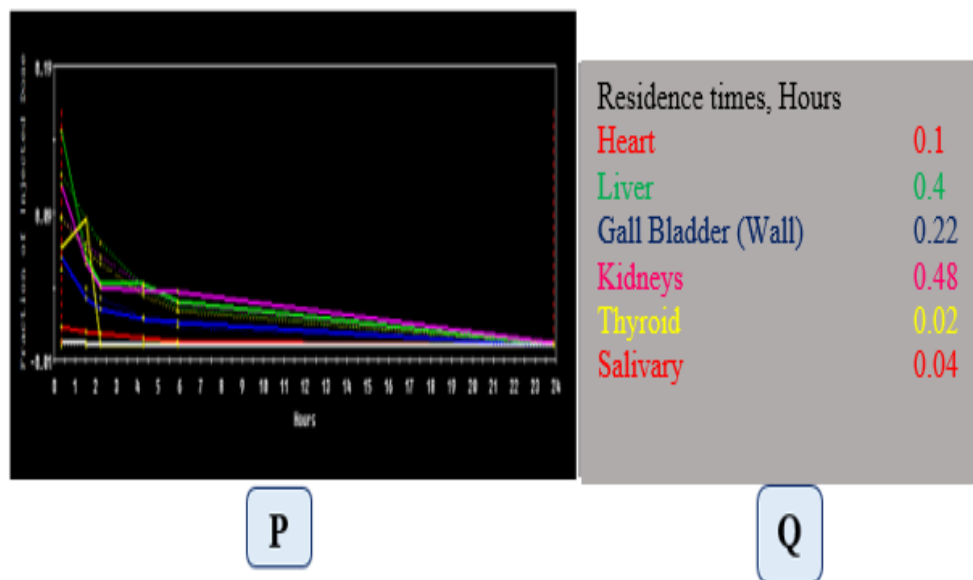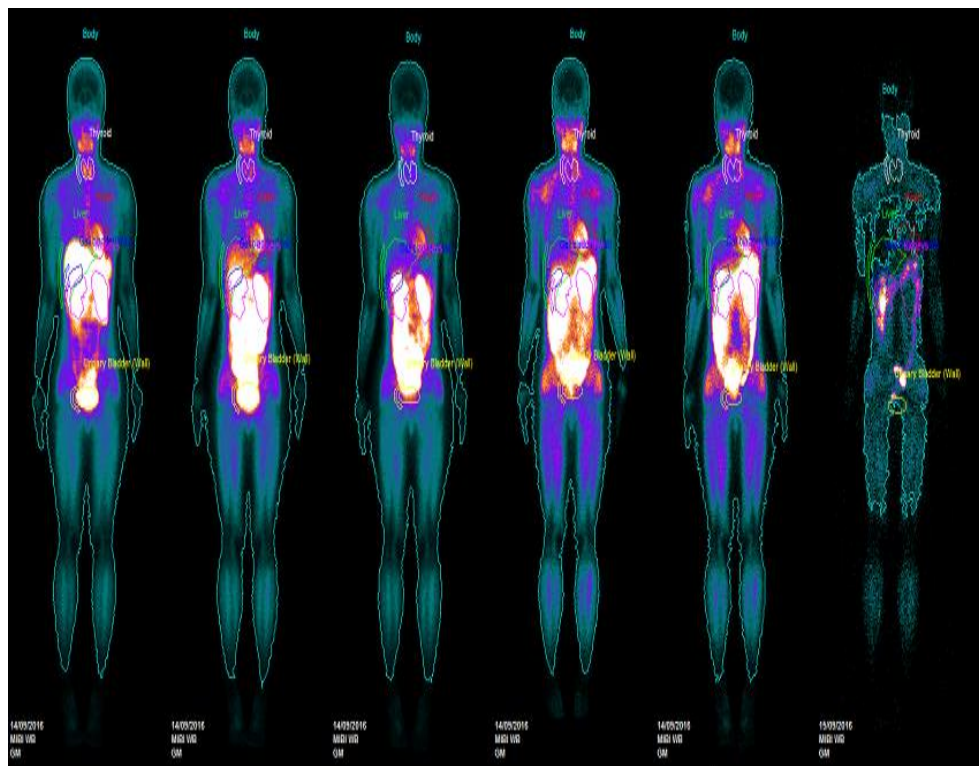 - **Isotope half-life**: Time in hours.

Figure H.6: Dialogue for entering information of patient and radiotracer

- After entering all of the required parameters, time-activity curves were automatically displayed for each defined organ (P).

- Horizontal axis shows the time units in hours, while the vertical axis indicates the activity as a fraction of injected dose.

- The residence time for each organ is shown in (Q)

Figure H.7: The results of residence time with related time-activity curves from Dosimetry Toolkit

APPENDIX H

Qualitative risk levels recommended by ACR and RSNA

Qualitative risk levels recommended by ACR and RSNA with background radiation

Negligible risk: less than 2 days of natural background exposure

Minimal risk: more than 2 days and up to 1 month of natural background exposure

Very low risk: more than 1 month and up to 8 months of natural background exposure

Low risk: more than 8 months and up to 6 years of natural background exposure

Moderate risk: more than 6 years of natural background exposure

Table H.1: The quantification of risk of cancer incidence

Quantification	Risk of cancer incidence
Negligible	< 1 in a million
Minimal	1 in a million to 1 in 100000
Very low	1 in 100000 to 1 in 10000
Low	1 in 10000 to 1 in 1000
Moderate	1 in 500 to 1 in 1000

VITA

NAME: Miss. Hnin Nitar

SEX: Female

NATIONALITY: Myanmar

DATE OF BIRTH: 23 June 1990

PLACE OF BIRTH: Meikhtila, Myanmar

INSTITUTIONS ATTENDED: University of Medical Technology,

Yangon, Myanmar, 2011:

Bachelor of Medical Technology

(Medical Imaging Technology).

Chulalongkorn University, 2017:

Master of Science (Medical Imaging).

E-MAIL ADDRESS: hninnitar@gmail.com